

The Solar System Boron Abundance:  
A Measurement of Boron Concentrations  
in Carbonaceous Chondritic Meteorites

Thesis by  
Martha Carroll Riherd Weller

In Partial Fulfillment of the Requirements  
for the Degree of  
Doctor of Philosophy

California Institute of Technology  
Pasadena, California

1979

(Submitted November 30, 1978)

Acknowledgments

I would like to thank Professor Tom Tombrello for accepting me as a student. His suggestions on this and other projects have been extremely helpful. I am particularly grateful for his encouragement and extreme patience while I tried to figure out how to do research.

I am grateful to Professor D.S. Burnett for the use of his laboratory facilities and for many helpful discussions. I have also enjoyed many useful conversations with Marian Furst. Her assistance in the initial stages of this experiment helped solve many early problems.

I have benefitted from conversations with many persons while engaged in this project. I would like to mention, especially, Professor E.C. Stone, Professor Ward Whaling, Joe Griffith, and Harold Wilson.

The highly competent technical staff of the Kellogg Laboratory played an important part in this work. I wish to thank, in particular, Bud Warrick, Will Schick, and Don Woshnak.

There are many people who have provided encouragement and moral support at various crucial stages of my academic career. It would be impossible to list them all. However, I am especially grateful to Carol Hieronymus, Dr. Don Altieri, Professor Steve Baker, Professor G.J. Wasserburg, and my oral candidacy exam committee.

I also wish to acknowledge the love and support of my family. My husband, Bob, has provided moral support as well as valuable technical advice and assistance. My parents were concerned about my education even when I was not and have always been encouraging. My sisters and brother have also encouraged me.

Finally, I would like to dedicate this thesis to the memory of my youngest sister, Shelley Riherd Griffis. For many years, Shelley was interested in my research and in my career as a scientist. Her encouragement was of enormous importance to me and I have missed it these last two years.

This research project was supported in part by the National Science Foundation. Meteorite samples were generously supplied by R. Clarke (U.S. National Museum), E. Olsen (Field Museum, Chicago), C. Moore (Arizona State), J. Wasson (U.C.L.A.), D.B. Curtis (Los Alamos), and G.J. Wasserburg (Caltech).

Abstract

Boron concentrations were determined for six carbonaceous chondritic meteorites using the reaction  $^{11}\text{B}(\text{d},\text{p})^{12}\text{B}$ . The results imply a solar system B/H ratio of  $(2 \pm 1) \times 10^{-9}$ . Although this ratio is much lower than that determined from previous meteoritic measurements, it remains significantly higher than the B/H ratios determined from the solar photosphere and other astrophysical environments.

Light element abundance ratios obtained from both meteoritic and photospheric data are compared with calculated values. It is concluded that two contributions are probably necessary to account for the observed ratios. Lithium, beryllium and boron nuclei produced according to the standard galactic cosmic ray model are expected to contribute significantly to the observed abundances. However, a component arising from low-energy spallation of CNO nuclei also appears necessary. Several possibilities are considered for the origin of these low-energy particles. However, the data and calculations are too uncertain to permit any firm conclusions.

Table of Contents

I.	Introduction	1
II.	Experimental Procedure	5
	A. Sample Preparation	5
	B. $^{12}\text{B}$ Activation Analysis	7
	C. Contamination Effects	13
III.	Results	22
IV.	Light Element Abundances in the Solar System and Other Astrophysical Environments	27
V.	Nucleosynthesis of the Light Elements	32
	A. The Galactic Cosmic Ray Model	32
	B. Comparison of GCR Model Predictions with Observations	36
	C. Other Possibilities for Light Element Nucleosynthesis	38
	D. Possible Tests of Low-Energy Spallation Models	42
VI.	Conclusions	46
	Appendix A - Calculation of Boron Concentrations	48
	Appendix B - Calculation of Light Element Abundance Ratios	56
	References	63
	Tables	68
	Figures	94

## I. Introduction

Although most of the chemical elements were probably created by thermonuclear reactions in stars, three light elements, lithium, beryllium and boron, must have been produced elsewhere, since they are rapidly destroyed in the stellar environment. Many models have been proposed to explain the existence and abundances of these elements, the most successful being the galactic cosmic ray spallation model (see, e.g. Reeves et al., 1970; Meneguzzi et al., 1971). However, even this model does not seem to completely solve the problem of these light elements.

One of the major difficulties in understanding these light element abundances has been the inadequate and often conflicting data on their solar system abundances. The problem has been particularly bad in the case of boron: Measurements of boron in the solar photosphere (Hall and Engvöld, 1975; Kohl et al., 1977), the interstellar medium (Morton et al., 1974), and the star Vega (Boesgaard et al., 1974) imply  $B/H \approx 10^{-10}$  while Cameron et al. (1973) calculated a meteoritic  $B/H$  of  $1.5 \times 10^{-8}$  based on carbonaceous chondrite data obtained by Quijano-Rico and Wänke (1969). Other data from carbonaceous chondrites (Harder, 1961; Mills, 1968) suggest  $B/H = 5 \times 10^{-9}$ .

It is not necessarily required that the  $B/H$  value for the interstellar medium or for stars other than the sun agree with the meteorite value. However, good agreement is

expected between the solar photospheric boron abundance and that derived from analyses of carbonaceous chondritic meteorites. Carbonaceous chondrites resemble the solid material expected when a gas cloud of solar composition cools to temperatures of  $\sim 300$  °K at low pressure ( $10^{-4}$  -  $10^{-6}$  atmospheres). Thus, elements which are gases (carbon, nitrogen, oxygen, rare gases, and perhaps chlorine) are depleted in meteorites relative to the sun. However, non-gaseous elements are expected to be present at their solar values (Anders, 1971; Ross and Aller, 1976) and cases where elements are enriched in meteorites may provide important information. For example, the 200-fold enrichment of lithium (Nichiporuk and Moore, 1970; Grevesse, 1968) indicates thermonuclear destruction of solar lithium, either in an earlier, totally convective, phase of solar evolution or by burning at the base of the surface convection zone during the main sequence lifetime. Unfortunately, a similar explanation for the boron discrepancy does not seem likely. Beryllium should be destroyed at lower temperatures than boron and there seems to be a reasonable correspondence between photospheric and meteoritic beryllium abundances (Quandt and Herr, 1974; Chmielewski, 1975). It has also been suggested that boron may be enhanced in carbonaceous chondrites and that these meteorites do not provide a valid solar system abundance for this element (Hall and Engvöld, 1975; Morton et al., 1974; Boesgaard et al., 1974).

However, with the exception of lithium and possibly mercury (Reed, 1971), no other cases of element enrichment in carbonaceous chondrites relative to the solar photosphere are known and such an enrichment of boron would be difficult to explain.

As emphasized by Cameron et al. (1973), a B/H ratio of  $10^{-8}$  is too high to be compatible with otherwise attractive theories of galactic cosmic ray (GCR) nucleosynthesis of the light elements. The lower value of  $10^{-10}$  has been generally accepted as more compatible with GCR nucleosynthesis; however, as will be discussed later, the high implied Li/B ratio presents difficulties.

In view of the large difference between the meteoritic and solar boron abundances and the implications for light element nucleosynthesis, additional measurements of the meteoritic boron abundance seemed desirable. In Chapter II of this thesis, the experimental technique used for these measurements will be described. The results of these measurements will be presented in Chapter III and compared with other measurements of boron in carbonaceous chondrites. Chapter IV will consider boron abundances from other astrophysical environments. Possible explanations for the the discrepancies between these values and our measurements will be presented. In Chapter V, the various light element abundances will be compared with the predictions of the GCR model and the possibility of other contributions to these

abundances will be considered. Conclusions will be presented in Chapter VI.

## II. Experimental Procedure

Because of the complexity of boron chemistry and the relative inertness of boron isotopes to conventional neutron activation techniques, the development of modern methods of boron analysis for geochemical samples has been slower than that for other elements. In this work, the nuclear reaction  $^{11}\text{B}(d,p)^{12}\text{B}$  was used to determine boron concentrations in carbonaceous chondrites. This chapter describes the procedure for the  $^{12}\text{B}$  activation analysis of low-boron samples.

For samples with more than 10 ppm B, the  $^{12}\text{B}$  activation technique permits convenient, routine boron analysis without elaborate precautions and testing for contamination. However, at the 1 ppm level, sample contamination can become a major concern. Sample preparation procedures and tests for contamination were important for this experiment and are also discussed in this chapter.

### A. Sample Preparation

Samples of each of the three types of carbonaceous chondrites were obtained for analysis. C1 chondrites, considered to be the most primitive material in the solar system, are composed almost entirely of dark matrix material. Material from these meteorites crumbled easily and therefore required careful handling. C2 and C3 meteorites are characterized by small glassy spheres

(chondrules) imbedded in a matrix similar to that of the C1 chondrites. These samples were considerably more solid than the C1 samples. In addition to the meteorites, NBS glass standards containing about 350 ppm B and graphite control samples were also prepared and analyzed.

Because of the serious contamination problems encountered in this experiment, meteorite samples were selected and prepared with great care. All operations were carried out with pre-cleaned tools in a restricted-use laboratory which has a charcoal-filtered air supply system. Totally interior samples were obtained by chipping, sawing, or, in the case of the C1 meteorites, by carefully removing the external portions of the samples with tweezers. Chipped or sawed surfaces were sanded with coarse-grit silicon-carbide paper to remove any smeared metal and then ultrasonically rinsed in high-purity methanol. Surfaces cleaned in this way could be analyzed directly. However, because of sample thickness corrections required for analysis, only slices with plane parallel faces were considered suitable for irradiation. Glass standards were prepared in a similar manner, using different equipment to avoid cross-contamination of samples. The C1 meteorite samples (because of their friability), some Murchison (C2) samples and some graphite controls were powdered in a ball mill using a plastic ball and container. Grinding times for obtaining the powders varied from a few seconds for the C1

chondrites and graphite control samples to a few minutes for the Murchison samples. The powders were then pressed into 5 mm diameter pellets (20-50 mg) using a stainless steel die. No binder was necessary to obtain coherent pellets, although those from Allende were fragile.

It was necessary to use low-boron materials throughout the sample preparation and analysis procedures. Although boron is a rare element in the solar system, it is quite common in the laboratory environment. Pyrex glassware (4% B) and detergents containing boron were obvious problems and were not used. Table 1 shows the boron concentrations of other standard laboratory materials. These concentrations were measured by M. Furst using a nuclear track technique for boron analysis (Furst et al., 1976; Weller et al., 1978). Materials actually used in preparing samples for this experiment are indicated by asterisks.

#### B. $^{12}\text{B}$ Activation Analysis

The reaction  $^{11}\text{B}(d,p)^{12}\text{B}$  is particularly suitable for low-level boron analyses for several reasons. The cross section is large, ranging between 0.2 and 0.6 barns for deuteron energies between 1 and 2.8 MeV (Kavanagh and Barnes, 1958). Also, the beta-decay of  $^{12}\text{B}$  is almost exclusively to the ground state of  $^{12}\text{C}$  with a maximum decay energy of 13.4 MeV and a half-life of 20.4 msec. This unique decay signature allowed the yield of betas from  $^{12}\text{B}$  to be

determined despite significant background from other reactions.

The experimental arrangement for these measurements is shown schematically in Figure 1. One of the 24 targets in the holder was bombarded with about 150 nA of 2.8 MeV deuterons, confined within a beam spot size of about 3 mm x 3 mm. The maximum beam current was limited by the outgassing of the targets. The bombarding energy of 2.8 MeV was chosen to minimize the effects of background reactions. Deuterons with this energy penetrated about 50 microns into the samples. However, at energies below about 0.5 MeV, the cross section for the (d,p) reaction is quite small due to Coulomb barrier effects; thus, the actual thickness analyzed was about 35 microns, out of a total sample thickness of 0.5 to 1 mm. A 5 cm x 5 cm Pilot B plastic scintillator, located 6 mm behind the target, detected the betas, which had already lost an average energy of 2.5 MeV in the sample and in the material between the target and the detector. The single channel analyzer (SCA) had an energy window corresponding to an energy loss in the detector of 3.5 to 9.5 MeV. This means that most of the betas accepted by the SCA had initial energies between 6 and 12 MeV. Pulses from the SCA were then fed into four scalers which were gated to count in consecutive time intervals.

The counting sequence is shown in Figure 2a. The beam

was on the target for 30 msec. Because there was a delay of several msec between the signal for the beam to be deflected and the actual deflection of the beam, a 15 msec delay was introduced into the counting cycle to insure that the beam was not on the target during the first counting period. After this delay, four scalers were gated, in turn, for 15 msec counting periods. This cycle was repeated between 20,000 and 100,000 times, depending on the target and the beam current. Assuming constant background, the difference between any two scaler readings was proportional to the concentration of  $^{11}\text{B}$ .

There were two important background reactions in this experiment which caused a rather small signal to background ratio (roughly 1/20): (1.) The lithium content of chondrites is small (1 to 2 ppm), but the  $^7\text{Li}(d,p)^8\text{Li}$  reaction cross section is large and the 13.1 MeV beta-decay energy of  $^8\text{Li}$  made it impossible to discriminate between the  $^8\text{Li}$  and  $^{12}\text{B}$  spectra on the basis of energy. The yield of betas from  $^8\text{Li}$  was approximately equal to that from  $^{12}\text{B}$  for a target containing  $\text{Li/B} = 1.5$  by weight; however, the large difference in half-life (850 msec for  $^8\text{Li}$  vs. 20 msec for  $^{12}\text{B}$ ) enabled counts from  $^{12}\text{B}$  to be distinguished from those due to  $^8\text{Li}$ . (2.) Analysis of the decay rate of the induced radioactivity showed that most of the background for a meteorite sample was due to the beta decay of  $^{16}\text{N}$ , produced

in the reaction  $^{18}\text{O}(d,\alpha)^{16}\text{N}$ . This reaction does not have a large cross section, but oxygen is the most abundant element in carbonaceous chondrites.  $^{16}\text{N}$  decays primarily to excited states in  $^{16}\text{O}$ , emitting low-energy betas which were not counted. The high-energy gammas from the subsequent decay to the ground state did not contribute significantly to the observed background since plastic scintillators are inefficient detectors for gamma rays. However, betas with a maximum energy of 10.4 MeV are emitted in 26% of the  $^{16}\text{N}$  decays. Although the low-energy cut-off on the SCA was chosen to minimize the effect of this decay on the final error, these high-energy betas accounted for 95% of the meteorite background counts.

Although the half-lives of both  $^8\text{Li}$  (0.85 sec) and  $^{16}\text{N}$  (7.2 sec) are much longer than that for  $^{12}\text{B}$ , the background could not be considered constant. Such an assumption would have resulted in an overestimate of the boron concentration by about twenty percent. With four counting periods, one can, in principle, obtain a  $^{12}\text{B}$  yield which properly takes into account the decays of  $^8\text{Li}$  and  $^{16}\text{N}$ . However, for the meteorite samples, only a small error was made by assuming that the background was entirely due to  $^{16}\text{N}$ , and that it therefore decayed with a 7.2 sec half-life. The estimated error from this assumption was approximately 2%, compared to 10% from counting statistics alone. For the standard

samples which contained 100-200 times more lithium than the meteorites, the background was assumed to decay with an 0.85 sec half-life. Again, this introduced only a small error into the results.

Given these assumptions, only two counting periods are required to determine the  $^{12}\text{B}$  yield. Statistically, the most precise  $^{12}\text{B}$  yields were obtained by combining the four 15 msec counting periods into two 30 msec periods. All of the tabulated B concentrations were based on this procedure which is described in detail in Appendix A. Other differences in the number of counts (e.g. between the 1st and 2nd periods) were routinely checked and found to be consistent, indicating that the  $^{16}\text{N}$  and  $^8\text{Li}$  background corrections were effective. Figures 2b and 2c are examples of actual meteorite decay curves, both uncorrected and corrected for background.

To obtain the boron concentrations,  $^{12}\text{B}$  yields from meteoritic samples were compared with those from the National Bureau of Standards glass SRM 610 which contains 351 ppm B. The SRM 610 concentration was confirmed by comparison with Pyrex glass which has a well-known and well-controlled boron concentration. The results of these comparisons for different pieces of the NBS glass are shown in Table 7. In comparing meteorite yields with those for the NBS glass, a small correction (10%) was made which took into account the differences in deuteron energy loss between the sample and the standard. (The range of the deuterons, and

thus the thickness of material analyzed, is dependent on sample composition.) This correction is described in detail in Appendix A. A correction was also necessary for differences in the beta yields due to varying sample thicknesses. Compared to a thin sample, a thick sample degraded more betas below the SCA lower limit and, thus, a smaller fraction of the total spectrum was counted. This correction was typically 30%, but was as large as 100% in some cases; fortunately, it could be determined experimentally from "absorption" curves obtained by analysis of various thicknesses of Pyrex glass. Although high-energy betas were being counted, ionization losses dominated bremsstrahlung as the principal mechanism for energy loss since the absorbing materials were composed primarily of light elements. Thus, negligible error was introduced by assuming that the measured beta absorption curve for Pyrex applied to the meteorite samples as well. The uncertainty in the thickness corrections did not contribute significantly to the total error in the measured boron concentrations. The details of this correction are also discussed in Appendix A. Finally, to obtain the total boron content, it was assumed that the  $^{11}\text{B}/^{10}\text{B}$  ratio in meteorites is the same as the terrestrial ratio. Thus, no isotopic correction was necessary in comparing meteoritic and standard samples.

As an additional check on the  $^{12}\text{B}$  activation technique,

a comparison was made of boron concentrations obtained using this technique with those obtained by M. Furst using the nuclear track technique. Agreement to within 5% was obtained for pieces of glass containing about 90 ppm B.

The estimated error for a single measurement on a sample containing 1 ppm B is  $\pm 15\%$ . For samples with higher boron concentrations, the percentage error is smaller since most of the error arose from counting statistics.

### C. Contamination Effects

It was important to establish that the data were not seriously affected by contamination. Since this technique was instrumental, it was possible to re-analyze a given sample. However, when this was done, the measured boron concentration increased with each irradiation, sometimes by as much as a factor of 2-3. Even elaborate precautions in storage of the samples between irradiations failed to prevent this increase. Consequently, all reported results are based on the first analyses of freshly prepared samples.

The following tests were performed to determine whether results obtained from the initial analyses of samples were also affected by contamination. Recall that the important question is whether  $B/H = 10^{-10}$  or  $B/H = 1.5 \times 10^{-8}$ .

(1) Low boron control samples were prepared and analyzed in parallel with each batch of meteorites, and these samples consistently yielded much lower boron concentrations than the meteorites. If contamination had been introduced in any way

during sample preparation or analysis, it would have affected both meteorite and control samples. (2) The time between sample preparation and analysis as well as the total exposure time of the sample to the laboratory atmosphere were deliberately varied. These tests showed that contamination was not significant for our standard procedures. (3) Fresh surfaces of three Murchison slices were prepared under vacuum and then analyzed without atmospheric exposure. Results from one of these samples indicated a possible contamination effect of  $\leq 0.5$  ppm.

We now consider these test results in detail.

(1) A sample of reactor-grade graphite was prepared and analyzed along with meteorite samples during each  $^{12}\text{B}$  activation irradiation. The mechanical and surface properties of graphite made it a reasonable choice for a control sample, particularly for comparison with sawed meteorite surfaces. The graphite was guaranteed to have a boron content of less than 0.8 ppm and the average value (according to the manufacturer's specifications) was 0.4 ppm B. Individual analyses in this experiment yielded concentrations between 0.1 and 0.4 ppm with the standard deviation of a typical analysis being about 0.15 ppm. Thus, within errors, a value of 0.25 ppm B was obtained for all the graphite control samples. This sets an upper limit for the amount of contamination which is, at most, 25% of the observed meteorite values. Since a sample of the Murchison meteorite

was present in most of the irradiations, it was also possible to check for any correlation between the graphite and Murchison data which would have suggested a variable amount of contamination. No such correlation was observed.

Graphite samples were analyzed in the form of pellets as well as slices. No differences were seen between the sawed slices and the pellets. Thus, no correction for a "crushing blank" was applied to the meteorite results obtained from pellet samples.

(2) It was found that samples could not normally be stored for periods of a few weeks between irradiations without observing an increase in boron content. Consequently, it was necessary to demonstrate that the sample did not become contaminated in the time between preparation and the first analysis, i.e. to have some estimate of the rate of surface contamination. There were two times which required investigation: (a) the storage time between sample preparation and evacuation of the irradiation vacuum chamber and (b) the exposure time of a fresh sample surface to the laboratory atmosphere.

Normally, samples were stored in a dessicator for 10-20 hours prior to evacuation of the irradiation chamber. A series of slices of Murray and of graphite were prepared and the storage times were varied. The resulting boron concentrations are shown in Figure 3. No significant increases were observed except for the graphite sample which

was stored for 64 hours.

Between the time of sample preparation and the evacuation of the irradiation chamber, fresh sample surfaces were normally exposed to the laboratory atmosphere for 15-30 minutes. Slices of Murchison, Allende and Murray were prepared for which the laboratory exposure times were increased to 90 minutes and these samples were analyzed in parallel with slices having normal exposures. The results are shown in Figure 4. The scatter in the data at short exposures is typical of these samples and is ascribed to sampling. Considering this scatter, there was no significant increase in boron concentration with increased laboratory exposure time, except possibly for the Murray sample which had an extended exposure.

These results indicate that negligible boron contamination was acquired during the normal exposure and storage of freshly prepared samples prior to analysis. They also demonstrate that the actual meteorite samples did not "adsorb" boron contamination more rapidly than the control samples during this time. However, these results do not preclude the possibility that "instantaneous" contamination occurred when the meteorite surface was first exposed to the atmosphere.

(3) Three slices of Murchison were analyzed by  $^{12}\text{B}$  activation. Following the initial analyses, fresh surfaces were scraped on the samples without breaking the vacuum, and the samples were then re-analyzed. This procedure was

repeated several times, yielding the results shown in Figure 5.

Sample #1 was scraped twice with a quartz tool while under vacuum and a total of  $\sim 75\%$  of the irradiated surface material was removed. The data from this sample indicate no contamination.

For Sample #2, the surface was removed using a steel file. In this case, the sample was scraped four times and the entire top 230 microns were removed. Data from this sample indicate some possible surface contamination. Unfortunately, it was not possible to determine the absolute boron concentrations for these analyses. The energy window of the SCA for these analyses was significantly different from that of the other analyses and a much smaller fraction of the spectrum was counted. Since the beta energy loss correction to the data was determined for a different part of the spectrum, this correction could not be accurately made. However, a subsequent comparison of B concentrations obtained using different portions of the beta spectrum indicated that the B concentrations shown in Figure 5 should be taken as lower limits for the actual concentrations for this sample. Thus, the contamination level is, at most, 0.5 ppm B. Measurements on other samples suggest that the actual concentrations are 10-20% higher than these lower limits. These values are only slightly lower than many of those obtained from other analyses of this meteorite.

Sample #3 was also scraped with a steel file. This sample was scraped 7 times and a total of 420 microns of surface material was removed. Although this sample was seriously contaminated initially, the boron concentrations found after the sample had been scraped several times were well within the normal range of concentrations for this meteorite. Thus, this sample also indicates that our results were not seriously affected by contamination.

During the second surface removal experiment, the sample was analyzed twice between the second and third scraping. The results of the two analyses were consistent and indicate that, while under vacuum, contamination of a clean surface occurs very slowly, if at all.

Based on the above tests, contamination is not believed to be a serious source of error in these measurements. Nevertheless, the origin of the contamination was of some concern and attempts were made to determine its source. The following discussion summarizes what is known (and conjectured) about this contamination.

There was an apparent difference in the contamination rate of samples before and after irradiation which is believed to be significant, although this cannot be conclusively proved. Preferential contamination of radiation-damaged surfaces is moderately well documented for fluorine (Goldberg et al., 1975) and hydrogen (Leich et al., 1974). In this experiment, the evidence for radiation-

induced contamination came from measurements in which a sample was analyzed, exposed to air and then re-analyzed under vacuum. This experiment was done three times on a total of six meteorite and two graphite samples with atmospheric exposure times varying from 0.5 to 12 hours between measurements. In the first two experiments, all of the B concentrations increased by amounts ranging from 2 to 10 standard deviations. However, in the third irradiation which involved the shortest exposure time, two Murchison samples showed no significant increase. Thus, radiation damage appears to have had an important influence on the contamination rate, although other factors may also have existed.

An alternate explanation for these results is that most of the surface-adsorbed gases were removed when the samples were placed under vacuum and then contamination occurred immediately upon re-exposure to the atmosphere, regardless of whether the sample had been irradiated. This interpretation seems unlikely because surface-adsorbed gases would not be removed at the pressures used for these measurements ( $10^{-5}$ - $10^{-6}$  Torr), and rapid contamination has also been observed with the nuclear track analysis technique (Weller et al., 1978) which involved no vacuum. Nevertheless, experiments were performed to test this interpretation. Homogenized meteorite pellets were analyzed by  $^{12}\text{B}$  activation, but analysis of some pellets was done only

after the scattering chamber had been vented and re-evacuated. In two experiments, the pellets analyzed after venting showed boron concentrations which were 1 and 3 standard deviations higher than those obtained from pellets analyzed before venting. However, for the samples which had been irradiated before venting, the boron concentrations after venting were even higher. These results support the radiation-damage hypothesis, but still permit some contamination (up to ~0.5 ppm) of the samples which were pumped on and then exposed to air before analysis. However, only a few samples had this pressure history and they did not show systematically higher boron contents than the other samples.

The source of the contamination boron is not known. However, it is clearly airborne and limits on the size of the contaminating particles have been set based on measurements by M. Furst using the nuclear track technique (Weller et al., 1978). These measurements indicated an upper limit of  $\leq 10^9$  atoms of boron per contaminant particle. The most likely form of such small contaminant particles is aerosol droplets, e.g. sub-micron  $H_3BO_3$  solutions, presumably originating from sea spray. An observed correlation between high boron results for control (as well as meteorite) samples and certain local weather patterns suggests a second possible source of contamination. Extensive borate deposits are

located in the nearby deserts and it is likely that dust particles from these deposits are blown into our area by the occasional strong winds from the desert.

Since the source of the contaminant boron could not be definitely established or eliminated, it was necessary to establish criteria by which samples could be considered approximately free of contamination. Exposure of the samples to the laboratory atmosphere was minimized and samples were placed in the scattering chamber under vacuum within 24 hours of preparation. Analyses were accepted only if low boron concentrations were obtained from graphite control samples during the same irradiation. Finally, only the initial analysis of a surface was accepted. All analyses satisfying these requirements were assumed to be unaffected by contamination. (One additional requirement was imposed on the samples which had nothing to do with contamination: Since the data had to be corrected for differences in target thicknesses, only samples with plane parallel surfaces were accepted for analysis.)

### III. Results

Detailed results of these measurements are presented in Table 8 and Figure 6 on a sample-by-sample basis. The X's indicate analyses of different pellets prepared from aliquots of a single crushed sample while the other data represent the single analyses of samples which were prepared as slices. Typical errors for all the data are  $\pm 0.2$  ppm.

The reproducibility of these results was quite good. Duplicate bombardments of the same sample routinely gave results that agreed within statistical errors, provided that the vacuum system was not vented between irradiations. This reproducibility shows that the results are not anomalously low due to loss of volatile boron compounds by beam heating.

The homogenized pellets provide another test of reproducibility. Analyses of different pellets produced from aliquots of a given sample were in generally good agreement as is seen in Figure 6.

Some scatter is expected for different samples of the same meteorite, given the relatively small volume of material analyzed and the petrographic variability of carbonaceous chondrites; however, the results for the C2 meteorites, Murray and Murchison, are remarkably consistent. The Allende results show more scatter with values for individual samples ranging from 1 to 3 ppm. However,

this scatter is not unreasonable for these samples.

Most of the  $^{12}\text{B}$  activation results obtained after August 26, 1976 have been accepted. Murchison and Allende analyses prior to this date were made on samples of irregular thickness which resulted in very large uncertainties. These results were not tabulated because of the large errors. They are compatible with the later data, although there is some tendency for the Murchison values to be somewhat higher (2-3 ppm rather than 1-2 ppm) than those obtained later. Several later Murchison analyses were also rejected. Two of these samples had not been cleaned properly and therefore did not satisfy the criteria for sample acceptance. One other sample was shown by vacuum-scraping to be contaminated. Finally, the results from one sample were rejected because the usual SCA energy window was not used for these analyses.

Table 2 gives the average boron concentrations for the meteorites studied. Clearly, different ways of averaging the individual analyses would produce somewhat different results. For example, all samples were included in the averages, although omitting the highest values for Murchison and Allende (Figure 6) would have been permitted statistically. If the high results are excluded, the resulting boron concentrations for these meteorites become 1.5 and 1.3 ppm, respectively. The results in Table 2 differ slightly, but not significantly, from those given in Weller et al.(1977) and Weller et al.(1978).

The final column in Table 2 gives the atomic boron

abundances, relative to Si =  $10^6$ . Silicon contents for individual meteorites have been used where possible; otherwise, the silicon contents for the various C meteorite subgroups (Moore, 1971) were used. The progression of B/Si between the C3/C2/C1 meteorites is close to the 0.4/0.5/1 progression normally observed (Larimer and Anders, 1967; Anders et al., 1976) between the different types of C meteorites for moderately volatile elements.

The results of several measurements of boron in carbonaceous chondrites are presented in Table 3. The Allende result from Weller et al. refers only to the value obtained by nuclear track analysis. In addition to these measurements, Curtis et al. (1976) have determined boron concentrations in eight carbonaceous chondrites, obtaining results in agreement with those presented in Table 2, although actual values were not presented in their paper. There are obvious discrepancies between the early analyses and the more recent measurements which probably cannot be ascribed to sampling. The number of samples of each meteorite analyzed by  $^{12}\text{B}$  activation is indicated in Table 2. In the case of Allende, the samples were taken from two different specimens, each supplied from a different source. For the Murchison measurements, samples were taken from three different specimens, also from different sources. If the boron concentration in carbonaceous chondrites really varies between 1 and 10 ppm, high values should have been

observed in some of the  $^{12}\text{B}$  activation measurements. The low results of Curtis et al. and of Weller et al. also support the argument that the discrepancies are not due to sampling.

The differences between the low boron concentrations obtained in the most recent measurements and the early high results may represent the use of contaminated samples in the previous studies. Wänke (1978) has indicated that their carbonaceous chondrite samples were of poorer quality than their other samples and has also suggested that the location of their laboratory adjacent to a factory producing high-boron glass may have contributed to the contamination of these samples. It should be emphasized that the chemical and analysis procedures used by Quijano-Rico and Wänke produced low blanks and, ironically, have superior sensitivity and precision to those used for the  $^{12}\text{B}$  activation measurements. There is no reason to question the results of these workers for the ordinary and enstatite chondrites where larger and better quality samples were available for analysis. In fact, Curtis et al. (1976) have confirmed their results for these meteorites.

It should be noted that Curtis et al. now seem to be obtaining boron concentrations for some carbonaceous chondrites (Murchison and Lancé) which are lower than their earlier results and the results given in Table 2 (Curtis, 1978). The most obvious explanation for this new discrepancy

is that the earlier results as well as those in Table 2 are high due to contamination. The neutron-induced prompt gamma-ray analysis technique (Gladney et al., 1976) used by Curtis et al. is less sensitive to surface contamination than either the  $^{12}\text{B}$  activation technique or the nuclear track technique. Their new results for Murchison are consistent with, but somewhat lower than, the lower limit of 0.8 ppm found for one of the vacuum-scraped samples in this experiment. However, the results of the contamination tests discussed in the last chapter indicate that contamination did not seriously affect the results in Table 2. Throughout the remainder of this thesis, it will be assumed that the values given in this table reflect the approximate boron contents of carbonaceous chondrites.

Based on the results given in Table 2, the solar system B/H ratio is estimated to be  $(2 \pm 1) \times 10^{-9}$ . One may also calculate a B/H ratio based on the boron concentration of 0.8 ppm obtained as a lower limit for one of the vacuum-scraped Murchison samples. A value of  $1.5 \times 10^{-9}$  is determined if one assumes that the B/Si ratios are characterized by the progression between the different types of C meteorites which is observed for other moderately volatile elements. This value is not significantly different from that obtained from the other samples.

IV. Light Element Abundances in the Solar System and  
Other Astrophysical Environments

In attempts to clarify the creation process for the light elements, measurements have been made recently of the lithium, beryllium and boron abundances in several different astrophysical environments. Table 4 summarizes the results of these measurements relative to hydrogen abundances of 1. It is clear that the measured abundances of the light elements do not all agree for different environments and in this chapter, possible explanations will be offered.

Although there is no reason for the abundances to be the same in all of these environments, general agreement has been found between elemental abundances in the solar photosphere and those in carbonaceous chondrites except for elements that are normally in gaseous form. Unless the abundances of lithium, beryllium and boron have been influenced by processes which have not affected other elements, good agreement is expected between the solar photospheric and meteoritic abundances for these elements as well. The most widely accepted model for the synthesis of the light elements, the GCR model, predicts approximate agreement between solar system and interstellar medium abundances. This model also implies that the lithium, beryllium and boron abundances for main-sequence stars other than the sun should agree with the solar system values unless

the stellar abundances for these elements are modified by nuclear processes. However, this model does allow the relative abundances of elements and their isotopes in the cosmic rays to differ from their values in other environments.

It is seen from Table 4 that the meteoritic and solar photospheric abundances do not agree for any of the light elements. In the best case, that of beryllium, the discrepancy is a factor of three while, for lithium, there is a difference of nearly two orders of magnitude. The disagreement in lithium abundances is generally considered to be due to the destruction of lithium by nuclear reactions at the base of the solar photosphere or during an earlier phase of solar evolution. However, this explanation is unlikely to account for the discrepancies between the meteoritic and solar photospheric abundances of beryllium and boron. Since beryllium is destroyed at lower temperatures than boron, the difference between solar and meteoritic beryllium should be larger than that for boron. This does not appear to be the case. However, the large experimental errors do not allow a firm conclusion. If all the light elements have been destroyed to some extent in the solar photosphere, then the meteoritic abundances must be assumed to represent the solar system abundances for beryllium and boron as well as lithium.

The beryllium discrepancy is generally ignored and other explanations have been suggested for the discrepancy between the solar photospheric and meteoritic boron abundances. Several authors (Boesgaard et al., 1974; Audouze et al., 1973; Kohl et al., 1977) have suggested that boron may be anomalously enriched in carbonaceous chondrites relative to its actual solar system value. However, there is no obvious mechanism for such enrichment and, with the possible exception of mercury (Reed, 1971), it is not observed for other elements.

The possibility of experimental errors in either the solar photospheric or meteoritic measurements (or both) cannot be excluded. For example, contamination has already been discussed as a source of error in the meteoritic boron measurement. Photospheric measurements of both boron and beryllium are difficult and, for boron, two different measurements are not in agreement. If the higher value of Kohl et al. is chosen, then the discrepancy between meteoritic and photospheric boron abundances is not much worse than that for beryllium. On the other hand, if either the photospheric or meteoritic beryllium abundance were shown to be incorrect, the possibility of stellar destruction of boron might seem more plausible.

As mentioned earlier, independent of models of light element nucleosynthesis, there is no reason to expect solar

system abundances to agree with those observed in the interstellar medium or in other main sequence stars. However, the GCR model for light element creation predicts agreement for lithium, beryllium and boron in these environments. It is seen from Table 4 that, except for beryllium, the interstellar abundances are lower than the solar system values. Stellar abundances agree well with the solar photospheric values for boron and beryllium while the range of lithium values in stars may be attributed to varying degrees of stellar destruction of this element. Lithium abundances for the youngest stars where destruction has not occurred are in reasonable agreement with the meteoritic abundances.

It has been suggested that the apparent depletion of light elements in the interstellar medium relative to the solar system is not real, but rather is the result of accretion onto interstellar grains or concentration in molecules (Reeves, 1974; Boesgaard et al., 1974; Field, 1974). Light element nuclei which are present in the interstellar medium in these forms would not have been observed in the measurements quoted in Table 4.

The cosmic ray abundances of lithium, beryllium and boron are much higher than those in any other astrophysical environment. This is usually explained in terms of the GCR nucleosynthesis of these elements as will be discussed in

more detail in the next chapter.

In order to understand the creation process or processes responsible for the light elements, it would be useful to know their abundances in the various astrophysical environments. Although the solar system lithium and beryllium abundances seem to be established, the boron abundance is less certain. For the reasons discussed earlier, abundances in the interstellar medium should probably also be considered unknown and, thus, should not be used to place stringent constraints on models of light element nucleosynthesis.

In the next chapter, solar system abundances of the light elements will be compared with the predictions of the GCR model for light element nucleosynthesis. Other possible mechanisms for the creation of these elements will also be considered. Attention will be given to uncertainties in both the experimental data and the theoretical calculations.

## V. Nucleosynthesis of the Light Elements

The most widely accepted model for the nucleosynthesis of the light elements is the galactic cosmic ray (GCR) model proposed by Reeves et al. (1970) and expanded upon by many authors (Meneguzzi et al., 1971; Mitler, 1972; Reeves, 1974). In this chapter, the GCR model as presented by Meneguzzi et al. will be summarized and its predictions compared with the experimental data discussed in the previous chapter. The possibility of other contributions to the light element abundances will be considered and experiments will be suggested which could support or reject such contributions.

### A. The Galactic Cosmic Ray Model

The basic hypothesis of the GCR model is that the light element nuclei were produced by spallation reactions between galactic cosmic rays and the interstellar medium. Lithium, beryllium and boron nuclei which were stopped in the interstellar medium contributed to the solar system abundances for these elements while light element nuclei created with high energies are responsible for the relatively high abundances of these elements in cosmic rays.

In order to calculate the solar system abundances for the light elements, it is necessary to consider both creation and destruction processes for these elements. In the GCR model, a given nucleus of a given energy may be

produced in several ways. It may be the product of a reaction between galactic cosmic rays and the interstellar medium or it may be the daughter nucleus of an unstable isotope such as  $^{10}\text{Be}$ . It may also be part of an "injection spectrum" of cosmic rays from an unspecified source. In addition, a nucleus of higher energy may be slowed down to the appropriate energy. These nuclei may also be destroyed in a variety of ways. They may themselves undergo nuclear reactions. They may decay or escape from the galaxy. Finally, they may be slowed down below the appropriate energy.

Most of the processes mentioned above were included by Meneguzzi et al. in a diffusion equation for the abundance of a nucleus  $i$  having energy  $E$  per nucleon:

$$\frac{\partial N_i(E)}{\partial t} = -\frac{N_i(E)}{\tau_e} - \frac{N_i(E)}{\gamma\tau_i} + Q_i(E) + \frac{\partial}{\partial E} \left\{ -\left(\frac{\partial E}{\partial t}\right)_{i,E} N_i(E) \right\} + \sum_{j,k} n_j \int_0^\infty \left\{ N_k(E') v_k \sigma_{jki}(E',E) - N_i(E) v_i \sigma_{jik}(E,E') \right\} dE'. \quad (\text{V-1})$$

In this equation,  $N_i$  is the number of nuclei  $i$  per unit volume having an energy per nucleon between  $E$  and  $E + dE$ .  $\tau_e$  is the mean lifetime for escape from the galaxy,  $\tau_i$  is the mean decay time for a stationary nucleus  $i$  and  $Q_i(E)$  is the injection spectrum for that nucleus.  $(-\partial E/\partial t)$  is the rate of energy loss for the appropriate nucleus and  $\sigma_{jki}(E',E)$  is the cross section for the production of a

nucleus  $i$  with energy  $E$  per nucleon in a reaction between nuclei  $j$  and  $k$  where  $j$  is stationary and  $k$  has energy  $E'$  per nucleon and velocity  $v_k$ . Finally,  $n_j$  is the density of nuclei  $j$  in the interstellar medium.

In solving equation V-1, Meneguzzi et al. made several assumptions. It was assumed that the cosmic ray flux was in equilibrium. That is,  $\frac{\partial N_i(E)}{\partial t} = 0$ . It was also necessary to select an injection spectrum  $Q_i(E)$ . Several possibilities were considered, but a spectrum of the shape  $W^{-2.6}$  was suggested to be most appropriate where  $W$  is the total energy per nucleon of the cosmic ray nuclei. Chemical abundances in the injection spectrum were based on experimental data and lithium, beryllium and boron were assumed to be absent from the source. Although  $N_i(E)$  was calculated for all isotopes up to  $^{56}\text{Fe}$ , positive contributions due to spallation reactions were neglected for all nuclei having  $A > 15$ . In addition, only reactions involving at least one hydrogen or helium nucleus were considered. Finally, the cross sections  $\sigma_{jki}(E',E)$  were assumed to satisfy:

$$\sigma_{jki}(E',E) = \begin{cases} \sigma_{jki}(E') \delta(E-0) & \text{for } k = \text{protons or alphas} \\ & j = \text{heavier nuclei} \\ \sigma_{jki}(E') \delta(E-E') & k = \text{heavier nuclei} \\ & j = \text{protons or alphas} \\ \sigma_{jki}(E') \delta(E-E'/4) & k = j = \text{alphas} \end{cases}$$

The escape range  $\Lambda_e = v\tau_e$  was calculated from the

observed ratio of light elements to CNO nuclei at high energies in space. Using equation V-1, Meneguzzi et al. found  $\Lambda_e = 6.4 \text{ gm/cm}^2$ . This value was then assumed to be independent of energy.

Solution of equation V-1 gives the cosmic ray abundances of the light elements rather than the abundances in the interstellar medium. Contributions to the interstellar abundances arise primarily from two sources: Cosmic ray lithium, beryllium and boron nuclei are slowed to thermal energies and heavy nuclei in the interstellar medium are spalled by fast protons and alphas. These contributions are included in an equation for the rate of production of the light element nuclei:

$$\frac{\partial n_i}{\partial t} = N_i(E_0) \left( -\frac{\partial E}{\partial t} \right)_{i,E_0} + \sum_j n_j \int_0^\infty \left\{ \sigma_{j\beta i}(E') \phi_\beta(E') + \sigma_{j\alpha i}(E') \phi_\alpha(E') \right\} dE' \quad (V-2)$$

where  $E_0$  is a threshold energy below which particles may be considered thermalized. There should probably be a term in equation V-2 (as well as equation V-1) corresponding to the creation of nuclei by the decay of other nuclei although such a term was not included by Meneguzzi et al.

The value for  $E_0$  used by Meneguzzi et al. was 1 MeV/nucleon. This is clearly too high to be considered thermal. However, for the light elements, it can be shown that

$$\frac{\partial}{\partial E} \left\{ -\left( \frac{\partial E}{\partial t} \right)_{i,E} N_i(E) \right\} \approx 0$$

below energies of a few MeV per nucleon. Thus, the first term in equation V-2 is constant for  $E_0$  below these energies and may be evaluated at any low energy.

Since the creation rate given by equation V-2 is assumed to be time-independent, light element abundances in the interstellar medium may be calculated by multiplying this rate by the time throughout which creation has been occurring. Meneguzzi et al. estimated this time by equating the calculated Be/H ratio to an observed value of  $2 \times 10^{-11}$  and obtained a time of approximately  $10^{10}$  years.

#### B. Comparison of GCR Model Predictions with Observations

As mentioned above, the calculation of light element abundances in the GCR model requires knowledge of the length of time throughout which this process has been occurring. Since the abundance ratios do not require this information, this seems to be a more reasonable way to compare theoretical predictions with experimental observations of light element abundances.

Table 5 shows the experimental and theoretical abundance ratios.  ${}^7\text{Li}$  has been excluded from the table since it is generally agreed that most  ${}^7\text{Li}$  is created in processes other than cosmic ray spallation reactions. Three sets of experimental abundance ratios are given. In determining these ratios, the  ${}^6\text{Li}$  abundance was assumed to

be given by the meteoritic value for this nucleus. The two sets of solar abundance ratios, Solar 1 and Solar 2, correspond to the different B/H values obtained in the measurements of Hall and Engvöld (1975) and Kohl et al. (1977), respectively. The isotopic ratios used in calculating the observed nuclear abundances are the meteoritic values:  $^{11}\text{B}/^{10}\text{B} = 4.0 \pm 0.1$  (Shima, 1963) and  $^7\text{Li}/^6\text{Li} = 12.5 \pm 1.3$  (Bernas et al., 1968). The boron isotopic ratio has not been measured in the solar photosphere, but is expected to agree with the meteoritic value. Such measurements for lithium are irrelevant to this discussion since the meteoritic lithium abundance is assumed to be the correct solar system value. Finally, the last two sets of theoretical ratios given in Table 5 refer to calculations which will be discussed later in this chapter.

Although the agreement of the GCR ratios with experimental observations is not perfect for any set of data, the most significant discrepancy is that between the observed isotopic ratio for boron and the value predicted by the GCR model. The predicted ratios are uncertain due to errors in the cross sections used for calculating these values, but it is unlikely that this would account for the discrepancy between the observed boron isotopic ratio and that predicted by this model. Considering the cosmic ray

spectrum used in the GCR calculations, uncertainties of about 25% are expected based on results of similar calculations described in the appendix to this thesis. Although the GCR calculated ratios for  ${}^6\text{Li}$  and  ${}^9\text{Be}$  seem to be in reasonable agreement with at least one set of experimental data (Solar 2), the disagreement with the measured boron ratio suggests that significant amounts of the light elements may have been produced either by processes other than galactic cosmic ray interactions with the interstellar medium or by a cosmic ray spectrum which differs significantly from that of Meneguzzi et al.

### C. Other Possibilities for Light Element Nucleosynthesis

The injection spectrum,  $Q_i(E)$ , used by Meneguzzi et al. results in a cosmic ray flux,  $N_i(E)v_i$ , which has its maximum at  $E \approx 150$  MeV per nucleon and which drops off rapidly as the energy is decreased further. Since the spallation production rate of  ${}^{11}\text{B}$  compared to  ${}^{10}\text{B}$  is higher for incident energies below 100 MeV per nucleon, it seems reasonable to consider the possibility that substantial numbers of light element nuclei were produced by irradiation of either the interstellar medium or solar material by a flux of such low energy particles. Three such scenarios have been considered, all involving a particle flux of the form

$$\phi_i(E) = N_i(E)v_i = \phi_i E^{-a} \quad (V-3)$$

where  $E$  is the kinetic energy per nucleon of the incident particles. For each scenario, abundance ratios were calculated as described in the appendix. Since the experimental cross sections used in these calculations have large uncertainties, "exact" ratios will not be presented. Rather, the abundance ratios are expected to lie within a given range of values.

Due to solar modulation of the galactic cosmic ray spectrum, it is impossible to determine its spectral shape at energies below 100-200 MeV per nucleon. The injection spectrum,  $Q_i(E)$ , used by Meneguzzi et al. was chosen to reproduce the observed cosmic ray spectrum at high energies (above 500 MeV per nucleon) and was assumed to apply at low energies as well. However, a spectrum of the form indicated in equation V-3 would not necessarily be detected if it existed and cannot be refuted on the basis of the cosmic ray data. Such a spectrum would result in the light element abundance ratios shown in Figure 7 as a function of the exponent,  $a$ . As indicated in Table 5, for  $a = 1.8$ , the experimental data, Solar 2, are reproduced within errors. It does not appear possible, however, to reproduce either the Solar 1 or meteoritic data in this environment.

Low energy proton irradiation of solar gas or dust has been proposed (Lee et al., 1976; Heymann and Dziczkaniec, 1976) as a possible explanation for some of the isotopic

anomalies observed in meteorites. In particular, such a process might explain the  $^{26}\text{Al}$  anomalies observed in some Allende inclusions. If this proton irradiation were widespread, it would be expected to contribute significantly to the solar system abundances of lithium, beryllium and boron. If the proton spectral shape is assumed to be given by equation V-3, the resulting light element abundance ratios would be as shown in Figures 8 and 9 as a function of the exponent,  $a$ . It is seen from Figure 8 that, for  $a = 2.25$ , both the meteoritic and Solar 2 data are reproduced by proton irradiation of a gas of solar composition. It does not appear possible to reproduce the Solar 1 data by proton irradiation of either solar gas or solar dust due to the high experimental  $^6\text{Li}/^{10}\text{B}$  ratio.

It is unlikely that the light elements were created entirely by low energy processes. A more reasonable possibility is that the observed abundances are the result of spallation reactions involving both the high energy GCR spectrum suggested by Meneguzzi et al. and a low energy spectrum such as those described here. Given the uncertainties in the experimental and theoretical abundance ratios, it is impossible to determine unambiguously what fraction of the light elements were created by each process. However, some conclusions can be drawn from Figures 7-9 and from the results of Meneguzzi et al. For example, the

${}^6\text{Li}/{}^{10}\text{B}$  ratio of the Solar 1 experimental data is too large to be reproduced by a mixture of light elements produced with the GCR model and those produced in any of the low energy irradiations suggested above. Light elements produced by proton irradiation of solar dust cannot be combined, alone, with GCR light elements because the observed  ${}^{11}\text{B}/{}^{10}\text{B}$  ratio cannot be obtained. However, it appears that both the Solar 2 and meteoritic data can be reproduced by appropriate mixtures of light elements produced with the cosmic ray spectrum of Meneguzzi et al. and those produced either by a low energy cosmic ray spectrum or by proton irradiation of solar gas.

It is more difficult to reproduce the Solar 1 experimental data. The GCR model alone already over-produces  ${}^{10}\text{B}$  by a factor of 3-4 for this data set. This problem may be solved by assuming that the time throughout which creation took place was only  $<4 \times 10^9$  years instead of  $10^{10}$  years as suggested by Meneguzzi et al. However, the large  ${}^6\text{Li}/{}^{10}\text{B}$  ratio also presents a problem. The only obvious way to obtain such a high value is with a large flux of low energy alpha particles. Irradiation of material of solar composition would then produce large amounts of  ${}^6\text{Li}$  relative to other elements because of the  $\alpha + \alpha$  reaction and the relative abundance of  ${}^4\text{He}$  compared to CNO. The observed ratios might be reproduced by irradiation of solar material

with a low energy particle flux containing both protons and alpha particles.

#### D. Possible Tests of Low-Energy Spallation Models

Current light element abundance data and theoretical calculations are not accurate enough to permit us to choose between (or reject entirely) the proposed irradiation scenarios on the basis of the abundance data alone. However, light element production would probably not be the only observable effect of such low energy irradiations. It is likely that constraints could be placed on the irradiation process by consideration of other expected consequences of such an irradiation.

One of the anticipated effects of a low-energy flux of galactic cosmic rays is heating of the interstellar medium. This heating should be observed as ionization of interstellar hydrogen. The ionization rate could be used to set an upper limit on the flux of low energy particles and, thus, would limit the production rate of the light elements by such a spectrum.

Ionization of interstellar hydrogen has been observed and ionization rates have been calculated. The rate calculated by Field et al. (1969) of  $\zeta_H = 4 \times 10^{-16} \text{ sec}^{-1}$  could place important constraints on the number of light element nuclei which could be produced by a low energy cosmic ray spectrum. However, another calculation

(Hjellming et al., 1969) gives  $\zeta_H = 2 \times 10^{-15} \text{ sec}^{-1}$ . This ionization rate would probably permit a low energy flux large enough to create the observed meteoritic boron abundance and, thus, does not constrain this model.

If significant amounts of the light element nuclei were produced by proton irradiation of solar gas, other important consequences would be expected. Since the irradiation is assumed to have occurred near the time of condensation of the solar system, large quantities of  $^{10}\text{Be}$  ( $t_{\frac{1}{2}} = 2.5 \times 10^6$  years) would still have been present when condensation occurred. This isotope would have condensed in patterns characteristic of beryllium rather than boron and then would have decayed in situ. Since beryllium is a refractory element while boron is considered to have been moderately volatile under the conditions of solar condensation, it is likely that boron would have been excluded from high temperature condensates while beryllium, including  $^{10}\text{Be}$ , would be undepleted. Thus, this material would be expected to exhibit observable boron isotopic anomalies today.

Although no search has been made for boron isotopic anomalies, an upper limit of  $10^{16}$  atoms/gm has been found for the  $^{10}\text{B}$  content (and thus the original  $^{10}\text{Be}$  content) of some Ca-Al-rich Allende inclusions (Weller et al., 1978). For a Ca-Al-rich inclusion containing 20% Al (Grossman,

1975) and having  $^{26}\text{Al}/^{27}\text{Al} = 6 \times 10^{-5}$  initially (Lee et al., 1976), this would correspond to  $(^{10}\text{B} + ^{10}\text{Be})/^{26}\text{Al} \leq 3 \times 10^{-2}$  at the time of formation of the inclusion. If it is assumed that condensation occurred shortly after the irradiation and that neither Be nor Al were fractionated in these inclusions, some constraints may be placed on the shape of the proton spectrum. Assuming that boron was depleted in these inclusions,  $^{10}\text{Be}/^{26}\text{Al}$  ratios were calculated as a function of the exponent,  $a$ , in equation V-3. As illustrated in Figure 10, for irradiation of solar gas,  $a$  must be greater than 2.5 while, for irradiation of solar dust,  $a$  may be as small as 1.2.

The above discussion places very crude limits on the spectral shape allowed for a proton irradiation of solar material. However, the  $^{10}\text{Be}/^{26}\text{Al}$  upper limit discussed above is only applicable to a few Allende inclusions so far, and boron isotopic measurements on these inclusions would obviously be more useful. However, the existence of boron isotopic anomalies in these inclusions would not necessarily indicate a widespread proton irradiation. If the proton irradiation responsible for the  $^{26}\text{Al}$  affected the solar system as a whole, boron isotopic anomalies would also be expected in high temperature condensates contained in other meteorites. If these anomalies are not found, it would seem unlikely that significant amounts of lithium, beryllium

or boron could have been produced by proton irradiation of solar gas near the time of solar system condensation.

In addition to the anticipated boron anomalies, a proton irradiation of solar system material would result in anomalies for several other elements as discussed by Clayton et al. (1977). These anomalies have not been found and this may indicate that such a proton irradiation could not have occurred. However, the question is very much unresolved at the present time.

## VI. Conclusions

With this measurement of boron concentrations in carbonaceous chondrites, the uncertainty in the solar system boron abundance has been reduced by an order of magnitude. However, the discrepancy between the solar photospheric and meteoritic boron abundance is still at least a factor of five and may be larger if the upper limit of Hall and Engvöld (1975) is the correct solar value. It is not clear whether the meteoritic or photospheric abundance should be accepted as the solar system abundance for this element.

Although the solar system boron abundance remains uncertain, some statements can still be made about the creation of the light elements. Substantial fractions of the lithium, beryllium and boron abundances were probably produced according to the galactic cosmic ray model of Meneguzzi et al. (1971). However, this model does not reproduce the observed  $^{11}\text{B}/^{10}\text{B}$  ratio. Although the low energy calculations discussed in Appendix B are different from those of Meneguzzi et al., the errors involved in the two calculations should be comparable. These errors are not large enough to account for the difference between the observed  $^{11}\text{B}/^{10}\text{B}$  ratio and that calculated by Meneguzzi et al. In order to obtain the observed ratio, it is necessary to include contributions to the light element abundances due to

a spectrum of relatively low energy particles. A low energy cosmic ray component could probably reproduce the solar photospheric abundances if the boron concentration of Kohl et al.(1977) is accepted. These abundances as well as the meteoritic data may also be obtained by proton irradiation of solar gas. If the solar photospheric abundance of Hall and Engvold is accepted, a large flux of low energy alpha particles would be required to explain the high implied  ${}^6\text{Li}/{}^{10}\text{B}$  ratio.

It is difficult to make strong statements about the processes responsible for the solar system boron abundance when that abundance is still not well established. Although information about the shape of the galactic cosmic ray spectrum at low energies and about possible boron isotopic anomalies in meteorites might be useful in understanding the light element abundances, this does not seem to be the most important question. A discrepancy exists between the meteoritic and photospheric boron abundances and this discrepancy must be understood in terms of reasonable physical processes. When this issue is resolved, we may know how much boron there really is. That information is necessary if we expect to understand the processes responsible for the light element abundances.

Appendix A - Calculation of Boron Concentrations

In Section II-B, the procedure was briefly discussed for extracting boron concentrations from the data obtained from  $^{12}\text{B}$  activation analysis of a sample. In order to determine boron concentrations from the count yields,  $Y_i$ , of the four scalers, it was necessary first to distinguish between counts from  $^{12}\text{B}$  and counts from other background reactions. Once the yield,  $Y_B$ , due to  $^{12}\text{B}$  was obtained, the boron concentration could be calculated using the equation

$$\frac{Y_B}{f} = \left(\frac{Q}{e}\right) \left(\frac{n(\text{B})}{n(^{11}\text{B})} \frac{1}{m(^{11}\text{B})}\right) \left[ \int_0^{E_{\max}} \frac{\sigma(E)dE}{(-dE/d(\rho x))} \right] \quad (\text{A-1})$$

where  $(Q/e)$  is the number of incident deuterons,  $n(\text{B})$  and  $n(^{11}\text{B})$  are the mass fractions of total boron and  $^{11}\text{B}$ , respectively, in the sample and  $m(^{11}\text{B})$  is the atomic mass of  $^{11}\text{B}$ .  $\sigma(E)$  is the  $^{11}\text{B}(d,p)^{12}\text{B}$  reaction cross section and  $(-dE/d(\rho x))$  is the stopping power of the sample for deuterons.  $E_{\max}$  is the deuteron energy as it enters the sample. Finally,  $f$  is the fraction of betas from  $^{12}\text{B}$  which are actually counted.

Rather than using equation A-1, it was simpler to obtain boron concentrations for the meteoritic samples by comparing the  $^{12}\text{B}$  yields with those from NBS standard glass samples containing a known amount of boron. Then, from equation A-1,

$$\frac{n_{\text{met}}(\text{B})}{n_{\text{NBS}}(\text{B})} = \left(\frac{Y_B^{\text{met}}}{Y_B^{\text{NBS}}}\right) \left(\frac{f_{\text{NBS}}}{f_{\text{met}}}\right) \left(\frac{Q_{\text{NBS}}}{Q_{\text{met}}}\right) \left(\frac{R_{\text{NBS}}}{R_{\text{met}}}\right) \left(\frac{I_{\text{NBS}}}{I_{\text{met}}}\right). \quad (\text{A-2})$$

In this equation,  $R = n(^{11}\text{B})/n(\text{B})$  and  $I = \int_0^{E_{\max}} \frac{\sigma(E)dE}{(-dE/d(\rho x))}$ .

Most of the ratios in equation A-2 may be determined easily.  $Q_{\text{NBS}}$  and  $Q_{\text{met}}$  were measured directly during the  $^{12}\text{B}$  activation analysis. Since the boron isotopic ratio is assumed to be the same for meteorites and for terrestrial samples, the ratio ( $R_{\text{NBS}}/R_{\text{met}}$ ) is unity. The procedure for obtaining  $Y_{\text{B}}^{\text{met}}$  and  $Y_{\text{B}}^{\text{NBS}}$  from the count yields,  $Y_i$ , is straight-forward and will be discussed in detail later in this appendix. The two remaining ratios are obtained less easily and will also be discussed in detail. When all of the ratios in equation A-2 are determined, the meteoritic boron concentrations can be obtained from the known concentration in the NBS standard.

### 1. Extraction of $^{12}\text{B}$ Yield from Background

For a system consisting of two beta emitters, x and y, it is possible to determine the number,  $N_i$ , of each isotope present at  $t = 0$  by counting for two consecutive time periods. If the first period begins at  $t = 0$  and each period lasts for a time T, then

$$N_x = \frac{Y_1 - Y_2 e^{T/\tau_y}}{(1 - e^{-T/\tau_x})(1 - e^{-T/\tau_x} e^{T/\tau_y})} \quad (\text{A-3})$$

where  $Y_1$  and  $Y_2$  are the total number of betas counted in each of the two periods.  $\tau_x$  and  $\tau_y$  are the mean lives of the beta emitters x and y, respectively.

Equations similar to equation A-3 may be used to obtain the  $^{12}\text{B}$  yields,  $Y_{\text{B}}^{\text{met}}$  and  $Y_{\text{B}}^{\text{NBS}}$ . As discussed in Section II-B, there were two major background reactions which contributed to the count yields,  $Y_i$ , of each of the four scalers. For meteoritic samples, the counts were assumed to arise only from the decays of  $^{12}\text{B}$  ( $\tau = 29.4$  msec) and  $^{16}\text{N}$  ( $\tau = 10.4$  sec) while, for the NBS glass, the counts were assumed to be due to  $^{12}\text{B}$  and  $^8\text{Li}$  ( $\tau = 1.21$  sec) decays. Although there were actually four 15 msec counting periods for these measurements, these periods were combined into two 30 msec periods for the purpose of data analysis. Thus, for our analyses, the expressions corresponding to equation A-3 were

$$Y_{\text{B}}^{\text{met}} = \frac{(Y_1 + Y_2) - 1.0029 (Y_3 + Y_4)}{0.4084} \quad (\text{A-4})$$

and

$$Y_{\text{B}}^{\text{NBS}} = \frac{(Y_1 + Y_2) - 1.0251 (Y_3 + Y_4)}{0.4032} \quad (\text{A-5})$$

for meteorite and NBS glass analyses, respectively.

## 2. Effects of Deuteron Energy Loss

The ratio ( $I_{\text{NBS}}/I_{\text{met}}$ ) in equation A-2 differs from unity only because the energy loss of the deuterons is different in the meteorites and the NBS glass samples. In order to determine this ratio, the stopping power for the deuterons was calculated as a function of energy for the different types of meteorites and for the NBS glass. The integrals,  $I_{\text{NBS}}$  and  $I_{\text{met}}$ , were then performed numerically.

For a material composed of several different elements, the stopping power is given by

$$\frac{dE}{d(\rho x)} = \sum_i n_i \left( \frac{dE}{d(\rho x)} \right)_i$$

where  $n_i$  is the mass fraction of element  $i$  in the sample and  $(dE/d(\rho x))_i$  is the stopping power in the element  $i$ . Table 6 shows the elemental compositions used for calculating  $dE/d(\rho x)$  for the various samples. Electronic stopping powers were obtained from Northcliffe and Schilling (1970). (Nuclear stopping is not important for the evaluation of  $I_{NBS}$  and  $I_{met}$ .)

Table 6 also shows the values of the integrals,  $I_{NBS}$  and  $I_{met}$ , for the various samples. Even in the worst case, the ratio,  $(I_{NBS}/I_{met})$ , differs from unity by only a few percent.

### 3. Effects of Beta Energy Loss

The quantities  $f_{NBS}$  and  $f_{met}$  in equation A-2 are influenced by many conditions including, among others, the solid angle subtended by the detector, the energy window on the single channel analyzer (SCA) and the counting cycle. However, most of these conditions are the same for both the meteorites and the NBS standards. As a result, the ratio  $(f_{NBS}/f_{met})$  is influenced only by differences in beta energy loss between the two samples.

Since the betas emitted in the  $^{12}B$  decays must pass through the sample to reach the detector, the pulses entering

the SCA will have different pulse height distributions corresponding to differences in beta energy loss for different samples. Thus, different fractions of the total beta spectrum may be accepted. The total energy lost by an electron passing through a sample is determined by two sample characteristics: its composition and its thickness. For these measurements, the beta energies were high enough that the electronic stopping power did not depend on the sample composition. Fortunately, the targets were composed primarily of light elements so that ionization losses dominated the total energy loss. Thus, for these samples, the ratio  $(f_{\text{NBS}}/f_{\text{met}})$  was a function only of the quantities  $(\rho d)_{\text{NBS}}$  and  $(\rho d)_{\text{met}}$ .

The ratio  $(f_{\text{NBS}}/f_{\text{met}})$  is not easy to calculate, but could be determined experimentally. Several pieces of Pyrex glass (4% B) of varying thickness were analyzed using the  $^{12}\text{B}$  activation technique. Since the samples were of uniform composition, the count yields from the various samples were expected to be related by

$$Y_{\text{B}}^i = \left( \frac{f_i}{f_j} \right) Y_{\text{B}}^j.$$

The results of these analyses are shown in Figure 11. The  $^{12}\text{B}$  yields were shown to satisfy an equation of the form

$$Y_{\text{B}}(d) = e^{-A\rho d} Y_{\text{B}}(0)$$

where  $A = 1.45 \text{ cm}^2/\text{gm}$ . This result is expected to apply for

the meteorites and NBS samples as well. Thus,

$$\left(\frac{f_{\text{NBS}}}{f_{\text{met}}}\right) = \exp A[(\rho d)_{\text{met}} - (\rho d)_{\text{NBS}}]. \quad (\text{A-6})$$

For the samples used in these measurements, it was found that this ratio was not very sensitive to errors in A as long as A was the same for both meteoritic and standard samples. (A 15% change in the value of A caused only a 1-2 % change in most of the meteoritic B concentrations.) Target thicknesses were measured directly for all samples and average densities were also verified experimentally. Tables 7 and 8 give the values  $(\rho d)$  for all the meteorites and standard samples which were analyzed. The error in the ratio  $(f_{\text{NBS}}/f_{\text{met}})$  is expected to be less than 5% for all of the meteorite analyses.

#### 4. Determination of $n_{\text{NBS}}(\text{B})$

In order to determine meteoritic boron concentrations from equation A-2, it was necessary to verify the boron concentrations for the NBS standards. This was done by comparing the NBS glass samples with Pyrex glass which has a uniform and well-controlled boron concentration. Boron concentrations obtained in this way are shown in Table 7 for all of the NBS samples which were used as standards.

It was also possible to verify the standard concentrations using equation A-1. Although the value of f in this equation was not precisely known, it could be estimated. The

resulting boron concentrations were consistent with those obtained by comparison with the Pyrex.

### 5. Meteoritic Boron Abundances

Meteoritic boron abundances may now be calculated from equation A-2. Table 7 shows the counts obtained in the different scalers for all analyses of NBS standards. Similarly, Table 8 shows the yields obtained from analyses of meteoritic samples. With the information in these tables and in Table 6, meteoritic boron concentrations can be obtained. These concentrations are shown in the last column of Table 8.

For nine of the analyses in Table 8, it was necessary to apply an additional correction to the data. Samples and standards were normally mounted in the target holder on clean tantalum disks to minimize contamination. After August 26, 1976, it was realized that two different thicknesses of tantalum had been used for several analyses. In seven cases, it was found that the tantalum thicknesses were different for the NBS standards and for the meteorite samples. To obtain the correct boron concentrations for these meteorites, it was necessary to include an additional correction factor of 0.8 in equation A-2. (This factor was determined experimentally by measurements similar to those performed to determine the thickness coefficient, A.) For the samples Murchison 9 and Allende 1C, it was uncertain whether this correction was

necessary. The correction was made, but the uncertainty is reflected in the errors for these two samples. All of the other errors quoted in the table include only statistics.

## Appendix B - Calculation of Light Element Abundance Ratios

In recent years, theoretical light element abundance ratios have been calculated by many authors in attempts to explain the observed abundance ratios. The results of another such calculation have been presented in Chapter V of this thesis. This appendix describes in detail the calculations which were performed in obtaining the results shown in Figures 7, 8, and 9 of that chapter.

For a given astrophysical environment, one expects that the light element nuclei may be produced or destroyed through a variety of mechanisms. For example, in the interaction of galactic cosmic rays with the interstellar medium, high energy protons and alpha particles may spall stationary heavy nuclei to produce relatively low energy light element nuclei which are then stopped in the interstellar medium. High energy light element nuclei may be produced by collisions of heavy-ion cosmic rays with hydrogen and helium in the interstellar medium. These high energy nuclei may then be destroyed by further spallation reactions or they may be stopped in the interstellar medium. They may also "leak out" of the galaxy. Obviously, stationary light elements may also be destroyed through spallation reactions.

The most accurate calculations of the light element abundance ratios include all of these creation and

destruction processes. Such a calculation was performed by Meneguzzi et al. (1971): Cosmic ray source spectra and interstellar abundances were chosen, the relevant spallation cross sections were estimated and diffusion equations were solved for each of the light elements. The light element abundance ratios could then be calculated.

In the calculations described here, a much simpler procedure was followed. Approximations have been made concerning many of the creation and destruction processes mentioned earlier. However, it will be argued that, for the conditions considered in these calculations, these approximations are appropriate.

The creation rate per unit volume for light elements of mass  $A$  and energy  $E_f$  per nucleon is given by

$$\dot{N}_A^c(E_f) = \sum_{i,j} n_j \int_0^\infty \phi_i(E) \sigma_{jiA}(E, E_f) dE \quad (B-1)$$

where  $n_j$  is the number density of stationary nuclei  $j$  and  $\phi_i(E)$  is the flux of nuclei  $i$  having energy  $E$  per nucleon. In these calculations,  $\phi_i(E)$  is assumed to be of the form  $\phi_i E^{-a}$ . Finally,  $\sigma_{jiA}(E, E_f)$  is the cross section for producing nuclei of mass  $A$  and energy  $E_f$  per nucleon in a spallation reaction with nucleus  $i$  incident on nucleus  $j$  at an energy  $E$  per nucleon.

Equation B-1 is not sufficient by itself to permit calculation of the light element abundance ratios. Nuclei

produced with high energies contribute to the cosmic ray abundances rather than the solar system or interstellar medium abundances. Equation B-1 also does not allow for destruction or loss of light element nuclei. Additional assumptions must be made and equation B-1 must be modified before light element abundances can be calculated.

In general, the cross sections  $\sigma_{jiA}(E, E_f)$  are not known. Instead, the quantity which is usually measured is

$$\sigma_{jiA}(E) = \int_0^{\infty} \sigma_{jiA}(E, E_f) dE_f .$$

To determine  $\dot{N}_A^C(E_f)$ , it is necessary to make some assumptions about the relationship between  $\sigma_{jiA}(E)$  and  $\sigma_{jiA}(E, E_f)$ . In these calculations, spallation reactions were considered for cosmic ray protons and alphas on stationary carbon, nitrogen and oxygen (CNO), for cosmic ray CNO on stationary hydrogen and helium, and for cosmic ray alphas on stationary helium. It was assumed that, for protons and alphas of any energy on stationary CNO, the product nuclei had low energies. For spallation reactions between cosmic ray CNO and stationary hydrogen or helium, it was assumed that the product nuclei had an energy per nucleon equivalent to that of the incident particle. For the case of cosmic ray alphas on stationary helium, it is clear that neither of these extremes is valid. However, since the cross section for the production of the light

element nuclei is significant only at low energies (Figure 32), and since the reactions are endoergic, it is clear that only low energy nuclei will be produced.

As mentioned earlier, only nuclei which are stopped will contribute to solar system abundances and some nuclei may be destroyed or lost before they are stopped. It can be shown that, for nuclei created with energies below 200 MeV per nucleon, most light elements will be stopped before they are lost or destroyed while for creation energies above 300 MeV per nucleon, the path length for destruction or loss is much smaller than that for stopping. Thus, these nuclei do not contribute to the solar system abundances. In the energy region between 200 MeV per nucleon and 300 MeV per nucleon, the situation is obviously more complicated. However, for a flux of the form  $E^{-a}$  and with the assumptions which have already been made about the energies of the product nuclei, the contributions to the light element abundances are negligible for nuclei created in this energy region.

These assumptions may be summarized in an equation for the rate of production,  $\dot{n}_A$ , of light element nuclei of mass A which contribute to the solar system abundances:

$$\begin{aligned} \dot{n}_A = & \sum_{i=p,\alpha} \sum_{\substack{j=He, \\ CNO}} n_j \phi_i \int_0^{\infty} E^{-a} \sigma_{jiA}(E) dE \\ & + \sum_{i=CNO} \sum_{\substack{j=H, \\ He}} n_j \phi_i \int_0^{200 \text{ MeV/n}} E^{-a} \sigma_{jiA}(E) dE. \end{aligned} \quad (B-2)$$

It is generally assumed that the fluxes  $\phi_i$  and abundances  $n_j$  are independent of time so that  $\dot{n}_A$  is directly proportional to  $n_A$ . Alternatively,  $n_j$  may be considered to be a time-averaged density and  $\phi_i$  an integrated flux or fluence. Then,  $\dot{n}_A$  may be replaced by  $n_A$  in equation B-2 and the light element abundance ratios may be calculated.

In these calculations, three possible scenarios were considered for the creation of the light elements: proton irradiation of a gas of solar composition, proton irradiation of solar dust, and interaction of a low energy component of galactic cosmic rays with the interstellar medium. The abundances  $n_j$  and the fluxes  $\phi_i$  used for each calculation are shown in Table 9.

One of the major difficulties in calculating light element abundance ratios is that the relevant cross sections  $\sigma_{jiA}(E)$  are either not well known or not measured at all. Comparisons of recently measured cross sections with theoretical estimates used in previous calculations do not inspire confidence in the theoretical estimates. Thus, in comparing calculated abundance ratios with the observed values, it is important to consider the uncertainties in the calculations as well as those in the observed ratios. In these calculations, an attempt has been made to estimate the uncertainties in the calculated ratios.

The cross sections which were used in obtaining the

results of Figures 7, 8, and 9 are shown in Figures 11-31. Typical errors are shown for experimental data for all measurements where the errors were reported. Maximum and minimum values,  $I_{ij}^{A+}$  and  $I_{ij}^{A-}$ , were calculated for the integrals in equation A-2 by taking the dotted lines in the figures as upper and lower limits, respectively, for the appropriate cross sections. It should be noted that cross-section measurements do not exist for spallation reactions involving alpha particles on oxygen nuclei. In previous calculations of light element abundances, it has been assumed that these cross sections were the same as those for alpha particles on carbon nuclei. The same assumption was made here. Finally, all cross sections were assumed to be constant for energies above 1 GeV per nucleon.

Once the integrals  $I_{ij}^{A+}$  and  $I_{ij}^{A-}$  were calculated, average creation rates and errors were calculated using the following formulae:

$$\dot{n}_A = \sum_{i=p,\alpha} \sum_{\substack{j=He, \\ CNO}} n_j \phi_i \left( \frac{I_{ij}^{A+} + I_{ij}^{A-}}{2} \right) + \sum_{i=CNO} \sum_{\substack{j=H, \\ He}} n_j \phi_i \left( \frac{I_{ij}^{A+} + I_{ij}^{A-}}{2} \right) \quad (A-3)$$

and

$$\begin{aligned} (\Delta \dot{n}_A)^2 = & \sum_{i=p,\alpha} \sum_{\substack{j=CNO, \\ He}} n_j^2 \phi_i^2 \left( \frac{I_{ij}^{A+} - I_{ij}^{A-}}{2} \right)^2 \\ & + \sum_{i=CNO} \sum_{\substack{j=H, \\ He}} n_j^2 \phi_i^2 \left( \frac{I_{ij}^{A+} - I_{ij}^{A-}}{2} \right)^2. \end{aligned} \quad (A-4)$$

Table 10 shows the average creation rates obtained from the low energy GCR spectra for several values of  $a$ . In this table, the contributions due to cosmic ray CNO and cosmic ray protons and alphas are also indicated separately. As indicated earlier, it was assumed that  $n_A$  is directly proportional to  $\dot{n}_A$ . Thus, abundance ratios were obtained from creation rate ratios and errors in the abundance ratios were calculated according to

$$\Delta\left(\frac{n_A}{n_{A'}}\right) = \left(\frac{n_A}{n_{A'}}\right) \left\{ \left(\frac{\Delta\dot{n}_A}{\dot{n}_A}\right)^2 + \left(\frac{\Delta\dot{n}_{A'}}{\dot{n}_{A'}}\right)^2 \right\}^{1/2}. \quad (B-5)$$

These calculations were performed for values of  $a$  between 1.5 and 5.5.

In Figures 7, 8, and 9, the average abundance ratios,  $(n_A/n_{10})_{ave}$ , have not been plotted. Instead, to emphasize the uncertainties in these ratios, bands have been plotted for each ratio,  $(n_A/n_{10})$ , with boundaries corresponding to

$$\left(\frac{n_A}{n_{10}}\right)_{ave} - \Delta\left(\frac{n_A}{n_{10}}\right) \leq \left(\frac{n_A}{n_{10}}\right) \leq \left(\frac{n_A}{n_{10}}\right)_{ave} + \Delta\left(\frac{n_A}{n_{10}}\right). \quad (B-6)$$

In light of the large uncertainties in the cross sections required for determining these ratios, it seems unreasonable to require that the observed abundance ratios be reproduced by the average calculated values for a given energy spectrum. A more reasonable condition is to require that, for a given energy spectrum, the observed abundance ratios lie within the bounds indicated by B-6.

REFERENCES

- Anders, E., 1971, *Geochim. Cosmochim. Acta* 35, 516.
- Anders, E., Higuchi, H., Ganapathy, R. and Morgan, J. W.,  
1976, *Geochim. Cosmochim. Acta* 40, 1131.
- Audouze, J., Lequeux, J. and Reeves, H., 1973, *Astron. and  
Astrophys.* 28, 85.
- Bernas, R., Epherre, M., Gradsztajn, E., Klapisch, R. and  
Yiou, F., 1965, *Phys. Letters* 15, 147.
- Bernas, R., Gradsztajn, E. and Yaniv, A., 1968, in  
Meteorite Research, ed. P. M. Millman (Reidel), p. 123.
- Bodansky, D., Jacobs, W. W. and Oberg, D. L., 1975, *Ap. J.*  
202, 222.
- Boesgaard, A. M., 1974, *Astron. and Astrophys.* 34, 9.
- Boesgaard, A. M., Praderie, F., Leckrone, D. S., Faraggiana,  
R. and Hack, M., 1974, *Ap. J. (Letters)* 194, L143.
- Boesgaard, A. M., 1976, *Ap. J.* 210, 466.
- Cameron, A. G. W., Colgate, S. A. and Grossman, L., 1973,  
*Nature* 243, 204.
- Chmielewski, Y., Müller, E. A. and Brault, J. W., 1975,  
*Astron. and Astrophys.* 42, 37.
- Clayton, D. D., Dwek, E. and Woosley, S. E., 1977, *Ap. J.*  
214, 300.
- Conti, P. S. and Danziger, I. J., 1966, *Ap. J.* 146, 383.
- Curtis, D. B., Gladney, E. S. and Journey, E. T., 1976,  
*Meteoritics* 11, 267.

- Curtis, D. B., 1978, private communication.
- Davids, C. N., Laumer, H. and Austin, S. M., 1970, Phys. Rev. C 1, 270.
- Epherre, M., 1972, Ph.D. Thesis, Univ. de Paris-Sud, Centre D'Orsay.
- Field, G. B., Goldsmith, D. W. and Habing, H. J., 1969, Ap. J. (Letters) 155, L149.
- Field, G. B., 1974, Ap. J. 187, 453.
- Fontes, P., Perron, C., Lestringuez, J., Yiou, F. and Bernas, R., 1971, Nucl. Phys. A165, 405.
- Fontes, P., 1975, Ph.D. Thesis, Univ. de Paris-Sud, Centre D'Orsay.
- Furst, M., Lowenstam, H. A. and Burnett, D. S., 1976, Geochim. Cosmochim. Acta 40, 1381.
- Furukawa, M., Shizuri, K., Komura, K., Sakamoto, K. and Tanaka, S., 1971, Nucl. Phys. A174, 539.
- Gladney, E. S., Journey, E. T. and Curtis, D. B., 1976, Anal. Chem. 48, 2139.
- Goldberg, R. H., Burnett, D. S., and Tombrello, T. A., 1975, Proc. Sixth Lunar Sci. Conf., Geochim. Cosmochim. Acta, Supl. 6, Vol. 2, 2189.
- Grevesse, N., 1968, Solar Physics 5, 159.
- Grossman, L., 1975, Geochim. Cosmochim. Acta 39, 433.
- Hall, D. N. B. and Engvöld, O., 1975, Ap. J. 197, 513.
- Harder, H., 1961, Nachr. Akad. Wiss. Math.-Phys. Göttingen 1, 1.

- Herbig, G. H., 1965, Ap. J. 141, 588.
- Heymann, D. and Dziczkaniec, M., 1976, Science 191, 79.
- Hjellming, R. M., Gordon, C. P. and Gordon, K. J., 1969,  
Astron. and Astrophys. 2, 202.
- Jacobs, W. W., Bodansky, D., Chamberlin, D. and Oberg, D. L.,  
1974, Phys. Rev. C 9, 2134.
- Jung, M., Jacquot, C., Baixeras-Aiguabella, C., Schmitt, R.  
and Braun, H., 1970, Phys. Rev. C 1, 435.
- Kavanagh, R. W. and Barnes, C. A., 1958, Phys. Rev. 112,  
503.
- King, C. H., Austin, S. M., Rossner, H. H. and Chien, W. S.,  
1977, Phys. Rev. C 16, 1712.
- Kohl, J. L., Parkinson, W. H. and Withbroe, G. W., 1977,  
Ap. J. (Letters) 212, L101.
- Larimer, J. W. and Anders, E., 1967, Geochim. Cosmochim.  
Acta 31, 1239.
- Laumer, H., Austin, S. M., Panggabean, L. M. and Davids,  
C. N., 1973, Phys. Rev. C 8, 483.
- Lee, T., Papanastassiou, D. A. and Wasserburg, G. J., 1976,  
Geophys. Res. Letters 3, 109.
- Leich, D. A., Goldberg, R. H., Burnett, D. S. and Tombrello,  
T. A., 1974, Proc. Fifth Lunar Sci. Conf., Geochim.  
Cosmochim. Acta, Suppl. 5, Vol. 2, 1869.
- Lestringuez, J., Raisbeck, G. M., Yiou, F. and Brnas, R.,  
1971, Phys. Lett. 36B, 331.

- Mathews, G. J., 1977, Ph.D. Thesis, University of Maryland.
- Meneguzzi, M., Audouze, J. and Reeves, H., 1971, *Astron. and Astrophys.* 15, 337.
- Mills, A.A., 1968, *Nature* 220, 1113.
- Mitler, H. E., 1972, *Astrophys. and Space Sci.* 17, 186.
- Moore, C. B., 1971, in Handbook of Elemental Abundances in Meteorites, ed. B. Mason (Gordon and Breach), p. 125.
- Morton, D. C., Smith, A. M. and Stecher, J. P., 1974, *Ap. J. (Letters)* 189, L109.
- Moyle, R. A., Glagola, B. G., Mathews, G. J. and Viola, V. E., 1978, University of Maryland preprint #ORO-5172-0007.
- Nichiporuk, W. and Moore, C. B., 1970, *Earth Planet. Sci. Lett.* 2, 280.
- Northcliffe, L. C. and Schilling, R. F., 1970, *Nuclear Data Tables* A7, 233.
- Quandt, U. and Herr, W., 1974, *Earth Planet. Sci. Lett.* 24, 53.
- Quijano-Rico, M. and Wanke, H., 1969, in Meteorite Research, ed. P. M. Millman (Reidel), p.132.
- Radin, J., 1970, *Phys. Rev. C* 2, 793.
- Radin, J., 1971, *Phys. Rev. C* 4, 1010.
- Raisbeck, G. M., Lestringuez, J. and Yiou, F., 1972, *Phys. Rev. C* 6, 685.
- Raisbeck, G. M. and Yiou, F., 1975, *Phys. Rev. (Letters)* 35, 155.
- Reed, G. W., 1971, in Handbook of Elemental Abundances in Meteorites, ed. B. Mason (Gordon and Breach), p. 487.

- Reeves, H., Fowler, W. A. and Hoyle, F., 1970, Nature 221, 727.
- Reeves, H., 1974, Ann. Rev. Astron. and Astrophys. 12, 437.
- Roche, C. T., Clark, R. G., Mathews, G. J. and Viola, V. E., 1976, Phys. Rev. C 14, 410.
- Ross, J. E. and Aller, L. H., 1974, Solar Physics 36, 11.
- Ross, J. E. and Aller, L. H., 1976, Science 191, 1223.
- Rudy, C., Vandenbosch, R., Russo, P. and Braithwaite, W. J., 1972, Nucl. Phys. A188, 430.
- Shapiro, M. M. and Silberberg, R., 1970, Ann. Rev. Nucl. Sci. 20, 323.
- Shima, M., 1963, Geochim. Cosmochim. Acta 27, 911.
- Traub, W. A. and Carleton, N. P., 1973, Ap. J. (Letters) 184, L11.
- Wänke, H., 1978, private communication.
- Weller, M. R., Furst, M. J., Tombrello, T. A. and Burnett, D. S., 1977, Ap. J. (Letters) 214, L39.
- Weller, M. R., Furst, M. J., Tombrello, T. A. and Burnett, D. S., 1978, Geochim. Cosmochim. Acta 42, 999.
- Yiou, F., Baril, M., Dufaure de Citres, J., Fontes, P., Gradsztajn, E. and Bernas, R., 1968, Phys. Rev. 166, 968.
- Yiou, F., Seide, C. and Bernas, R., 1969, J. Geophys. Res. 74, 2447.

Table 1

Boron concentrations of laboratory materials. These concentrations were measured by M. Furst using a nuclear track technique (Furst et al., 1976; Weller et al., 1978). Materials used in preparing samples for this experiment are denoted by asterisks. (See Section II-A.)

Table 1

Boron Concentrations of Laboratory Materials, ppm

Stainless steel labware	
pellet press cylinder*	14
pellet press ring (440 C)*	6
mortar (440 C)	4
ball mill container	1.5
Tantalum*	≤ 0.3
Tungsten carbide ball mill container	10,000
Hardened steel ball mill container	45
Sandpaper (Bueheler, 600 grit)*	3-5
Agate	
mortar (Fisher)	36
mortar (Van Waters-Rogers)	24
ball mill container (Spex)	48
Sapphire ball mill container	84
Aluminum oxide 0.3 micron powder (Bueheler)	1
Epoxy (Techkits E7)	≤ 0.3
Powder paper (Glassine, Lily)*	2-7
Transparent plastics	≤ 0.3
Filter paper (Whatman HP2)	3
Adhesive tape (Scotch Magic)	~30

Table 2

Average boron concentrations in carbonaceous chondrites. The average boron concentrations for six carbonaceous chondrites are shown in this table. Results from homogenized aliquots of a given sample were averaged together and considered as a single sample for the purposes of this table. The final column gives the atomic boron abundances relative to Si =  $10^6$ . The progression of B/Si between the C3/C2/C1 meteorites is typical of that observed for moderately volatile elements. (See Chapter III.)

Table 2

Average Boron Concentrations in  
Carbonaceous Chondrites

Type	Meteorite	No. Samples Analyzed	Average B ppm	Atomic B/Si <sub>6</sub> (10 <sup>-6</sup> )
C1	Ivuna	1	3.1	77
	Orgueil	1	1.6	40
C2	Murray	6	1.4	29
	Murchison	13	1.8	37
C3	Allende	6	1.7	22
	Lancé	2	1.4	18

Table 3

Measurements of boron concentrations in carbonaceous chondrites. This table gives the results of several recent measurements of boron in carbonaceous chondrites. The Allende result from Weller et al. (1978) refers only to the value obtained from the nuclear track analysis data. (See Chapter III.)

Table 3

Measurements of Boron  
in  
Carbonaceous Chondrites

<u>Type</u>	<u>Meteorite</u>	<u>Average B (ppm)</u>	<u>Reference</u>
C1	Orgueil	5.0	Harder(1961)
		5.2	Mills(1968)
		1.6	this work
	Ivuna	7.1	Mills(1968)
		3.1	this work
C2	Murray	1.4	this work
		9.4	Quijano-Rico and Wänke(1969)
	Murchison	1.8	this work
C3-4	Allende	1.1	Weller <u>et al.</u> (1978)
		1.7	this work
	Lancé	1.4	this work
		6.4	Quijano-Rico and Wänke(1969)
	Vigarano	9.6	Quijano-Rico and Wänke(1969)
	Karoonda	5.6	Quijano-Rico and Wänke(1969)

Table 4

Light element abundance measurements relative to hydrogen. This table summarizes the results of recent measurements of light element abundances in several different astrophysical environments. Results are given relative to a hydrogen abundance of 1. (See Chapter IV.)

Table 4

Light Element Abundance Measurements  
Relative to Hydrogen

	<u>Abundance</u>	<u>Reference</u>
<u>Lithium:</u>		
Meteorites	$(1.6 \pm 0.8) \times 10^{-9}$	Quijano-Rico and Wänke(1969)
Solar Photosphere	$1.0 \times 10^{-11}$	Grevesse(1968)
Main Sequence Stars	$1 \times 10^{-9} - 9 \times 10^{-11}$	Herbig(1965)
		Conti and Danziger(1966)
Interstellar Medium	$(2.9 \pm 0.7) \times 10^{-10}$	Traub and Carleton(1973)
Cosmic Rays	$(2.76 \pm 0.34) \times 10^{-4}$	Shapiro and Silberberg(1970)
<u>Beryllium:</u>		
Meteorites	$(4 \pm 2) \times 10^{-11}$	Quandt and Herr(1974)
Solar Photosphere	$(1.2 \pm 0.15) \times 10^{-11}$	Ross and Aller(1974)
Main Sequence Stars	$(1.31 \pm 0.36) \times 10^{-11}$	Boesgaard(1976)
Interstellar Medium	$\leq 5 \times 10^{-11}$	Boesgaard(1974)
Cosmic Rays	$(1.90 \pm 0.52) \times 10^{-4}$	Shapiro and Silberberg(1970)
<u>Boron:</u>		
Meteorites	$(2 \pm 1) \times 10^{-9}$	this work
Solar Photosphere	$< (1.2 \pm 0.6) \times 10^{-10}$	Hall and Engvöld(1975)
	$(4 \pm 4) \times 10^{-10}$	Kohl <u>et al.</u> (1977)
	$(4 - 2) \times 10^{-10}$	
Main Sequence Stars	$(1.0 \pm 0.2) \times 10^{-10}$	Boesgaard <u>et al.</u> (1974)
Interstellar Medium	$< 7.6 \times 10^{-11}$	Morton <u>et al.</u> (1974)
Cosmic Rays	$(4.66 \pm 0.52) \times 10^{-4}$	Shapiro and Silberberg(1970)

Table 5

Comparison of experimental and calculated abundance ratios. This table lists the light element abundance ratios obtained from measurements of lithium, beryllium and boron in meteorites and the solar photosphere. The meteorite lithium concentration was used to calculate all of the observed  ${}^6\text{Li}/{}^{10}\text{B}$  ratios. The Solar 1 and Solar 2 data represent ratios obtained using the boron concentrations found by Hall and Engvöld (1975) and Kohl et al. (1977), respectively. The calculated GCR ratios are from Meneguzzi et al. The other two calculated data sets correspond to low energy irradiation of the interstellar medium and of solar gas as described in Section V-C. (See also Section V-B.)

Table 5

Comparison of Experimental  
and Calculated  
Abundance Ratios

	$\frac{6\text{Li}}{10\text{B}}$	$\frac{9\text{Be}}{10\text{B}}$	$\frac{11\text{B}}{10\text{B}}$
Meteoritic	$0.30 \pm 0.21$	$0.10 \pm 0.07$	$4.0 \pm 0.1$
Solar 1	$> (5.0 \pm 3.5)$	$> (0.54 \pm 0.28)$	$4.0 \pm 0.1$
Solar 2	$1.50 \pm 1.28$	$0.16 \pm 0.11$	$4.0 \pm 0.1$
Calculated GCR	0.95	0.23	2.44
Calculated Low Energy GCR ( $a = 1.8$ )	$1.35 \pm 0.20$	$0.23 \pm 0.03$	$4.2 \pm 0.4$
Calculated Solar Gas Irradiation ( $a = 2.25$ )	$0.53 \pm 0.08$	$0.14 \pm 0.02$	$4.5 \pm 0.9$

Table 6

This table gives the elemental compositions used to determine the deuteron stopping powers for the samples analyzed in these measurements. The numbers for each element represent its percentage of the total mass of the sample. The last row in the table gives the values of the integral  $I = \int_0^{2.8 \text{ MeV}} \frac{\sigma(E)dE}{(-dE/d(\rho x))}$  for each sample. (See Appendix A.)

Table 6

Elemental Composition of Samples

	NBS glass	C1 meteorites	C2 meteorites	C3 meteorites
H	0	2.21	1.43	0.23
C	0	3.10	2.48	0.47
O	46.32	44.19	42.40	37.68
Na	10.39	0.55	0.47	0.38
Mg	0	9.53	11.74	14.46
Al	1.06	0.87	1.14	1.33
Si	33.65	10.55	13.00	15.61
P	0	0.12	0.13	0.17
S	0	5.49	3.66	2.45
K	0	0.06	0.04	0.03
Ca	8.58	0.87	1.19	1.83
Ti	0	0.04	0.05	0.06
Cr	0	0.25	0.25	0.36
Mn	0	0.15	0.16	0.15
Fe	0	18.42	21.25	24.06
Co	0	0.05	0.06	0.06
Ni	0	0.97	1.20	1.29
I( $10^{-27}$ gm)	4.1	3.8	4.1	4.2

Table 7

This table shows the boron concentrations of four NBS glass samples as determined from comparisons with Pyrex glass. The table also shows the count yields from each of the four scalers for all irradiations where the samples were used as standards for comparison with meteoritic samples. Except for the standard 3E, the integrated charges,  $Q_{\text{NBS}}$ , for all of the standard analyses were  $6 \times 10^{-5} \text{C}$ . For 3E,  $Q_{\text{NBS}} = 2 \times 10^{-5} \text{C}$  on 10-13-78 and  $Q_{\text{NBS}} = 4 \times 10^{-5} \text{C}$  for the other analysis. For equivalent integrated charges, the differences in count yields are due to small differences in geometry and in the SCA energy window.

(See Appendix A.)

Table 7

Analyses of NBS Standards					
Sample	B(ppm)	$\rho d$ (mg/cm <sup>2</sup> )	Analysis Date	Scaler	Counts
1B $\alpha$	360 $\pm$ 5	85.0	8-18-76	1	394146
				2	314891
				3	266095
				4	234785
			8-19-76	1	422383
				2	339053
				3	285440
				4	253424
1D $\alpha$	366 $\pm$ 5	220.0	8-26-76	1	365464
				2	288583
				3	240930
				4	212309
			8-29-76	1	440596
				2	348079
				3	289943
				4	254736
			9-16-76	1	377264
				2	298041
				3	249500
				4	219680
			9-24-76	1	398251
				2	312195
				3	261636
				4	229615
			9-25-76	1	407503
				2	322604
				3	270342
				4	236406
1D $\beta$	340 $\pm$ 5	242.5	10-25-76	1	356461
				2	281719
				3	236199
				4	207377
			11-10-76	1	397206
				2	311658
				3	258978
				4	225910

Table 7 (Continued)

Sample	B(ppm)	$\rho d$ (mg/cm <sup>2</sup> )	Analysis Date	Scaler	Counts
1D $\beta$	340 $\pm$ 5	242.5	12-20-76	1	418165
				2	326711
				3	271477
				4	238462
3E	360 $\pm$ 5	222.5	10-7-78	1	295391
				2	231249
				3	193337
				4	169561
			10-13-78	1	207849
				2	164984
				3	138655
				4	122009

Table 8

This table gives the raw data obtained for all of the meteorite analyses which were accepted. Boron concentrations may be obtained from these data using the procedure described in Appendix A and the information given in Tables 6 and 7. As discussed in Appendix A, an additional correction factor of 0.8 was applied to nine of the meteorite samples. These samples are denoted by daggers. Sample numbers of the form I(A), I(B), etc. refer to pellets made from homogenized sample I.

(See Chapter III, Appendix A.)

Table 8

Analyses of Meteoritic Samples							
Meteorite	Sample No.	Analysis Date	Q( $\mu\text{C}$ )	$\rho\text{d}(\text{mg}/\text{cm}^2)$	Scaler	Counts	B(ppm)
Ivuna	1(A) <sup>†</sup>	8-18-76	180	186	1	30334	$2.81 \pm 0.21$
					2	28227	
					3	27225	
					4	26544	
	1(B) <sup>†</sup>	8-26-76	180	155	1	37269	$3.34 \pm 0.18$
					2	32814	
					3	31837	
					4	31397	
Orgueil	NMNH2216(A) <sup>†</sup>	9-24-76	180	156	1	32464	$1.54 \pm 0.19$
					2	31440	
					3	30792	
					4	30167	
	NMNH2216(B) <sup>†</sup>	9-24-76	180	181	1	31324	$1.60 \pm 0.20$
					2	30407	
					3	29501	
					4	29275	
Murray	1-1 <sup>†</sup>	8-26-76	180	226	1	30579	$1.74 \pm 0.17$
					2	29286	
					3	28538	
					4	27726	
	2-1 <sup>†</sup>	8-26-76	180	177	1	31143	$1.05 \pm 0.16$
					2	30038	
					3	29571	
					4	29218	

Table 8 (Continued)

Meteorite	Sample No.	Analysis Date	Q( $\mu\text{C}$ )	$\rho\text{d}(\text{mg}/\text{cm}^2)$	Scaler	Counts	B(ppm)
Murray	3 <sup>†</sup>	8-26-76	180	174	1	34089	1.62 ± 0.17
					2	32814	
					3	31837	
					4	31397	
	4	8-29-76	180	163	1	34158	2.14 ± 0.17
					2	32229	
					3	31189	
					4	30509	
	1-2	8-29-76	180	160	1	31556	1.02 ± 0.16
					2	30152	
					3	29761	
					4	29626	
2-2	8-29-76	180	154	1	31517	1.09 ± 0.16	
				2	30711		
				3	29700		
				4	30036		
Murchison	9 <sup>†</sup>	8-18-76	180	412	1	25146	2.32 ± 0.65
					2	24279	
					3	23637	
					4	22903	
	4-1	8-29-76	180	360	1	27747	1.66 ± 0.21
					2	26507	
					3	25935	
					4	25558	
	6	8-29-76	180	312	1	27858	1.79 ± 0.20
					2	26415	
					3	25568	
					4	25358	

Table 8 (Continued)

Meteorite	Sample No.	Analysis Date	Q( $\mu\text{C}$ )	$\rho_d(\text{mg}/\text{cm}^2)$	Scaler	Counts	B(ppm)
Murchison	4-2	9-16-76	180	286	1	27002	$1.32 \pm 0.22$
					2	25719	
					3	25650	
					4	24918	
	7(A)	9-16-76	180	214	1	25104	$1.10 \pm 0.18$
					2	24071	
					3	23547	
					4	23648	
	7(B)	9-16-76	180	274	1	22832	$1.15 \pm 0.19$
					2	22174	
					3	21658	
					4	21456	
	7(C)	9-16-76	180	292	1	20602	$1.38 \pm 0.19$
					2	19784	
					3	19281	
					4	18932	
	8(A)	9-24-76	180	83	1	29550	$1.29 \pm 0.15$
					2	28495	
					3	27837	
					4	27273	
8(B)	9-25-76	180	72	1	31714	$1.69 \pm 0.15$	
				2	29961		
				3	29138		
				4	28577		
2682-1	10-25-76	180	395	1	25940	$1.74 \pm 0.28$	
				2	24973		
				3	24433		
				4	24301		

Table 8 (Continued)

Meteorite	Sample No.	Analysis Date	Q( $\mu\text{C}$ )	$\rho\text{d}(\text{mg}/\text{cm}^2)$	Scaler	Counts	B(ppm)
Murchison	2682-2-1	11-10-76	180	443	1	21818	$1.72 \pm 0.24$
					2	20659	
					3	20273	
					4	19928	
	2682-3	11-10-76	180	358	1	23806	$3.07 \pm 0.21$
					2	22366	
					3	21159	
					4	20526	
	2682-4-1	12-20-76	180	292	1	28515	$1.43 \pm 0.20$
					2	27530	
					3	26847	
					4	26700	
	828-2-1	10-7-78	180	295	1	31131	$2.68 \pm 0.20$
					2	29510	
					3	28176	
					4	27538	
	2682-4-2	10-13-78	150	266	1	36476	$1.58 \pm 0.18$
					2	35117	
					3	33942	
					4	34137	
	828-2-2	10-13-78	150	260	1	34848	$1.31 \pm 0.18$
					2	34001	
					3	33043	
					4	32857	

Table 8 (Continued)

Meteorite	Sample No.	Analysis Date	Q( $\mu\text{C}$ )	$\rho d$ ( $\text{mg}/\text{cm}^2$ )	Scaler	Counts	B(ppm)
Allende	1C <sup>†</sup>	8-19-76	180	526	1	38464	2.91 ± 0.90
					2	37063	
					3	36134	
					4	35729	
	1A <sup>†</sup>	8-26-76	180	291	1	27726	2.31 ± 0.18
					2	26260	
					3	24997	
					4	24596	
	1B <sup>†</sup>	8-26-76	180	249	1	25333	0.99 ± 0.16
					2	24631	
					3	24165	
					4	23706	
2A	8-29-76	120	325	1	14982	1.42 ± 0.21	
				2	14195		
				3	13714		
				4	13771		
2B	8-29-76	120	328	1	14704	1.08 ± 0.21	
				2	14010		
				3	13963		
				4	13450		
2C	8-29-76	180	328	1	22370	1.61 ± 0.18	
				2	20975		
				3	20465		
				4	20042		

Table 8 (Continued)

Meteorite	Sample No.	Analysis Date	Q( $\mu\text{C}$ )	$\rho d(\text{mg}/\text{cm}^2)$	Scaler	Counts	B(ppm)
Lance	1	9-24-76	180	150	1	30049	$1.03 \pm 0.17$
					2	28665	
					3	28444	
					4	28025	
	2	9-24-76	180	441	1	22473	$1.67 \pm 0.23$
					2	21882	
					3	20964	
					4	21066	

Table 9

This table gives the elemental abundances and cosmic ray fluxes which were used in the calculations described in Appendix B. For the case of cosmic ray interaction with the interstellar medium, the abundances,  $n_i$ , and fluxes,  $\phi_i$ , are the same as those used by Mathews (1977) in a similar calculation.

Table 9

	Proton Irradiation of Solar Gas	Proton Irradiation of Solar Dust	Interaction of Cosmic Rays with Interstellar Medium
$n_H$	1.0	1.0	1.0
$n_{He}$	$6.95 \times 10^{-2}$	$6.95 \times 10^{-2}$	$6.95 \times 10^{-2}$
$n_C$	$3.71 \times 10^{-4}$	0	$3.71 \times 10^{-4}$
$n_N$	$1.18 \times 10^{-4}$	0	$1.18 \times 10^{-4}$
$n_O$	$6.76 \times 10^{-4}$	$6.76 \times 10^{-4}$	$6.76 \times 10^{-4}$
$\phi_H$	1.0	1.0	1.0
$\phi_{He}$	0	0	0.1
$\phi_C$	0	0	$1.77 \times 10^{-3}$
$\phi_N$	0	0	$4.80 \times 10^{-4}$
$\phi_O$	0	0	$1.72 \times 10^{-3}$

Table 10

This table shows the average creation rates for the various light elements obtained from the interaction of low energy galactic cosmic rays with the interstellar medium. The table also distinguishes between the contribution due to cosmic ray CNO nuclei and that due to cosmic ray protons and alpha particles.

(See Appendix B.)

Table 10

Light Element Creation Rates

		CNO Contribution	p, $\alpha$ Contribution	Total Creation Rate
${}^6\text{Li}$ : a =	1.5	$1.75 \times 10^{-29}$	$2.28 \times 10^{-29}$	$4.03 \times 10^{-29}$
	2.0	$2.52 \times 10^{-30}$	$4.59 \times 10^{-30}$	$7.11 \times 10^{-30}$
	2.5	$4.14 \times 10^{-31}$	$1.14 \times 10^{-30}$	$1.55 \times 10^{-30}$
	3.0	$7.86 \times 10^{-32}$	$2.70 \times 10^{-31}$	$3.49 \times 10^{-31}$
	4.0	$4.61 \times 10^{-33}$	$1.88 \times 10^{-32}$	$2.34 \times 10^{-32}$
	5.0	$4.61 \times 10^{-34}$	$1.43 \times 10^{-33}$	$1.90 \times 10^{-33}$
${}^9\text{Be}$ : a =	1.5	$5.31 \times 10^{-30}$	$2.56 \times 10^{-30}$	$7.87 \times 10^{-30}$
	2.0	$8.11 \times 10^{-31}$	$3.14 \times 10^{-31}$	$1.13 \times 10^{-30}$
	2.5	$1.42 \times 10^{-31}$	$5.31 \times 10^{-32}$	$1.95 \times 10^{-31}$
	3.0	$2.84 \times 10^{-32}$	$1.20 \times 10^{-32}$	$4.04 \times 10^{-32}$
	4.0	$1.91 \times 10^{-33}$	$5.85 \times 10^{-34}$	$2.50 \times 10^{-33}$
	5.0	$1.08 \times 10^{-34}$	$4.11 \times 10^{-35}$	$1.50 \times 10^{-34}$
${}^{10}\text{B}$ : a =	1.5	$2.52 \times 10^{-29}$	$1.10 \times 10^{-29}$	$3.53 \times 10^{-29}$
	2.0	$4.92 \times 10^{-30}$	$1.25 \times 10^{-30}$	$6.17 \times 10^{-30}$
	2.5	$6.91 \times 10^{-31}$	$2.18 \times 10^{-31}$	$9.09 \times 10^{-31}$
	3.0	$1.43 \times 10^{-31}$	$4.02 \times 10^{-32}$	$1.83 \times 10^{-31}$
	4.0	$8.85 \times 10^{-33}$	$3.08 \times 10^{-33}$	$1.19 \times 10^{-32}$
	5.0	$8.00 \times 10^{-34}$	$2.91 \times 10^{-34}$	$1.09 \times 10^{-33}$
${}^{11}\text{B}$ : a =	1.5	$9.44 \times 10^{-29}$	$3.51 \times 10^{-29}$	$1.30 \times 10^{-28}$
	2.0	$1.73 \times 10^{-29}$	$5.41 \times 10^{-30}$	$2.27 \times 10^{-29}$
	2.5	$3.81 \times 10^{-30}$	$1.16 \times 10^{-30}$	$4.97 \times 10^{-30}$
	3.0	$9.90 \times 10^{-31}$	$2.99 \times 10^{-31}$	$1.29 \times 10^{-30}$
	4.0	$9.61 \times 10^{-32}$	$2.80 \times 10^{-32}$	$1.24 \times 10^{-31}$
	5.0	$1.28 \times 10^{-32}$	$3.54 \times 10^{-33}$	$1.64 \times 10^{-32}$

Figure 1

Schematic experimental arrangement for  $^{12}\text{B}$  activation measurement. To maximize counting efficiency, the target holder is mounted off-center and the plastic scintillator is mounted on a re-entrant, Pb-shielded tube in the scattering chamber. To minimize background, only the high energy portion of the beta spectrum is allowed to pass the single channel analyzer. The beam is pulsed and counts are acquired sequentially in each of the 4 scalers according to the counting cycle shown in Figure 2.

(See Section II-B.)

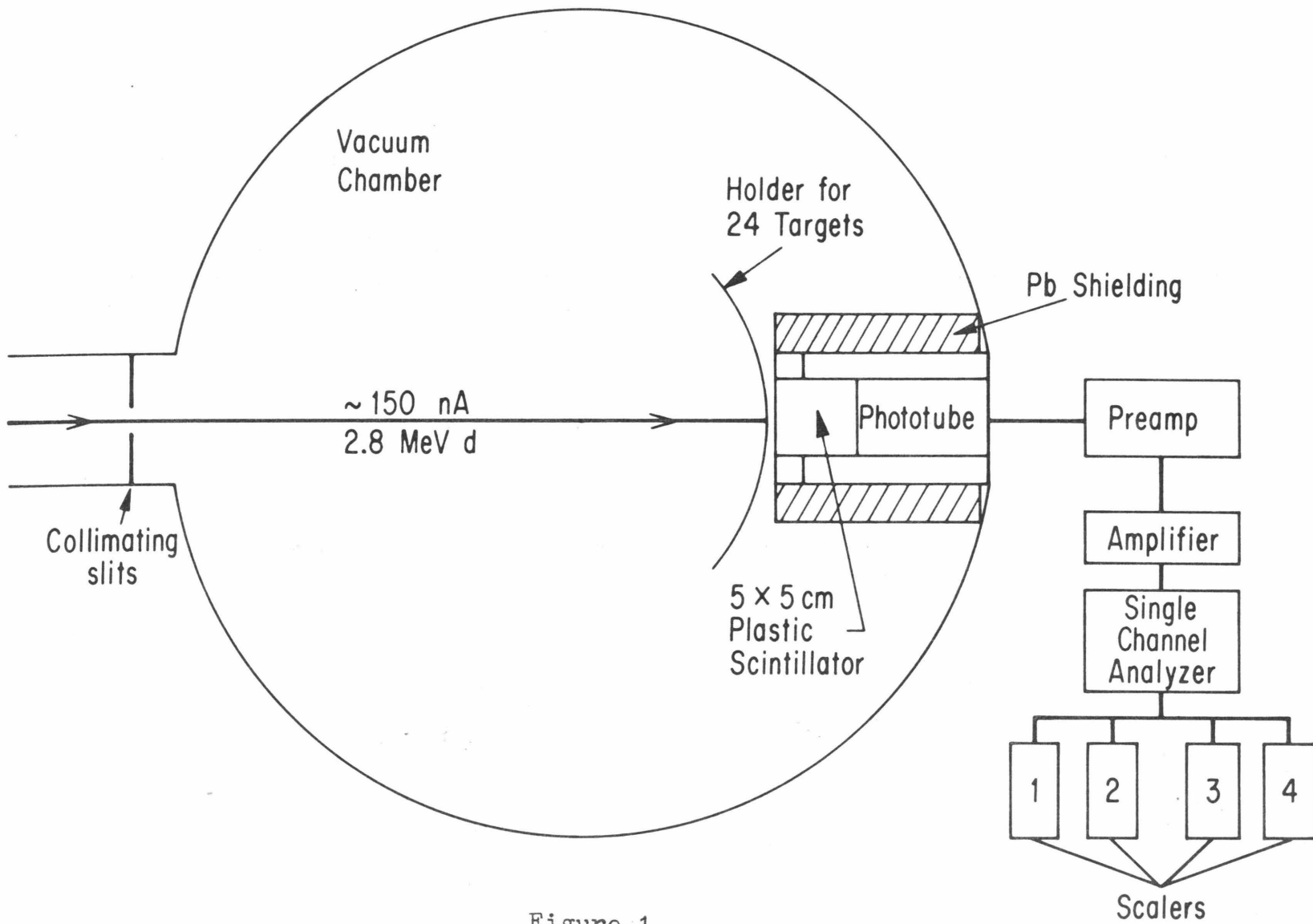


Figure 1

Figure 2

- a) Counting cycle for  $^{12}\text{B}$  pulsed beam activation measurement. The delay between 30-45 msec was to insure that the beam was totally deflected from the target before counting began. The Y values indicate the number of counts in the four successive counting intervals after beam deflection. The decrease from  $Y_1$  to  $Y_4$  schematically indicates the  $^{12}\text{B}$  decay.
  - b) Example of an uncorrected decay curve for a meteorite (Ivuna) sample. Decay time is measured after the start of interval  $Y_1$  (Fig 2a).
  - c) Background-corrected decay curve of data from Fig 2b. The corrected activity follows the 20 msec decay of  $^{12}\text{B}$ .
- (See Section II-B.)

### $^{11}\text{B}(d,p)^{12}\text{B}$ Counting Cycle

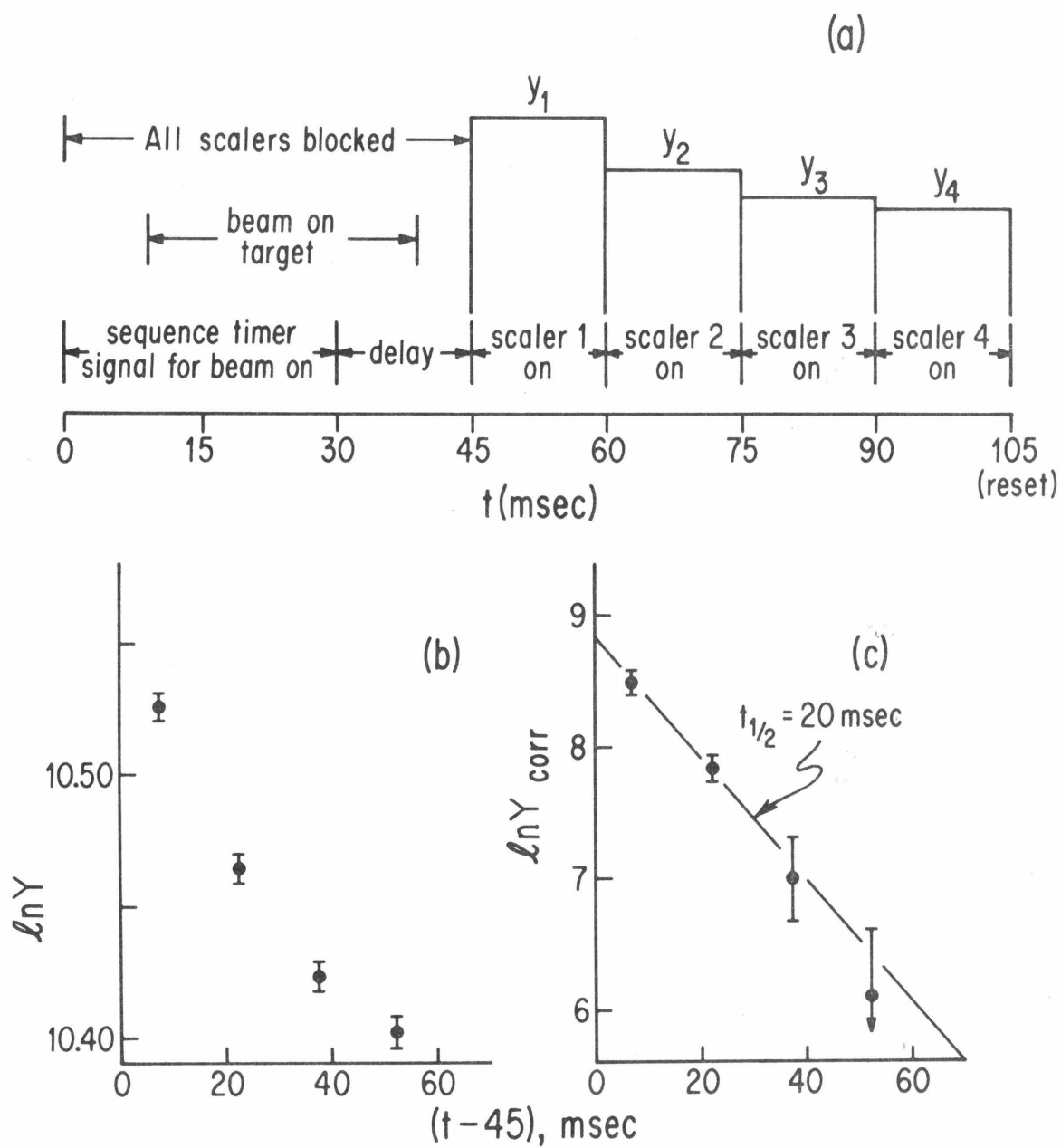


Figure 2

Figure 3

This figure shows the results of tests to determine whether boron concentrations were dependent on sample storage time (i.e. the time between sample preparation and analysis) due to the influence of airborne contamination. Typical storage times for  $^{12}\text{B}$  measurements were 10-20 hours in a dessicator. No significant increases were observed except for the graphite control sample at 64 hours. Additional data suggest that even this may be atypical. (See Section II-C.)

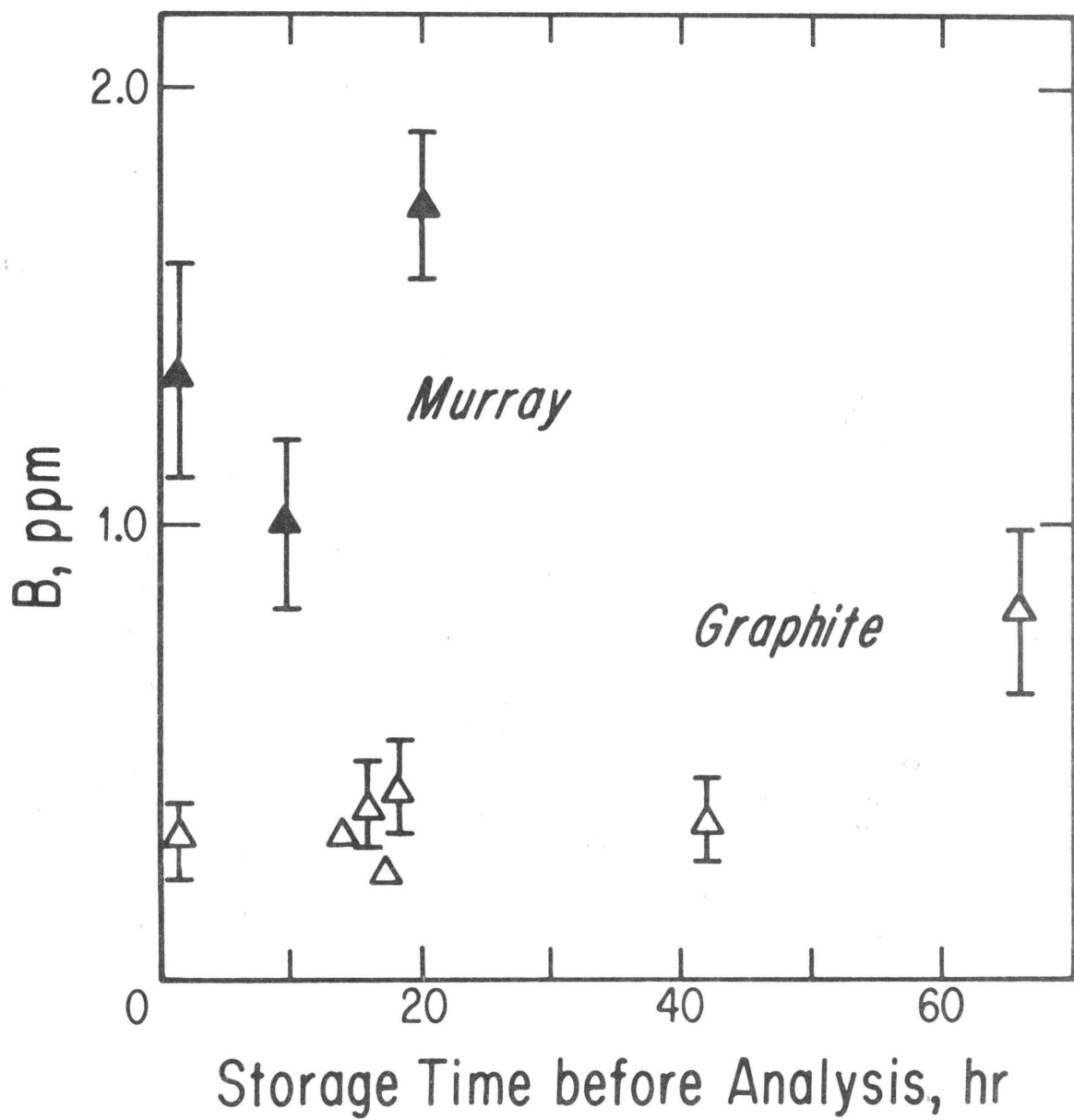


Figure 3

Figure 4

This figure shows the results of tests to determine whether boron concentrations depended on the exposure time of the sample to laboratory air due to airborne contamination. Typical exposure times for  $^{12}\text{B}$  measurements were 20 minutes. No significant increases were observed except possibly for the Murray point at 90 minutes.

(See Section II-C.)

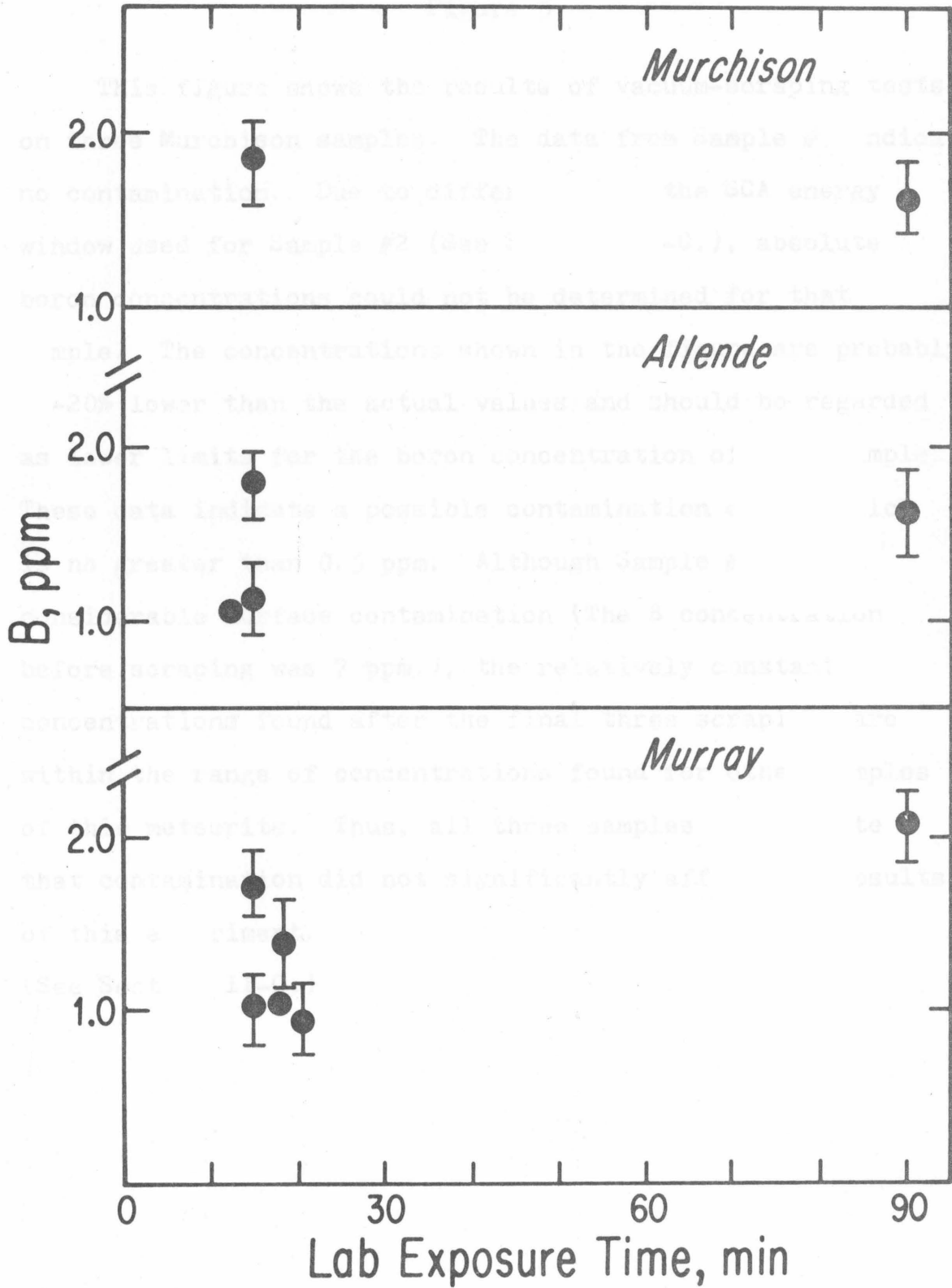


Figure 4

Figure 5

This figure shows the results of vacuum-scraping tests on three Murchison samples. The data from Sample #1 indicate no contamination. Due to differences in the SCA energy window used for Sample #2 (See Section II-C.), absolute boron concentrations could not be determined for that sample. The concentrations shown in the figure are probably 10-20% lower than the actual values and should be regarded as lower limits for the boron concentration of that sample. These data indicate a possible contamination effect which is no greater than 0.5 ppm. Although Sample #3 showed considerable surface contamination (The B concentration before scraping was 7 ppm.), the relatively constant concentrations found after the final three scrapings are within the range of concentrations found for other samples of this meteorite. Thus, all three samples demonstrate that contamination did not significantly affect the results of this experiment.

(See Section II-C.)

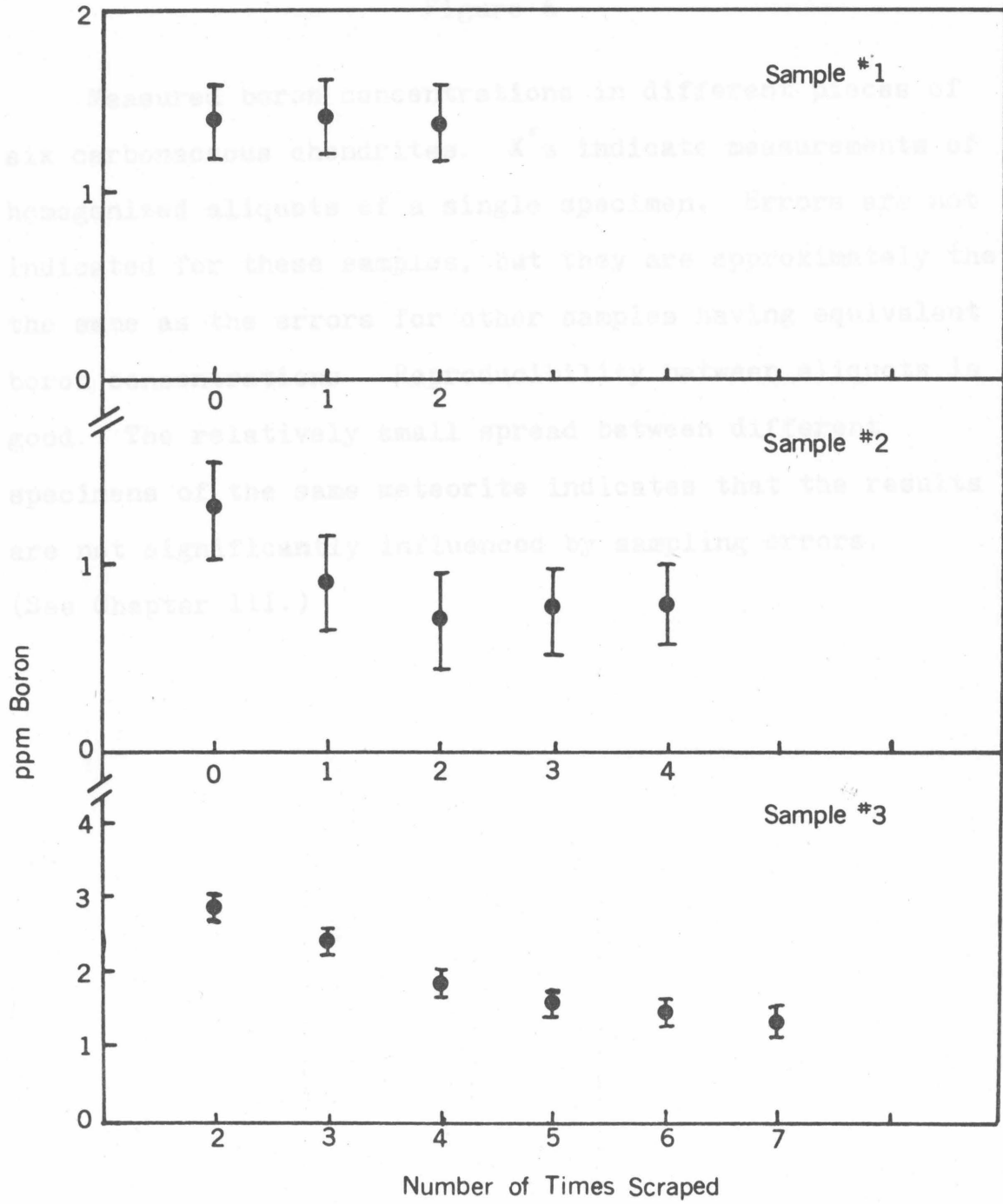


Figure 5

Figure 6

Measured boron concentrations in different pieces of six carbonaceous chondrites. X's indicate measurements of homogenized aliquots of a single specimen. Errors are not indicated for these samples, but they are approximately the same as the errors for other samples having equivalent boron concentrations. Reproducibility between aliquots is good. The relatively small spread between different specimens of the same meteorite indicates that the results are not significantly influenced by sampling errors. (See Chapter III.)

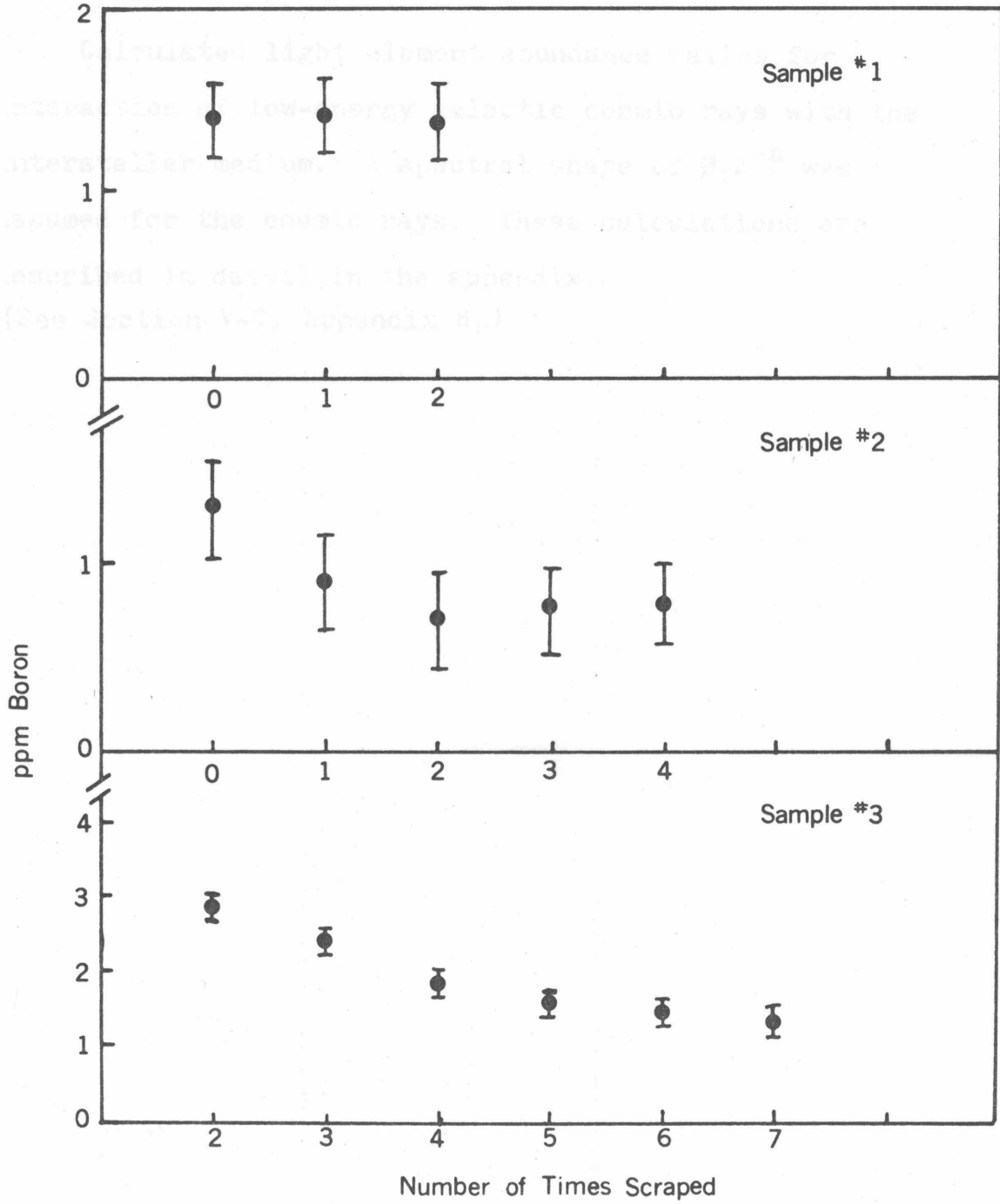


Figure 5

Figure 7

Calculated light element abundance ratios for interaction of low-energy galactic cosmic rays with the interstellar medium. A spectral shape of  $\phi_i E^{-a}$  was assumed for the cosmic rays. These calculations are described in detail in the appendix. (See Section V-C, Appendix B.)

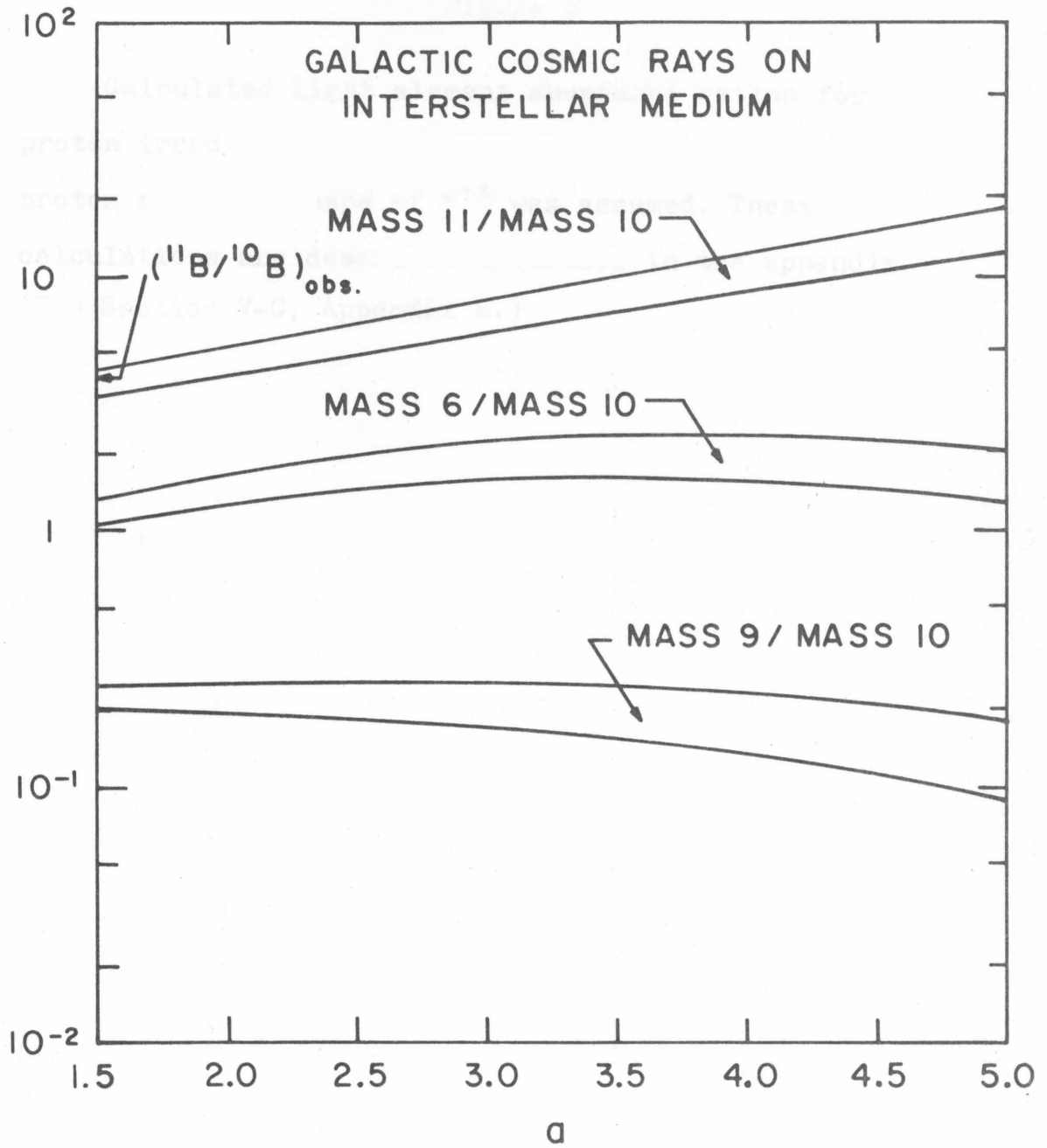


Figure 7

Figure 8

Calculated light element abundance ratios for proton irradiation of a gas of solar composition. A proton spectral shape of  $E^{-a}$  was assumed. These calculations are described in detail in the appendix. (See Section V-C, Appendix B.)

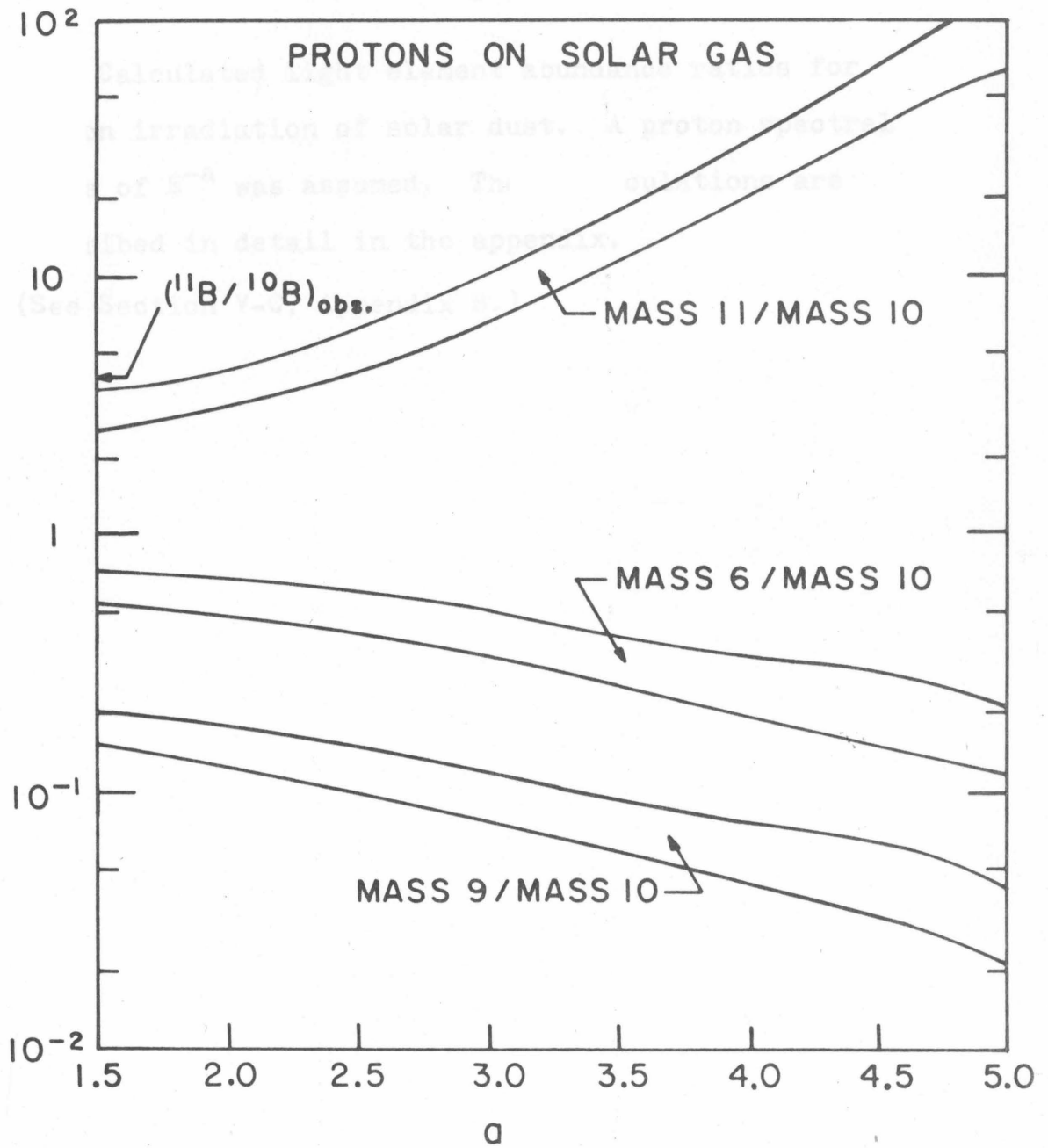


Figure 8

Figure 9

Calculated light element abundance ratios for proton irradiation of solar dust. A proton spectral shape of  $E^{-a}$  was assumed. These calculations are described in detail in the appendix.

(See Section V-C, Appendix B.)

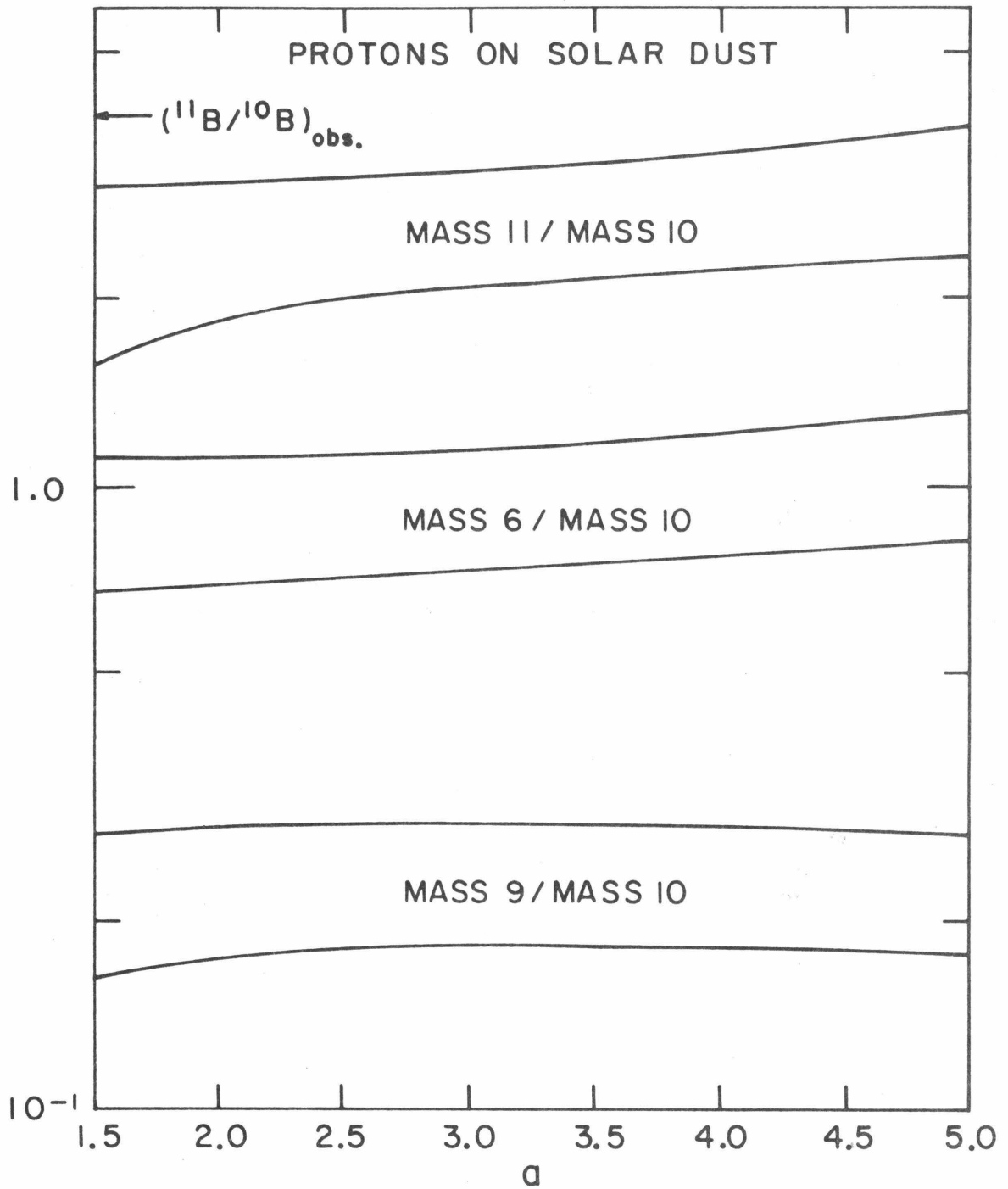


Figure 9

Figure 10

$^{10}\text{Be}/^{26}\text{Al}$  production ratio for irradiation of a solar gas or dust of solar composition with a proton spectrum of the form  $E^{-a}$ . These ratios may be uncertain by as much as a factor of two due to uncertainties in the production cross sections for both  $^{10}\text{Be}$  and  $^{26}\text{Al}$ . The  $^{10}\text{Be}/^{26}\text{Al}$  ratio is a steep function of  $a$  because  $^{10}\text{Be}$  is produced only at high energies, whereas  $^{26}\text{Al}$  has significant low energy production. The chemical systematics of the Allende Ca-Al-rich inclusions indicate that  $^{10}\text{Be}/^{26}\text{Al}$  should be unfractionated in their formation; thus the calculations can be compared with an experimental upper limit (dotted line) based on taking the measured  $^{10}\text{B}$  content as an upper limit to the initial  $^{10}\text{Be}$ . Cross sections used in these calculations were obtained from: Roche et al. (1976), Davids et al. (1970), Laumer et al. (1973), Epherre (1972), Yiou et al. (1969), Yiou et al. (1968), Mathews (1977), King et al. (1977), Bodansky et al. (1975), Jacobs et al. (1974), Fontes et al. (1971), Lestringuez et al. (1971), Raisbeck et al. (1972), Raisbeck and Yiou (1975), Jung et al. (1970), Furukawa et al. (1971) and Reeves (1974).

(See Section V-D.)

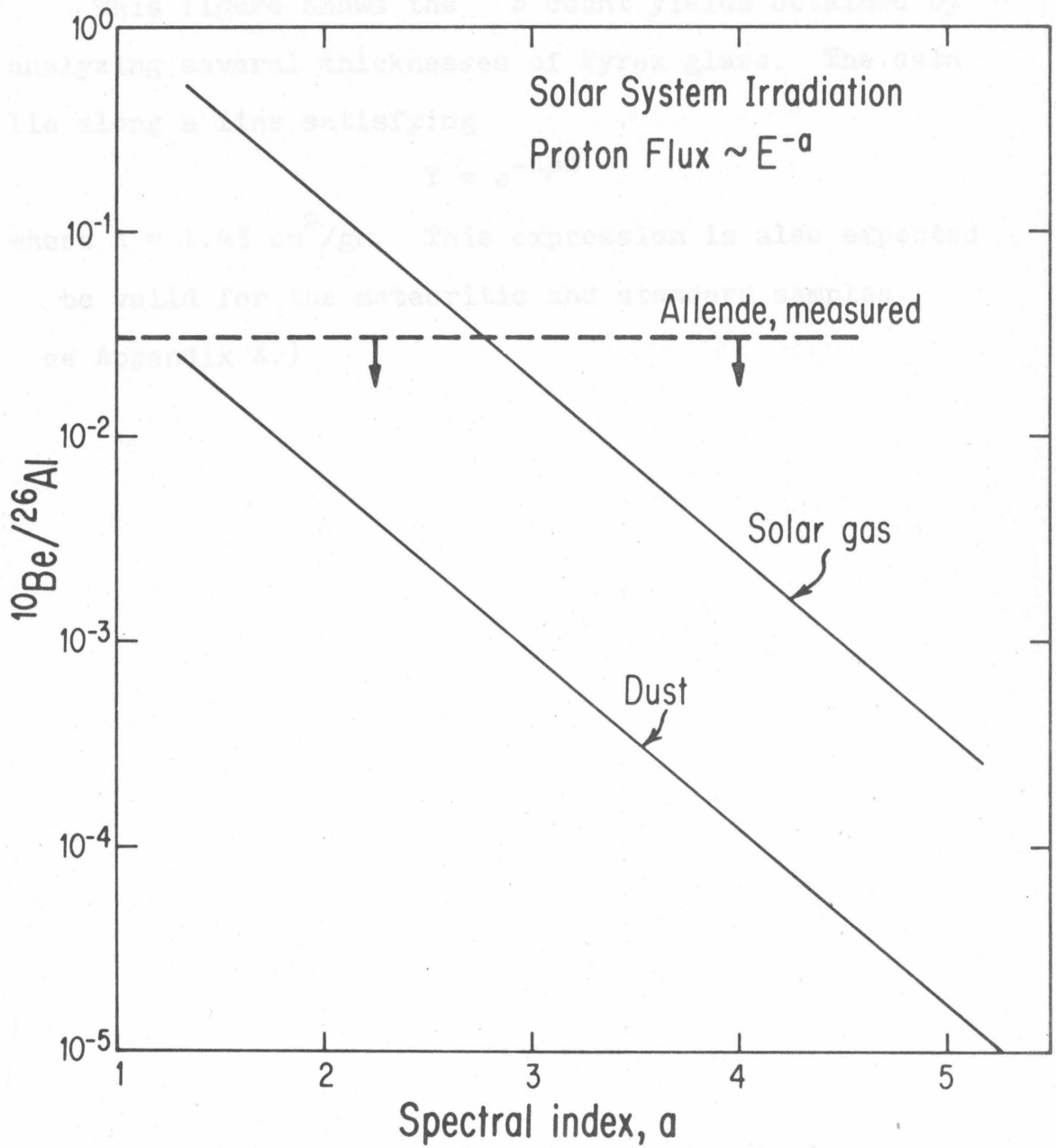


Figure 10

Figure 11

This figure shows the  $^{12}\text{B}$  count yields obtained by analyzing several thicknesses of Pyrex glass. The data lie along a line satisfying

$$Y = e^{-A\rho d}$$

where  $A = 1.45 \text{ cm}^2/\text{gm}$ . This expression is also expected to be valid for the meteoritic and standard samples.

(See Appendix A.)

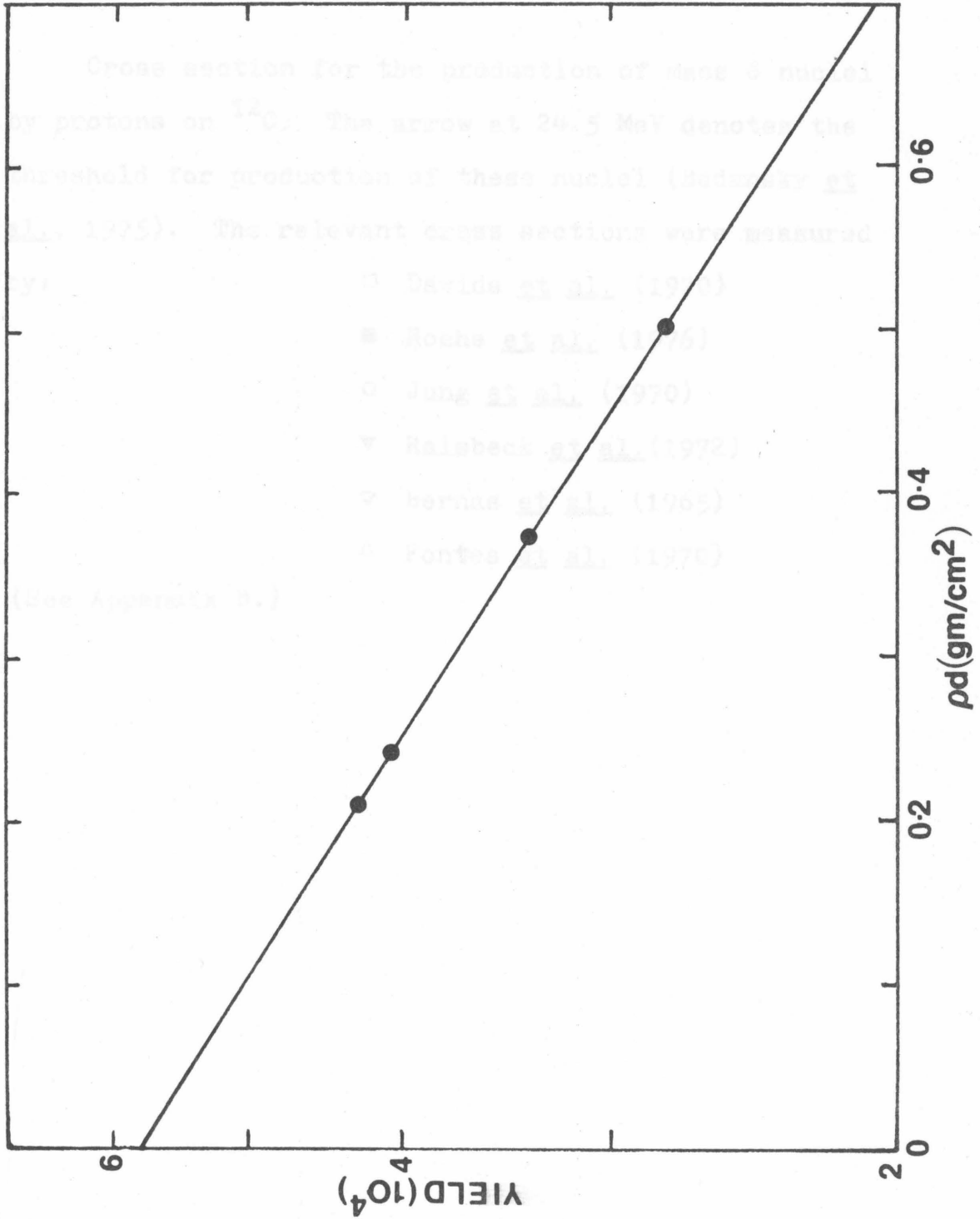


Figure 11

Figure 12

Cross section for the production of mass 6 nuclei by protons on  $^{12}\text{C}$ . The arrow at 24.5 MeV denotes the threshold for production of these nuclei (Bodansky et al., 1975). The relevant cross sections were measured by:

- Davids et al. (1970)
- Roche et al. (1976)
- Jung et al. (1970)
- ▼ Raisbeck et al. (1972)
- ▽ Bernas et al. (1965)
- △ Fontes et al. (1970)

(See Appendix B.)

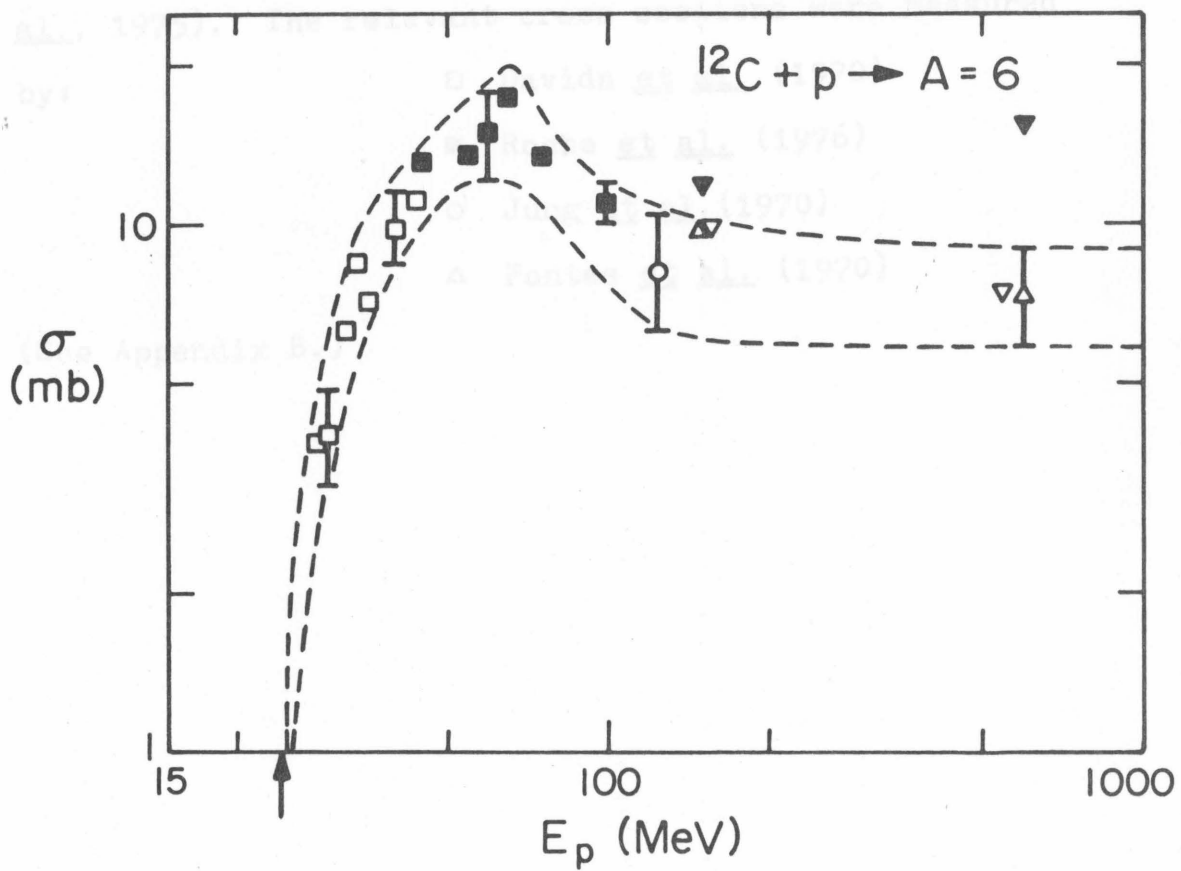


Figure 12

Figure 13

Cross section for production of mass 9 nuclei by protons on  $^{12}\text{C}$ . The arrow at 28.5 MeV denotes the threshold for production of these nuclei (Bodansky et al., 1975). The relevant cross sections were measured by:

- Davids et al. (1970)
- Roche et al. (1976)
- Jung et al. (1970)
- △ Fontes et al. (1970)

(See Appendix B.)

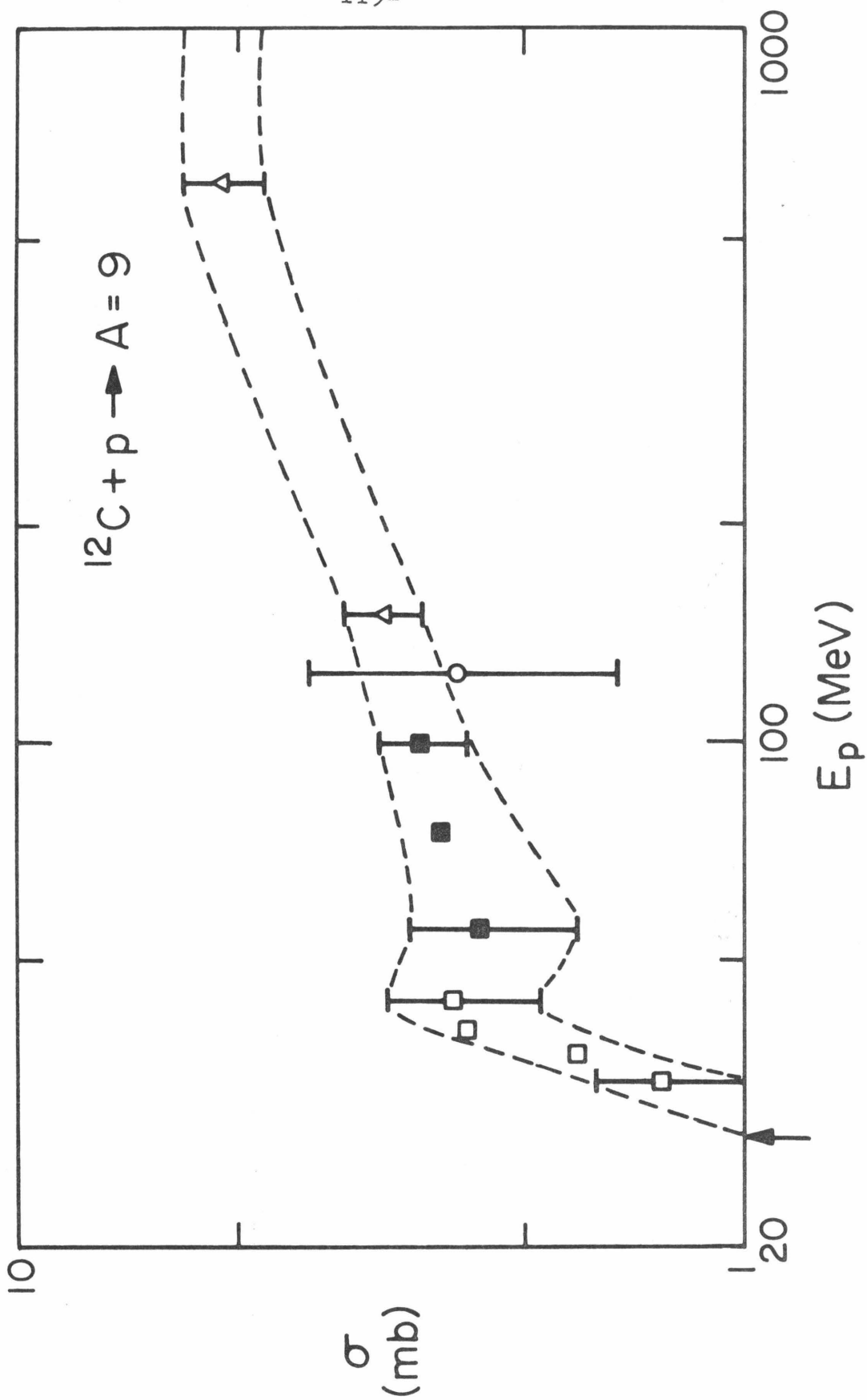


Figure 13

Figure 14

Cross section for production of mass 10 nuclei by protons on  $^{12}\text{C}$ . The arrow at 21.3 MeV denotes the threshold for production of these nuclei (Bodansky et al., 1975). The relevant cross sections were measured by:

- Davids et al. (1970)
- Roche et al. (1976)
- △ Fontes et al. (1970)

(See Appendix B.)

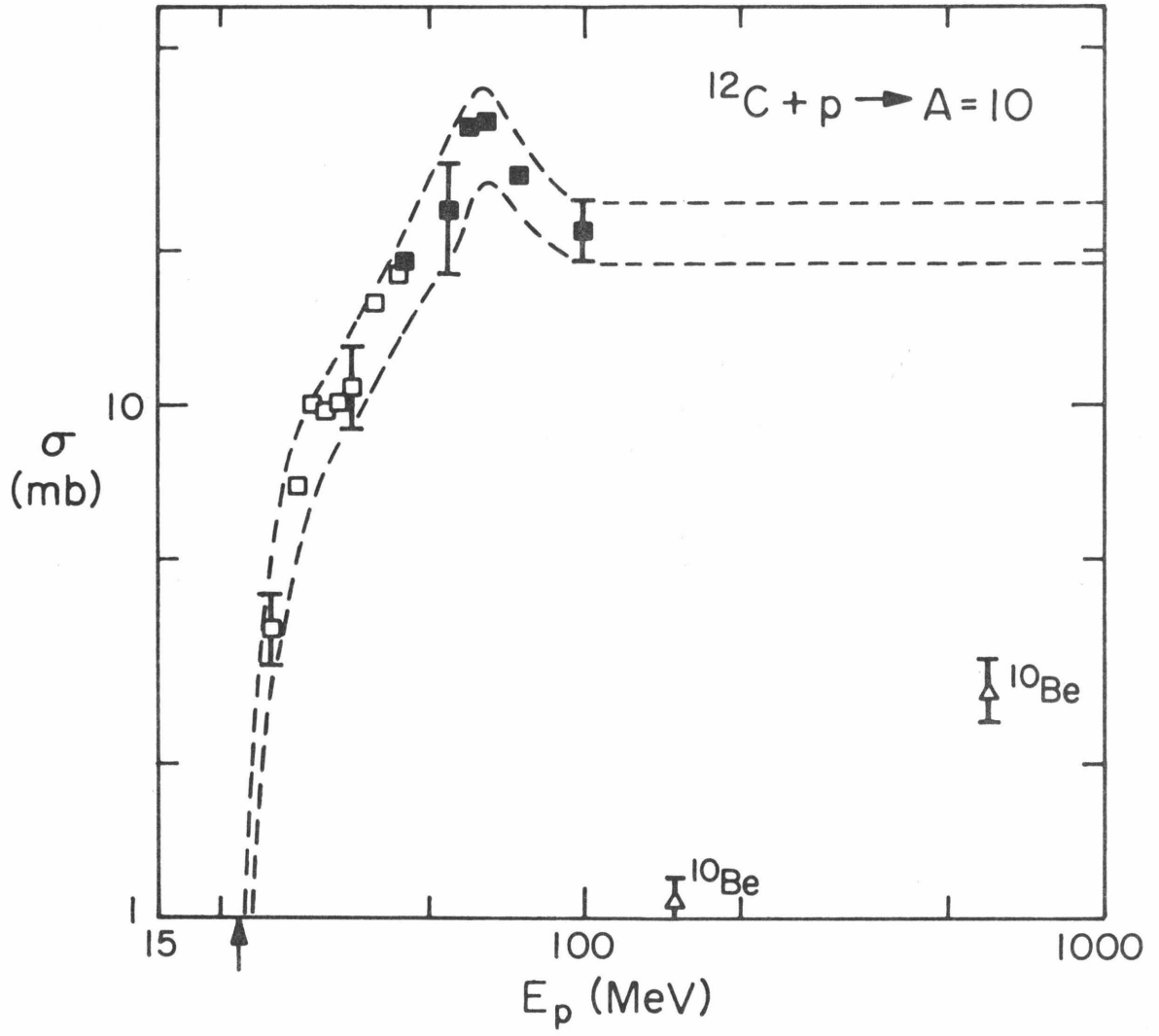


Figure 14

Figure 15

Cross section for the production of mass 11 nuclei by protons on  $^{12}\text{C}$ . The arrow at 17.3 MeV denotes the threshold for production of these nuclei (Bodansky et al., 1975). The relevant cross sections were measured

by:

- Davids et al. (1970)
- Roche et al. (1976)

(See Appendix B.)

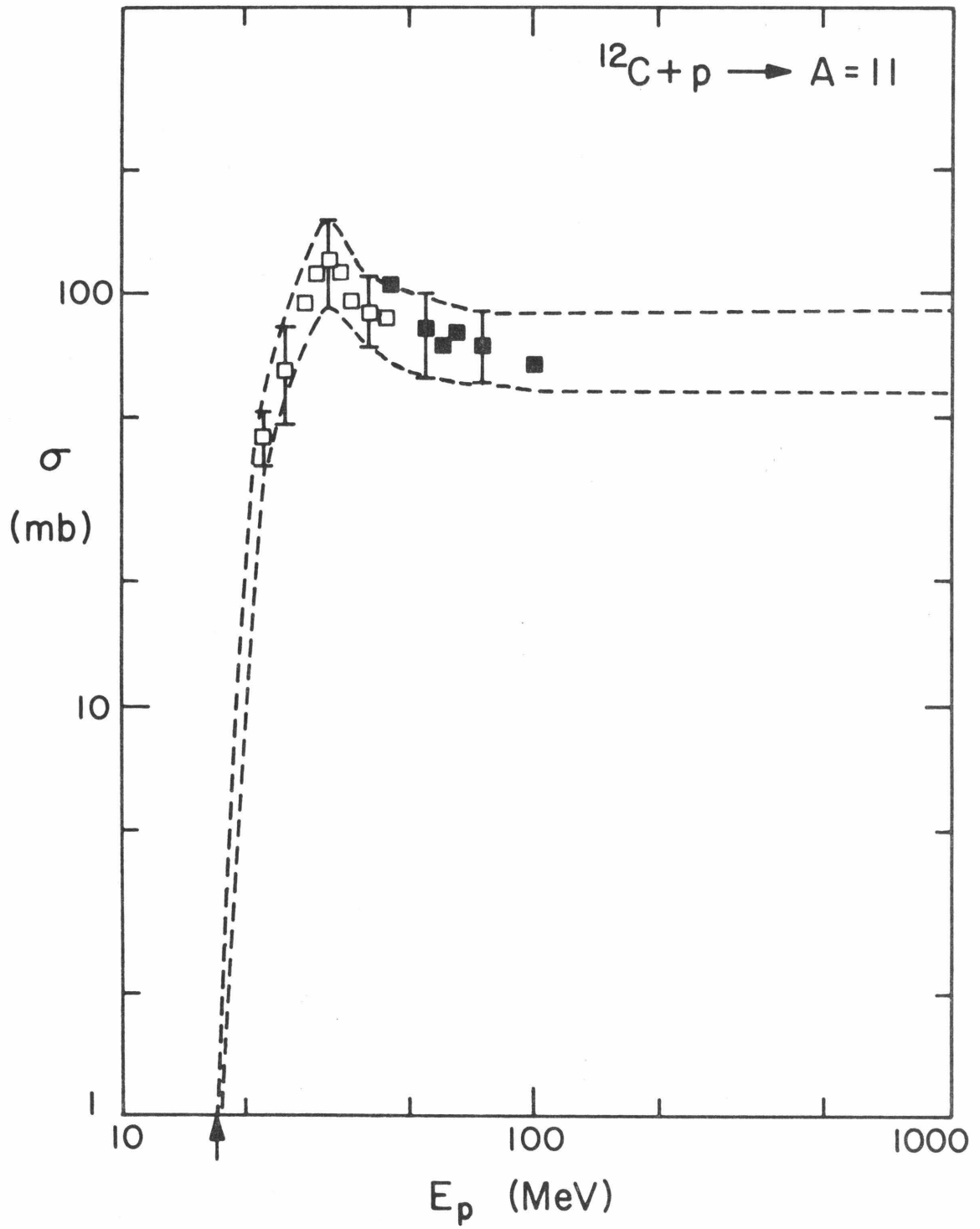


Figure 15

Figure 16

Cross section for the production of mass 6 nuclei by protons on  $^{14}\text{N}$ . The arrow at 17.2 MeV denotes the threshold for production of these nuclei (Bodansky et al., 1975). The relevant cross sections were measured by:

○ Jung et al. (1970)

● Laumer et al. (1973)

(See Appendix B.)

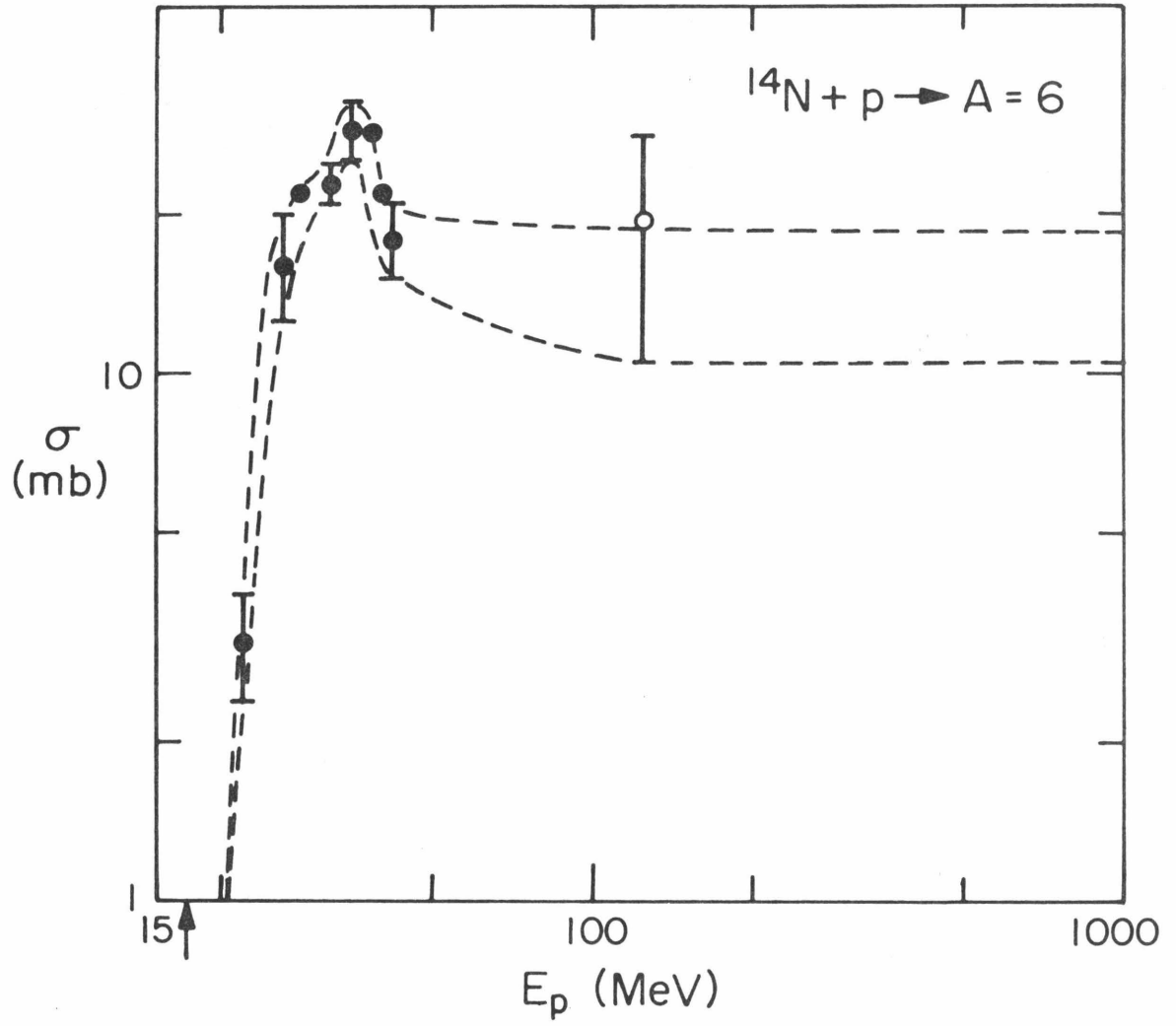


Figure 16.

Figure 17

Cross section for the production of  ${}^9\text{Be}$  by protons on  ${}^{14}\text{N}$ . The arrow at 19.5 MeV denotes the threshold for production of this nucleus (Bodansky et al., 1975).

The relevant cross sections were measured by:

- Laumer et al. (1973)
- Jung et al. (1970)

(See Appendix B.)

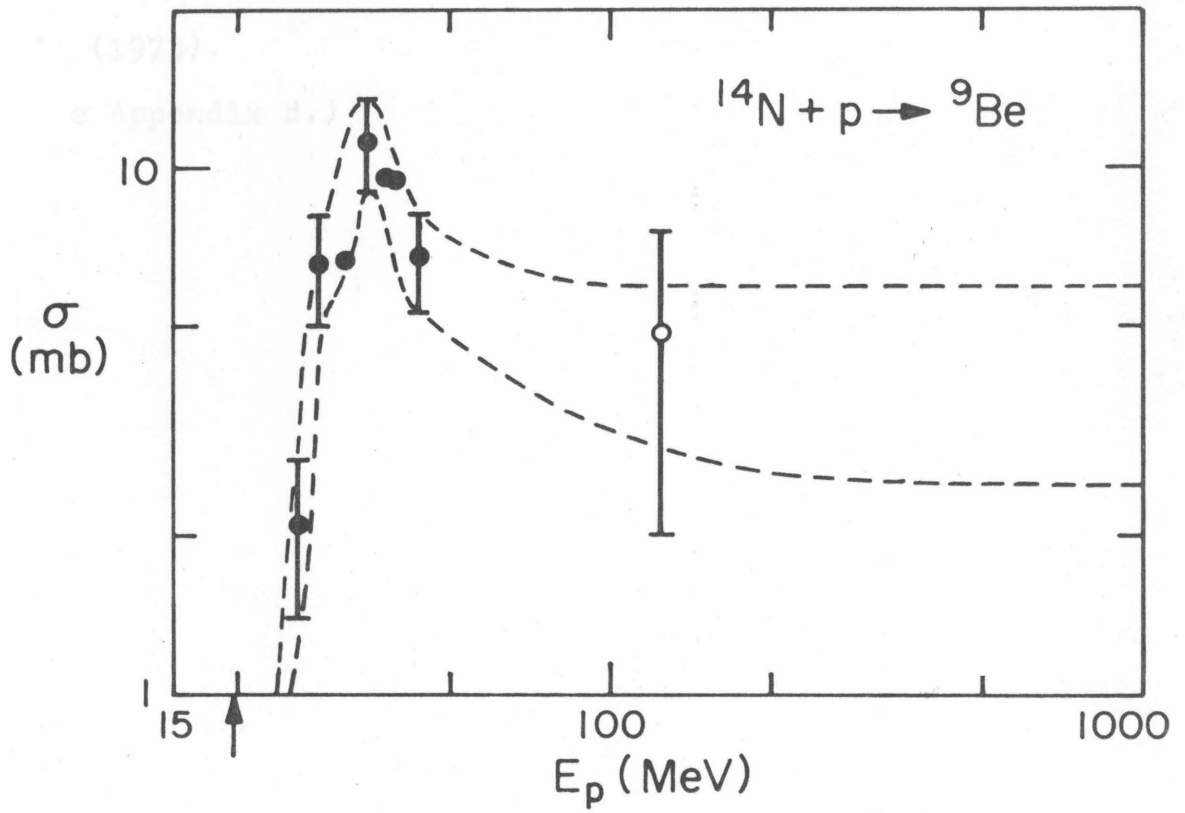


Figure 17

Figure 18

Cross section for the production of  $^{10}\text{B}$  by protons on  $^{14}\text{N}$ . The arrow at 12.4 MeV denotes the threshold for production of this nucleus (Bodansky et al., 1975). The relevant cross sections were measured by Laumer et al. (1973).

(See Appendix B.)

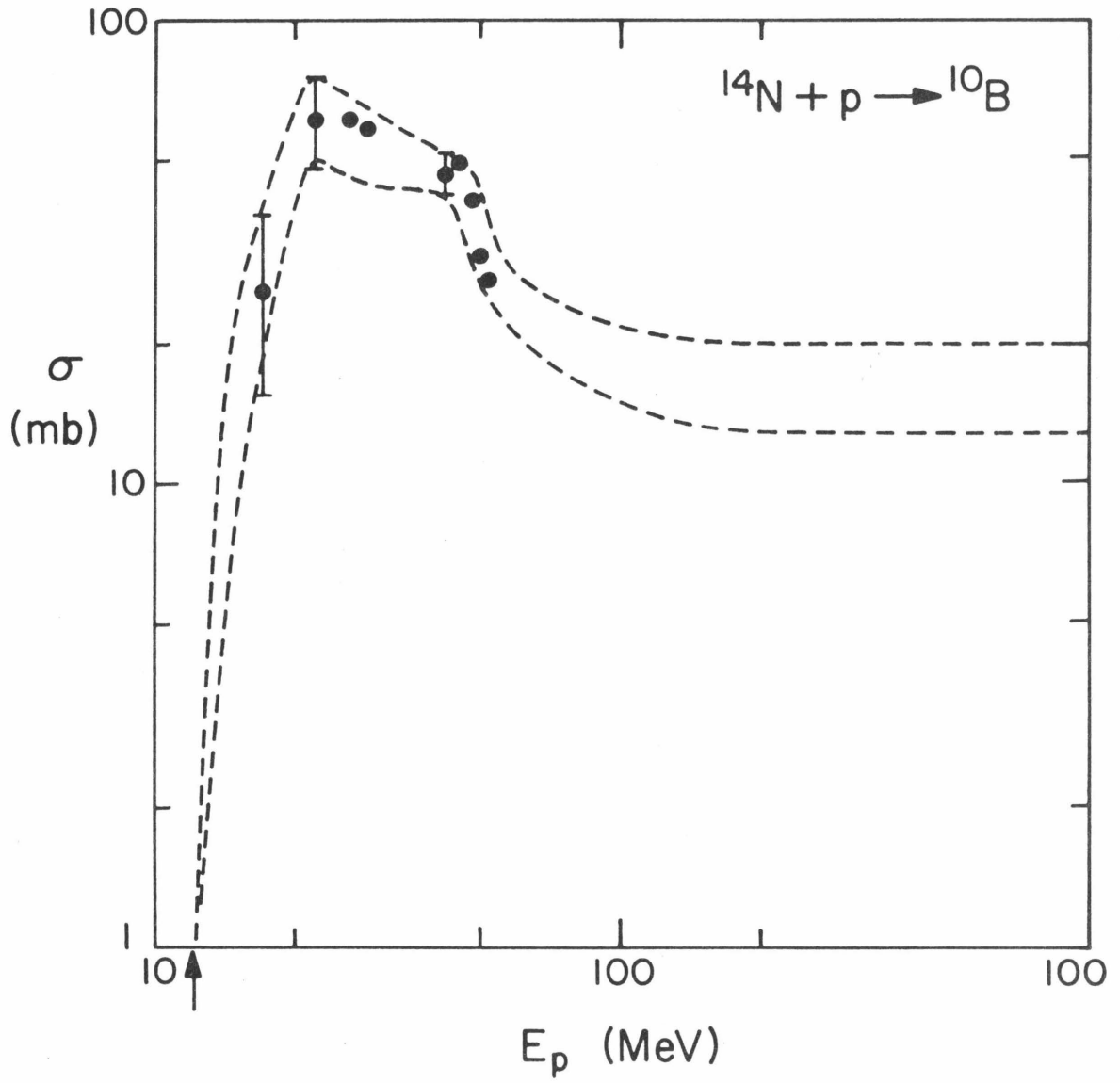


Figure 18

Figure 19

Cross section for production of mass 11 nuclei by protons on  $^{14}\text{N}$ . The arrow at 3.1 MeV denotes the threshold for the production of these nuclei (Bodansky et al., 1975). The relevant cross sections were

measured by:

▲ Jacobs et al. (1974)

● Laumer et al. (1973)

(See Appendix B.)

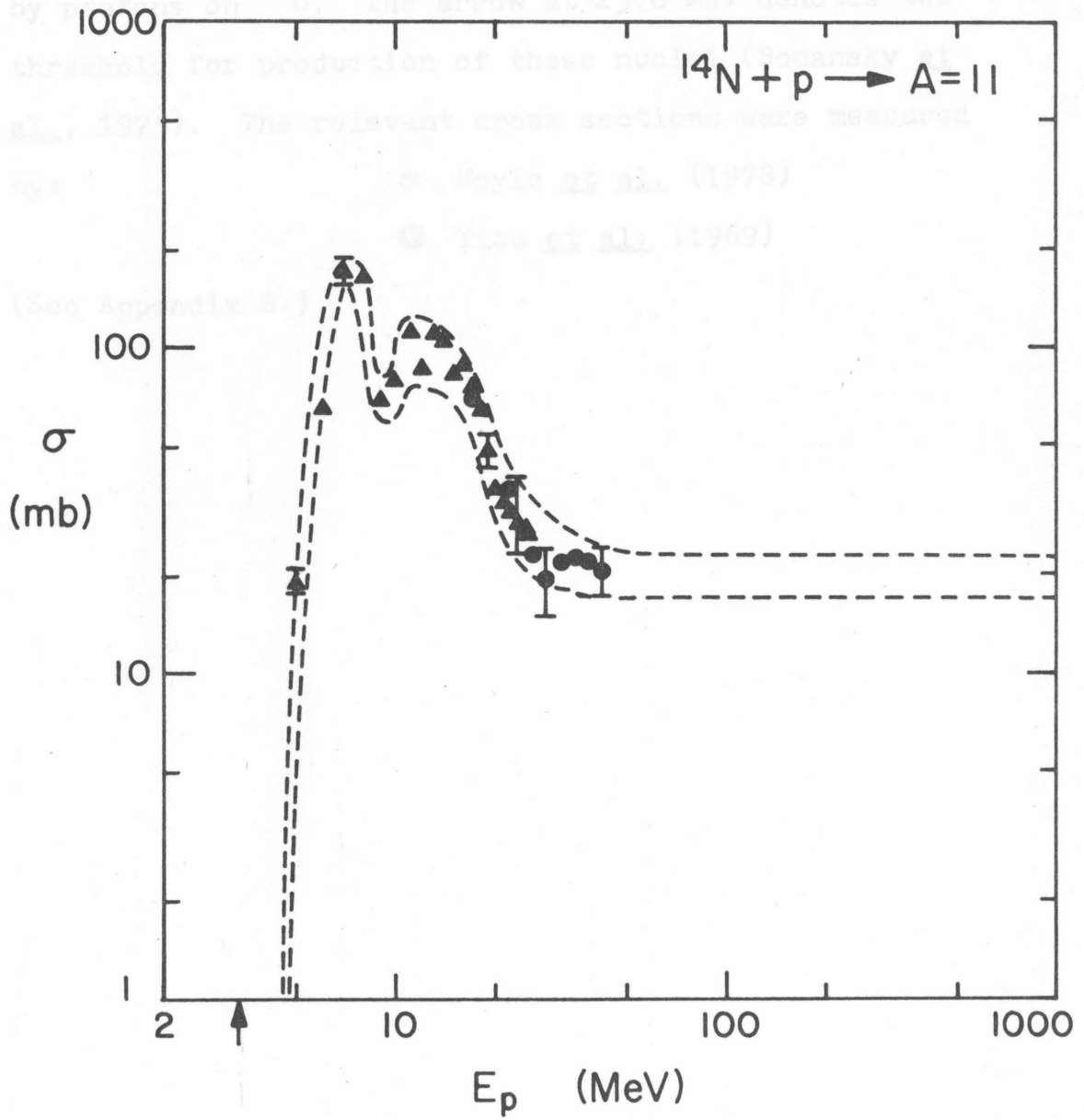


Figure 19

Figure 20

Cross section for the production of mass 6 nuclei by protons on  $^{16}\text{O}$ . The arrow at 23.6 MeV denotes the threshold for production of these nuclei (Bodansky et al., 1975). The relevant cross sections were measured

by:

\* Moyle et al. (1978)

⊙ Yiou et al. (1969)

(See Appendix B.)

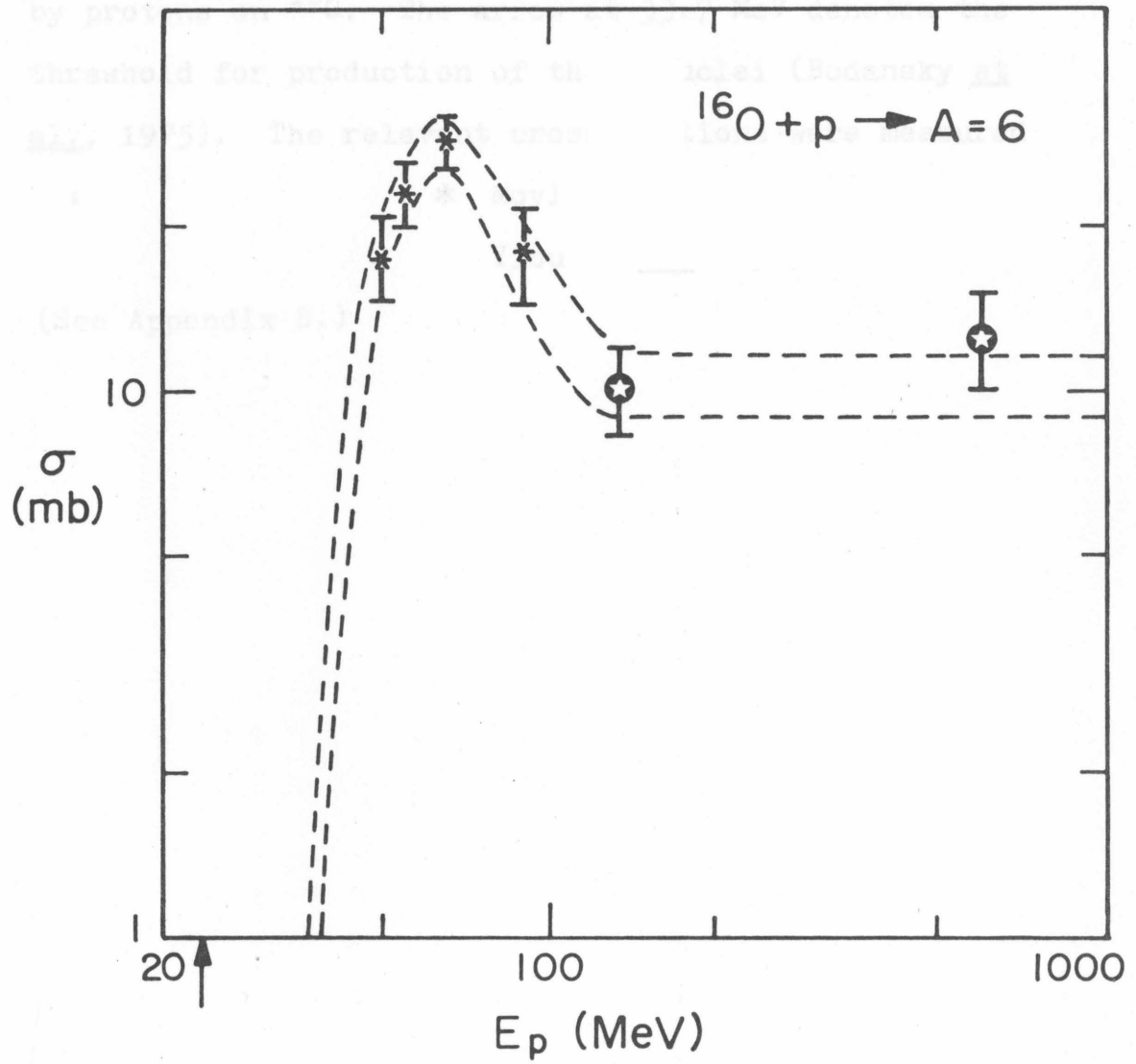


Figure 20

Figure 21

Cross section for the production of mass 9 nuclei by protons on  $^{16}\text{O}$ . The arrow at 33.7 MeV denotes the threshold for production of these nuclei (Bodansky et al., 1975). The relevant cross sections were measured

by:

\* Moyle et al. (1978)

⊙ Yiou et al. (1969)

(See Appendix B.)

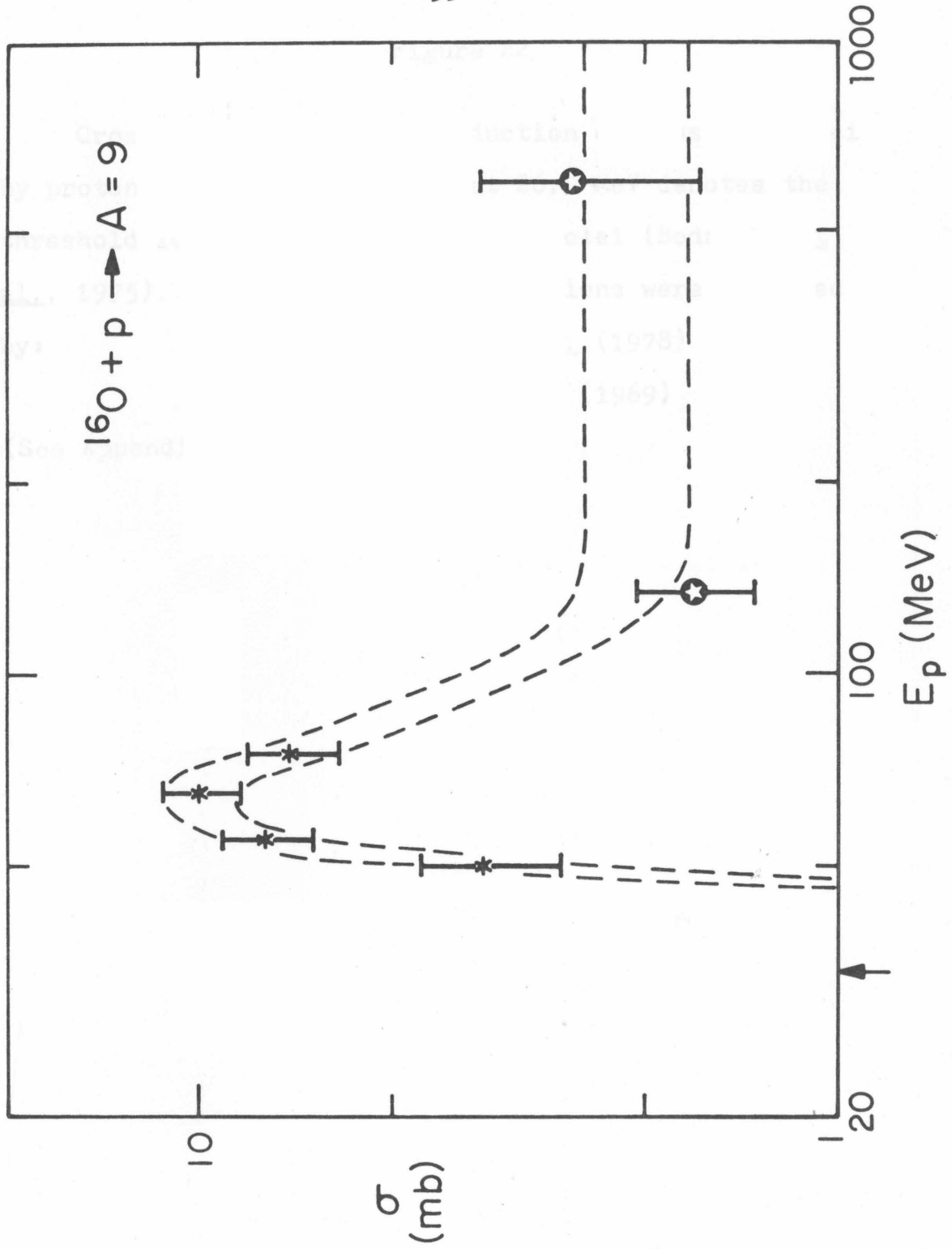


Figure 21

Figure 22

Cross section for the production of mass 10 nuclei by protons on  $^{16}\text{O}$ . The arrow at 26.9 MeV denotes the threshold for production of these nuclei (Bodansky et al., 1975). The relevant cross sections were measured

by:

- \* Moyle et al. (1978)
- ⊛ Yiou et al. (1969)

(See Appendix B.)

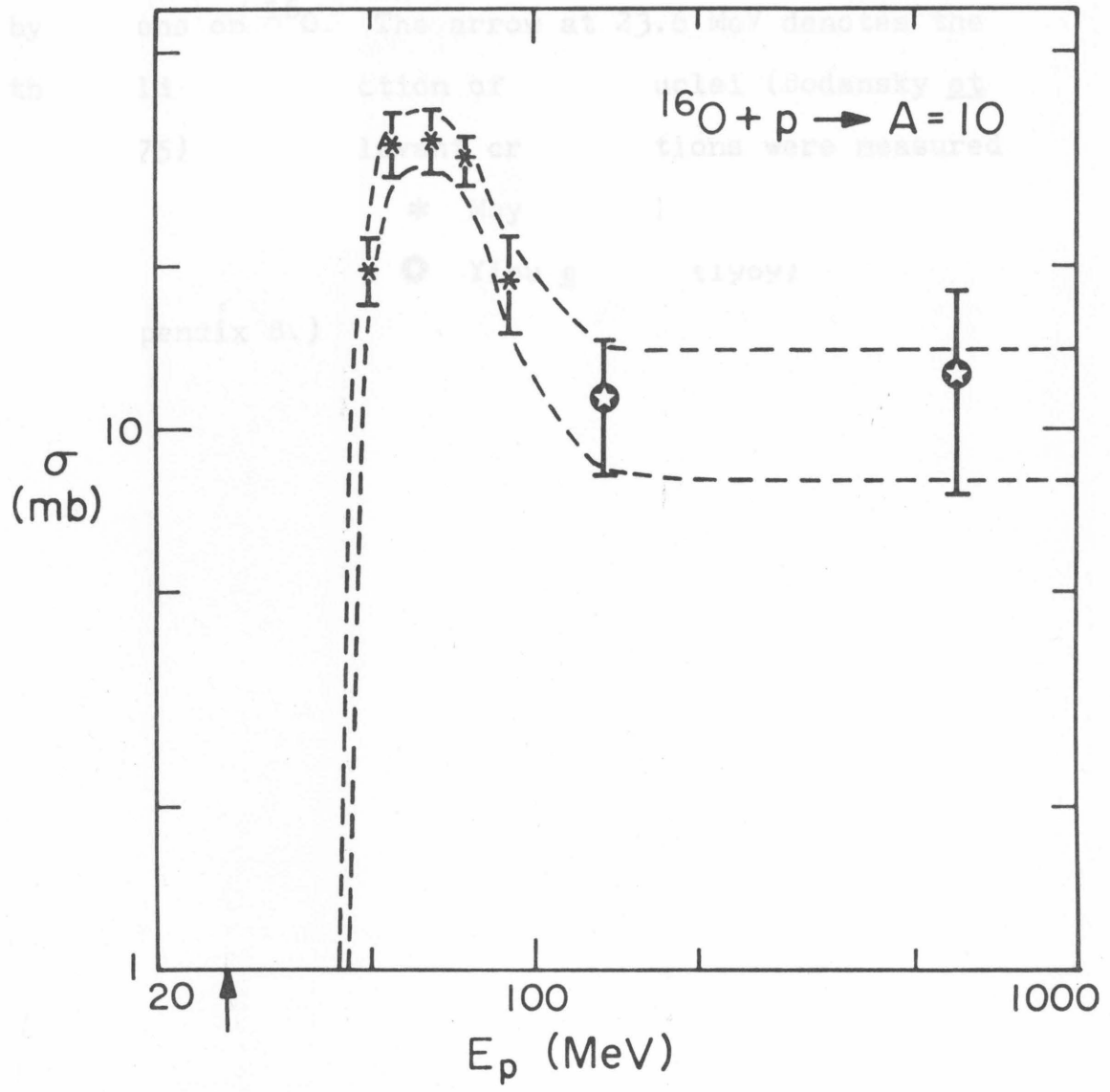


Figure 22

Figure 23

Cross section for the production of mass 11 nuclei by protons on  $^{16}\text{O}$ . The arrow at 23.6 MeV denotes the threshold for production of these nuclei (Bodansky et al., 1975). The relevant cross sections were measured

by:

\* Moyle et al. (1978)

⊙ Yiou et al. (1969)

(See Appendix B.)

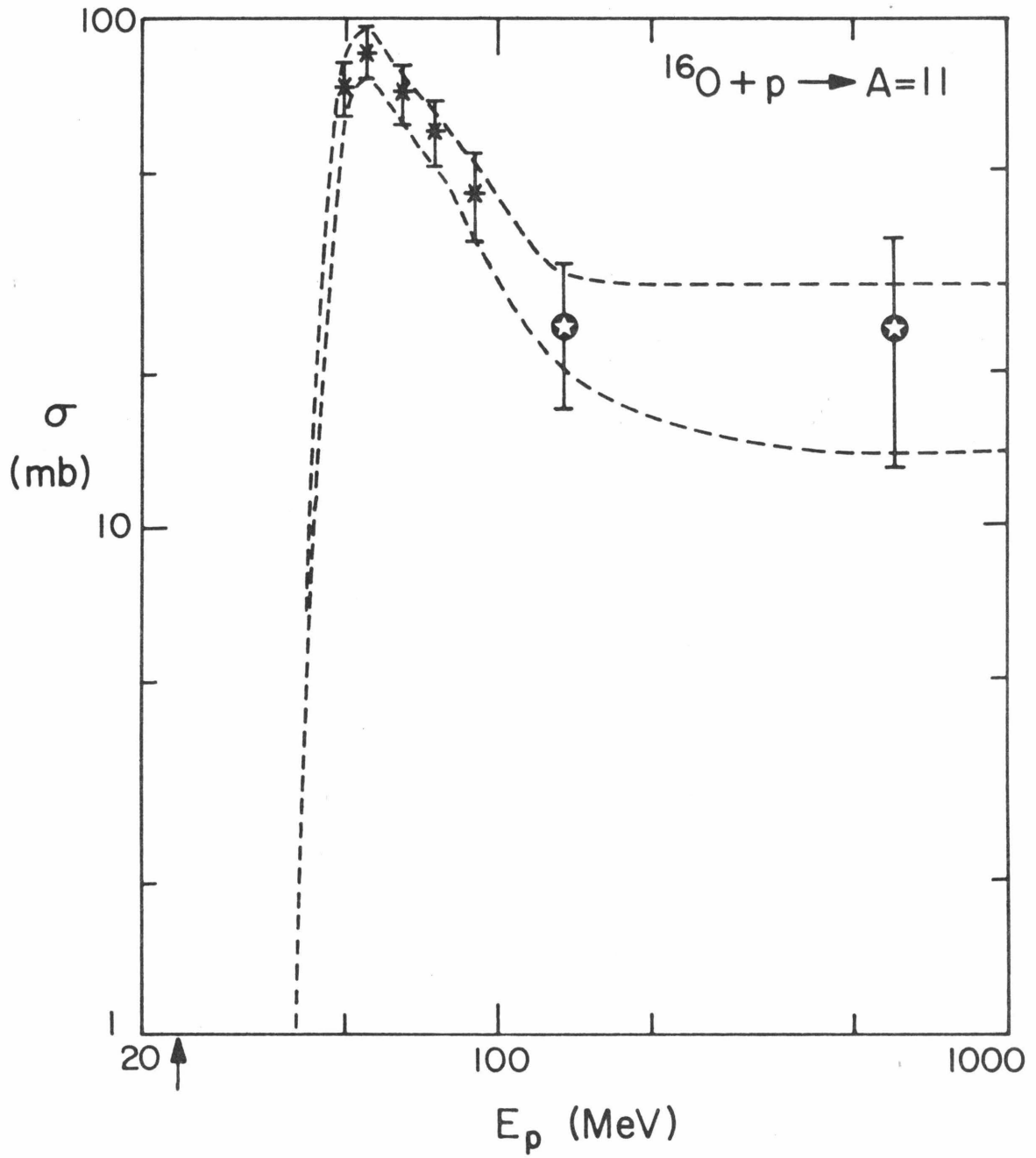


Figure 23

Figure 24

Cross section for the production of mass 6 nuclei by alphas on  $^{12}\text{C}$ . The arrow at 7.9 MeV per nucleon denotes the threshold for production of these nuclei (Bodansky et al., 1975). The relevant cross sections

were measured by:

- ◇ Rudy et al. (1972)
- ◆ Fontes et al. (1971)
- Jung et al. (1970)
- ▼ Raisbeck et al. (1972)

(See Appendix B.)

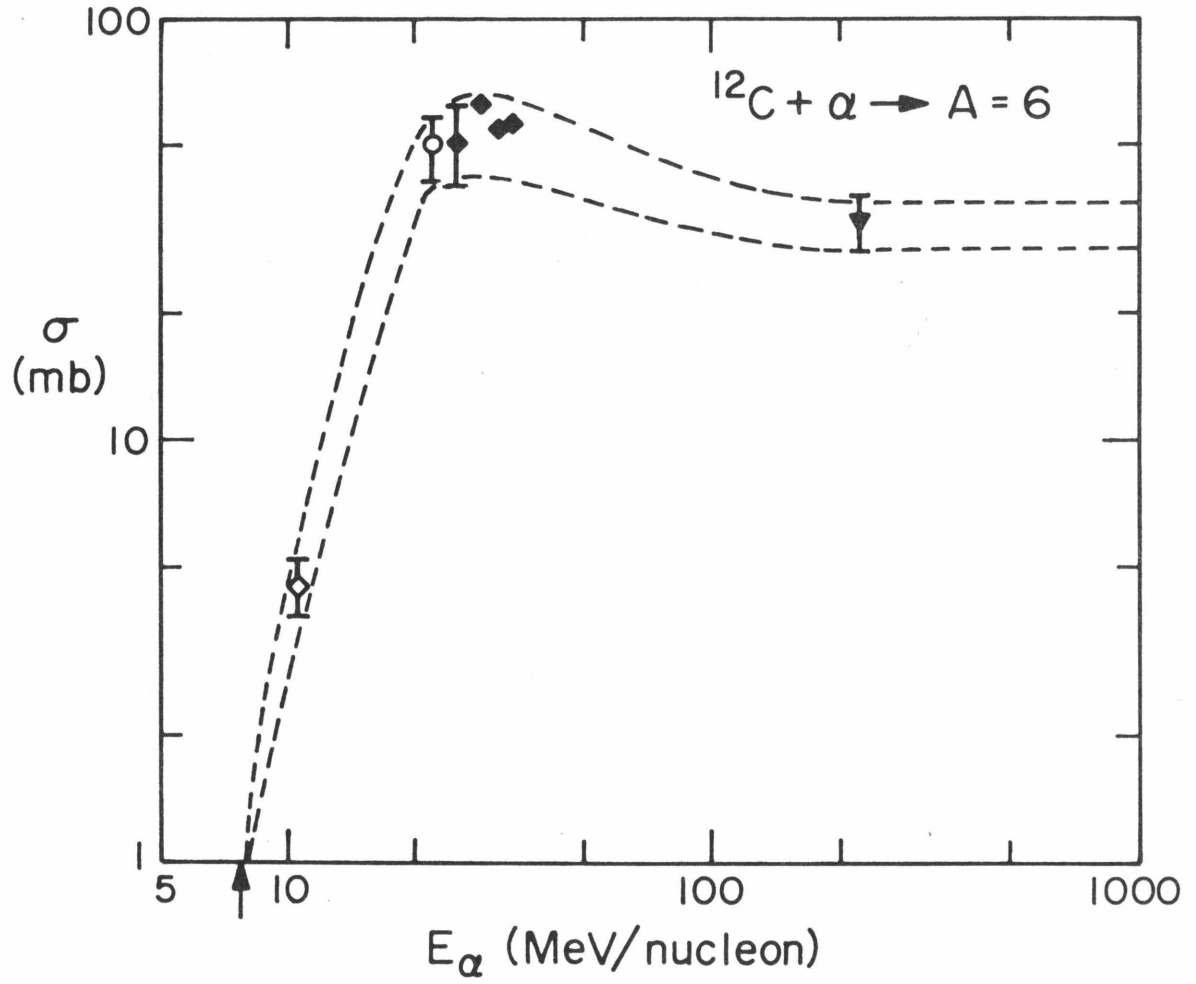


Figure 24

Figure 25

Cross section for the production of mass 9 nuclei by alphas on  $^{12}\text{C}$ . The arrow at 8.2 MeV per nucleon denotes the threshold for production of these nuclei (Bodansky et al., 1975). The relevant cross sections

were measured by:

- ◇ Rudy et al. (1972)
- Fontes (1975)
- Jung et al. (1970)
- ◆ Fontes et al. (1971)
- + Lestringuez et al. (1971)
- × Raisbeck and Yiou (1975)

(See Appendix B.)

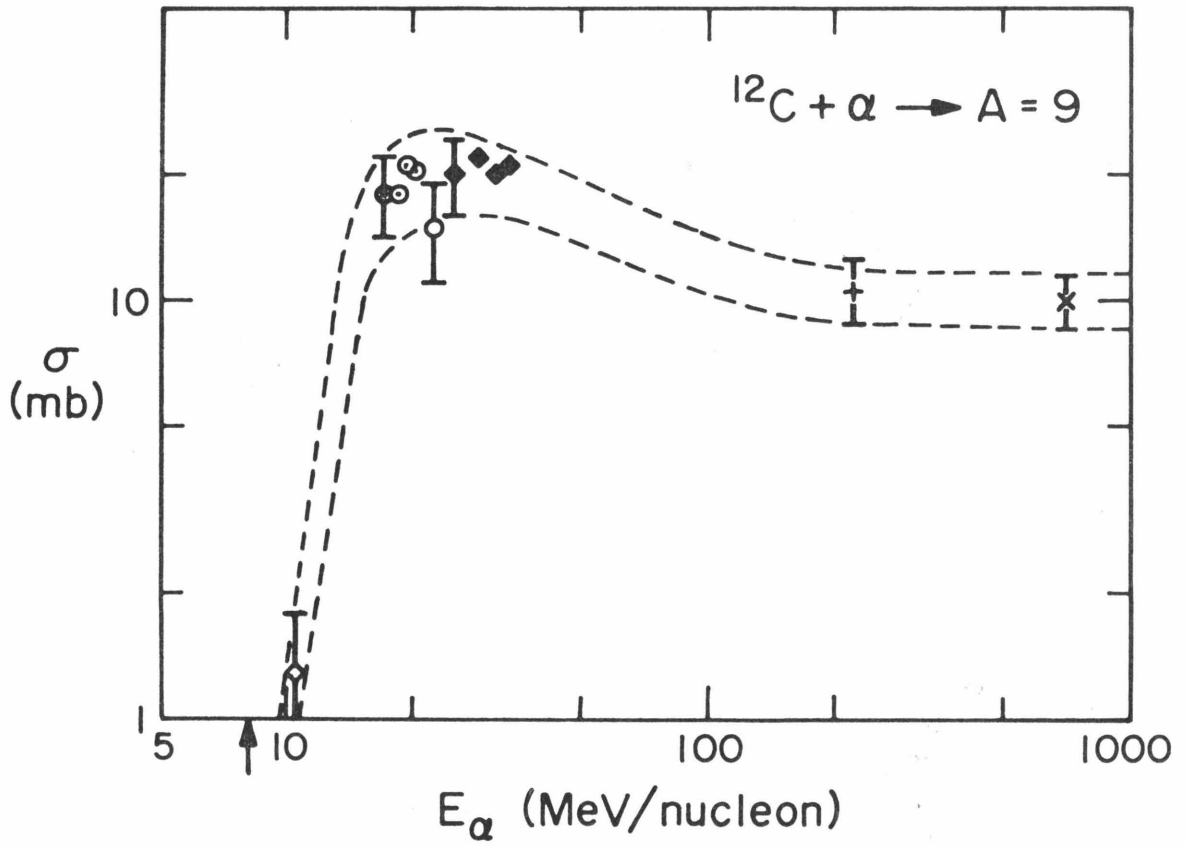


Figure 25

Figure 26

Cross section for production of mass 10 nuclei by alphas on  $^{12}\text{C}$ . The arrow at 7.9 MeV per nucleon denotes the threshold for production of these nuclei (Bodansky et al., 1975). The relevant cross sections were

measured by:

- ◇ Rudy et al. (1972)
- ⊙ Fontes (1975)
- Jung et al. (1970)
- ◆ Fontes et al. (1971)
- + Lestringuez et al. (1971)
- × Raisbeck and Yiou (1975)

(See Appendix B.)

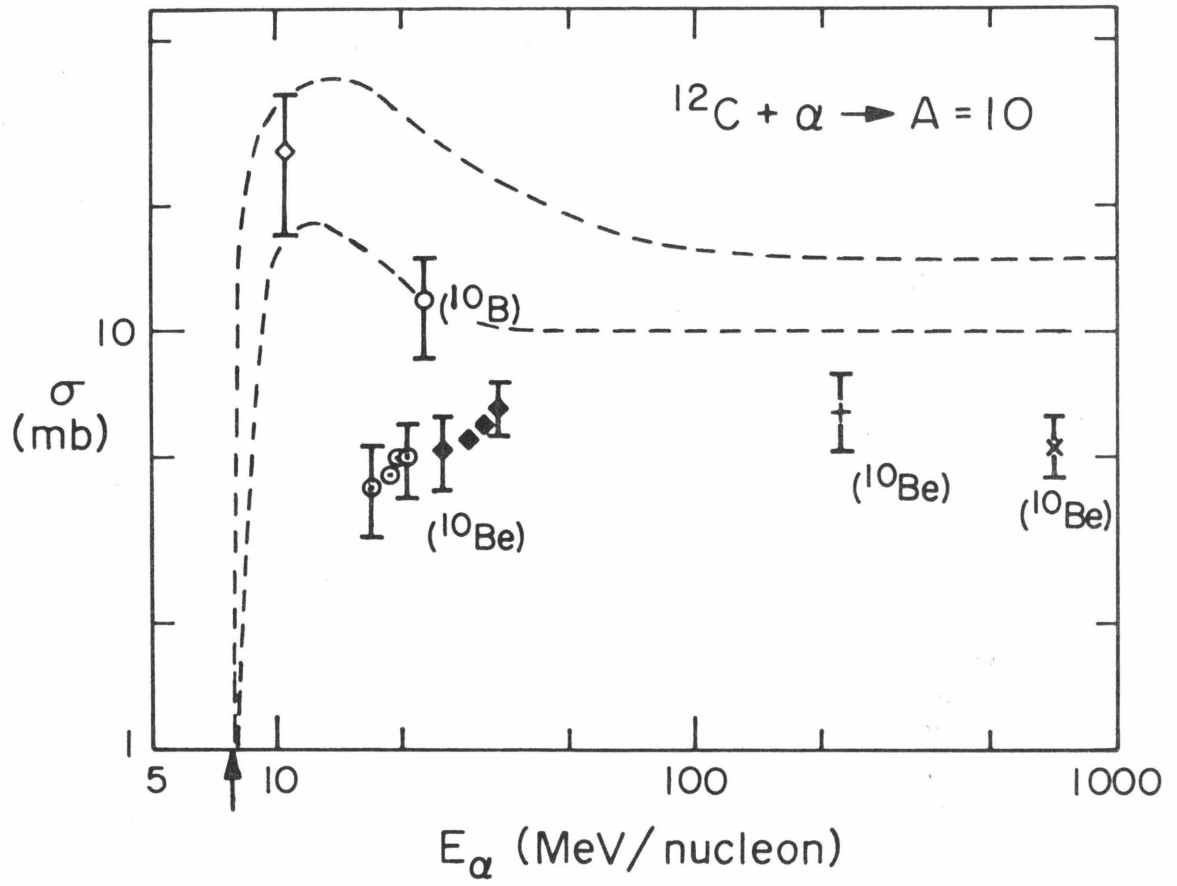


Figure 26

Figure 27

Cross section for the production of mass 11 nuclei by alphas on  $^{12}\text{C}$ . The arrow at 5.3 MeV per nucleon denotes the threshold for production of these nuclei (Bodansky et al., 1975). The relevant cross sections were measured by:

- ◇ Rudy et al. (1972)
- Jung et al. (1970)
- ◇ Radin (1970, 1971)

(See Appendix B.)

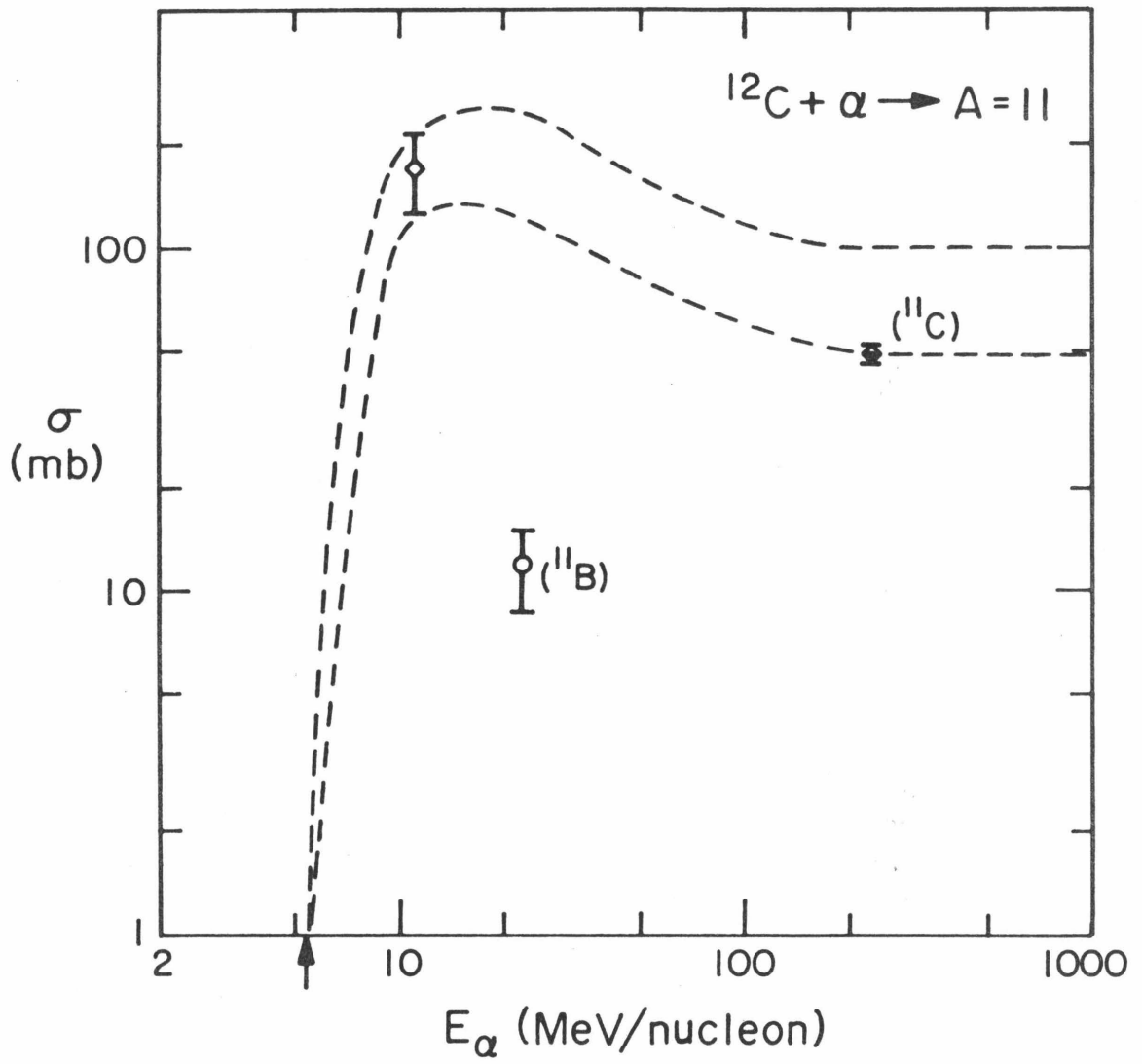


Figure 27

Figure 28

Cross section for the production of mass 6 nuclei by alphas on  $^{14}\text{N}$ . The arrow at 2.8 MeV per nucleon denotes the threshold for production of these nuclei (Bodansky et al., 1975). The relevant cross sections were measured by:

- Jung et al. (1970)
- Jacobs et al. (1974)

(See Appendix B.)

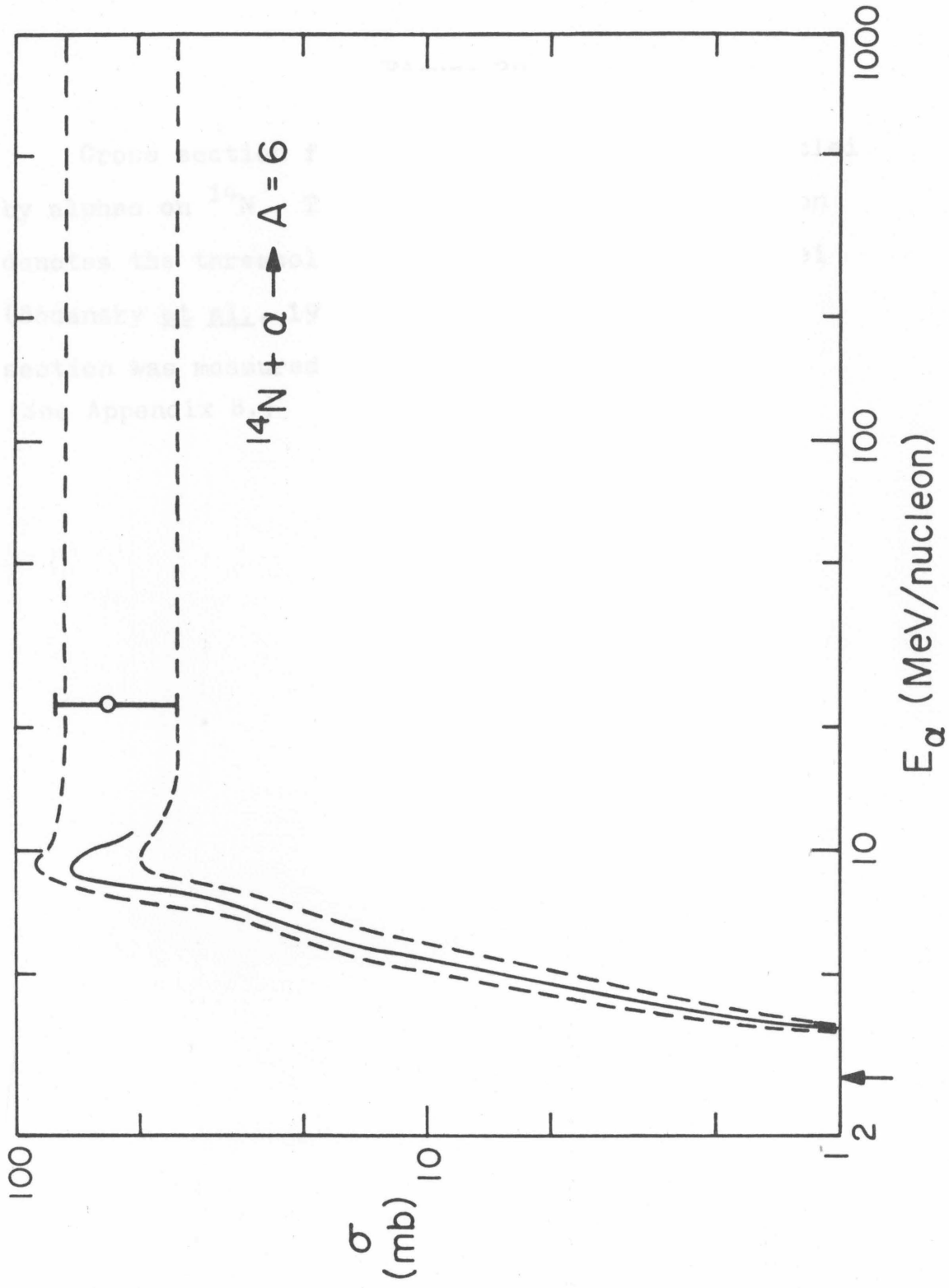


Figure 28

Figure 29

Cross section for the production of mass 9 nuclei by alphas on  $^{14}\text{N}$ . The arrow at 5.85 MeV per nucleon denotes the threshold for production of these nuclei (Bodansky et al., 1975). The experimental cross section was measured by Jung et al. (1970). (See Appendix B.)

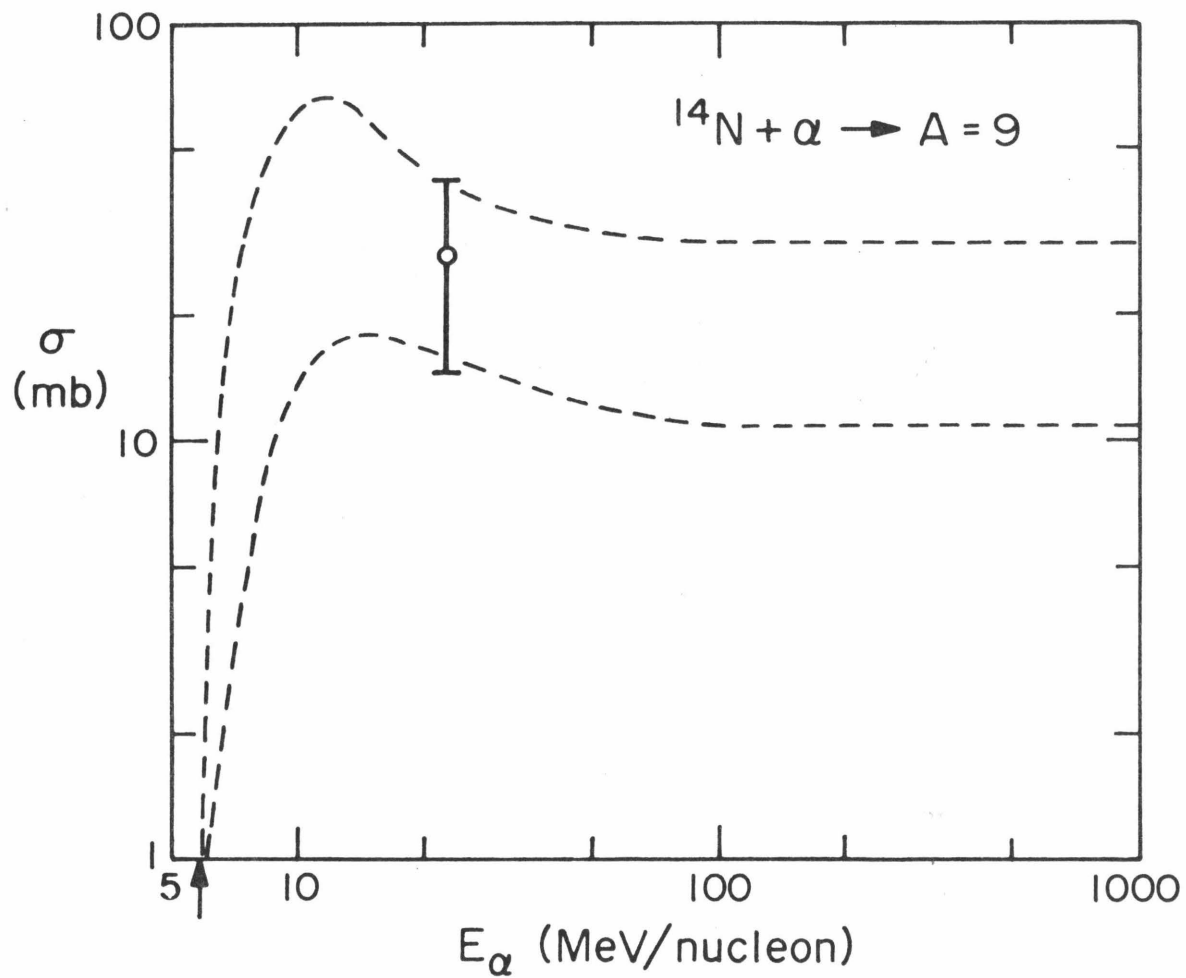


Figure 29

Figure 30

Cross section for the production of mass 10 nuclei by alphas on  $^{14}\text{N}$ . The arrow at 3.7 MeV per nucleon denotes the threshold for production of these nuclei (Bodansky et al., 1975). The relevant cross sections were measured by:

▲ Jacobs et al. (1974)

○ Jung et al. (1970)

(See Appendix B.)

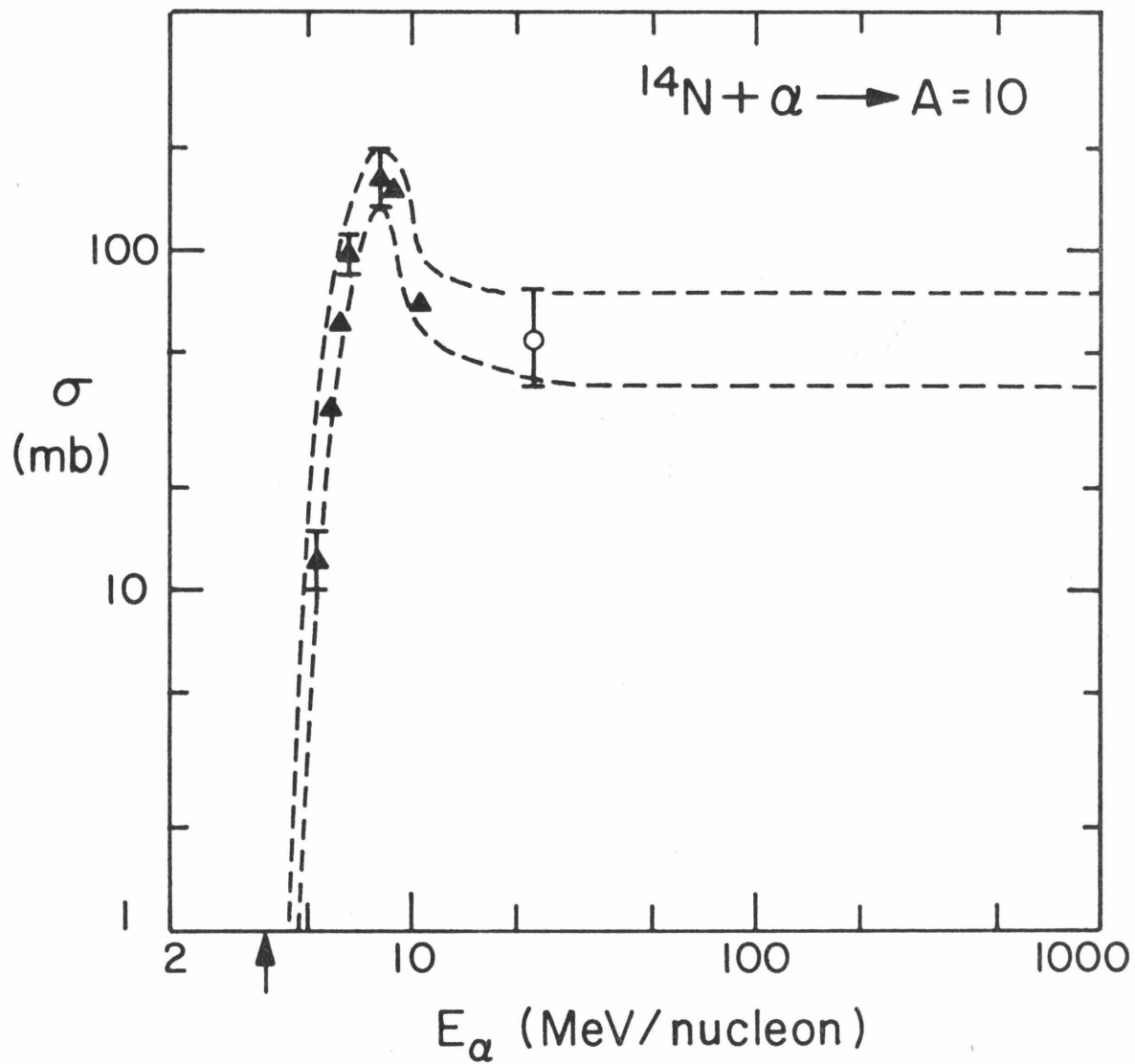


Figure 30

Figure 31

Cross section for the production of mass 11 nuclei by alphas on  $^{14}\text{N}$ . The arrow at 6.2 MeV per nucleon denotes the threshold for production of these nuclei (Bodansky et al., 1975). The experimental cross section was measured by Jung et al. (1970).  
(See Appendix B.)

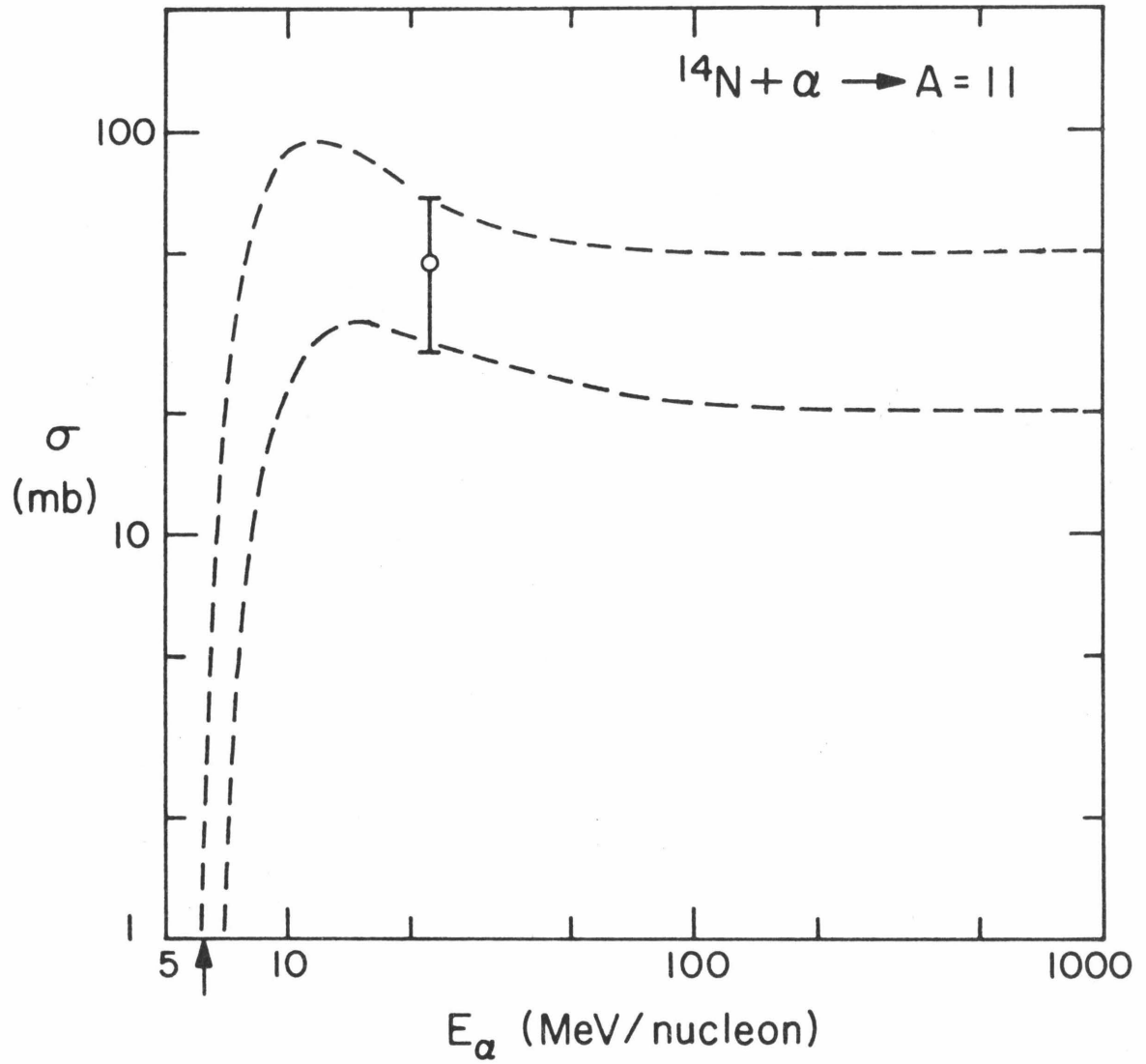


Figure 31

Figure 32

Cross section for the production of mass 6 nuclei by alphas on  ${}^4\text{He}$ . The arrow at 11.2 MeV per nucleon denotes the threshold for the production of these nuclei (Bodansky et al., 1975). The relevant cross sections were measured by:

☆ King et al. (1977)

★ Mathews (1977)

(See Appendix B.)

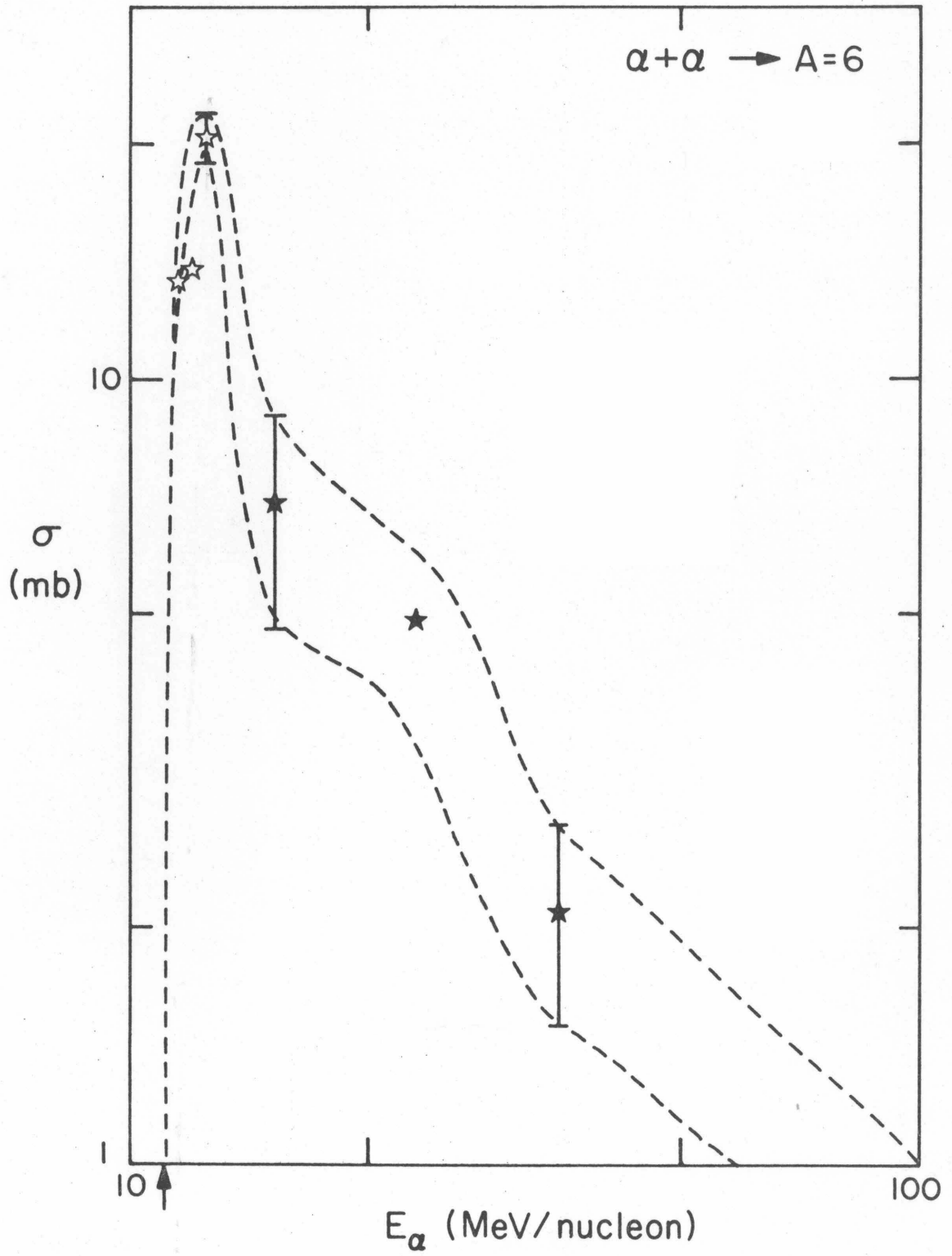


Figure 32